Confronting Dark Matter Powered Stars with Recent Results from Direct Detection Experiments: Modelling of Dark Star Atmospheres and Evolution

Diplomarbeit

vorgelegt von

Franziska Laatz

Institut für Experimentalphysik
Universität Hamburg

Hamburg,
Februar 2012

Erstgutachter: Prof. Dr. Dieter Horns
Zweitgutschter: Prof. Dr. Peter Hauschildt

Abstract

It is predicted that the first stars in the history of the Universe formed in mini-halos of 10^5 to 10^6 $M_\odot$, which also contain a large amount of Dark Matter (DM). These stars are believed to be very massive (M > 100 $M_\odot$). It has been proposed that self-annihilating DM could provide an additional source of energy, producing a new type of stable object, a Dark Matter powered star (Dark Star). The properties of such a Dark Star (DS) may be altered in comparison to a normal Pop III star. Dark Stars are predicted to be cooler, larger, more massive and potentially longer lived, due to their additional energy source.

Using the PHOENIX atmospheric code, stellar spectra of very massive DS are calculated to search for spectral signatures of such objects. PHOENIX is able to calculate atmospheres for a wide range of temperatures. The radiative transfer was calculated in non-local thermal equilibrium and several advanced line broadening options were included (Stark broadening and van der Waals broadening). No lithium lines useful for identifying DS have been found, while molecular hydrogen lines are good indicators for low temperature Pop III stars and early DS. The detectability of such stars via the James Webb Space Telescope (JWST) was investigated. Even for very optimistic assumptions, the JWST is not sensitive enough for detecting DS.

Recently, results from direct detection experiments searching for Weakly Interacting Massive Particles (WIMP, a DM candidate) have suggested low mass WIMPs (< 100 GeV). Furthermore, Pop III stars might not be as massive as previously expected (< 50 $M_\odot$) . The evolution of capture dominated Dark Stars was calculated using the Dark Star evolution code 'DarkStars' for several low mass WIMP scenarios and a variety of ambient DM densities and stellar masses. In conclusion, DS probably exclusively form in the central region of the DM halo, because otherwise it would be unlikely that the ambient WIMP density is high enough to support a DS on long timescales. Because low mass stars usually do not form in the central region of the DM halo, it is likely that DS usually have masses above 20 $M_\odot$.
The studies could be refined by studying different WIMP velocity dispersions and stellar velocities.

Kurzfassung

Es wird angenommen, dass sich die ersten Sterne (Pop III) in der Geschichte des Universums in Mini-Halos einer Gesamtmasse von 10^5 bis 10^6 Sonnenmassen ($M_\odot$) gebildet haben. Diese Halos enthalten außer konventioneller baryonischer Materie auch eine große Menge an Dunkler Materie. Die ersten, von schweren Elementen freien Sterne sind möglicherweise weitaus massiver (M $> 100\ M_\odot$) als die Sterne im heutigen Universum. Selbst annihilierende Dunkle Materie könnte eine zusätzliche Energiequelle für diese Sterne darstellen. Ein solcher von Dunkler Materie angetriebener Stern (Dunkler Stern, eng. Dark Star) hätte besondere Eigenschaften, die ihn stark von den normalen Pop III Sternen unterscheiden könnten. Dunkle Sterne sind vorraussichtlich kühler, größer und langlebiger aufgrund ihrer zusätzlichen Energiequelle.

Mit Hilfe des Programmpaketes PHOENIX, zur Simulation von Sternenatmosphären, wurden massive, primordiale Dark Stars simuliert und ihre Spektren zur anschließenden Analyse hinsichtlich spezifischer Signaturen von Dark Stars (z.B. Linien von Lithium oder molekularem Wasserstoff) berechnet. Der Strahlungstransport wurde im nicht lokalen thermischen Gleichgewicht berechnet und es wurden verschiedene Mechanismen, die zu einer Verbreiterung der Spektrallinien führen, berücksichtigt (Stark und Van der Waals Verbreiterung). Lithium Linien, die für die Identifikation von Dark Stars nützlich sein könnten, wurden nicht gefunden, während die beobachteten Linien molekularen Wasserstoffs ein guter Indikator für Pop III Sterne mit niedriger Temperatur oder Dark Stars sind. Die Möglichkeit einer Detektion massiver Dark Stars mit dem James Webb Space Telescope (JWST) wurde untersucht. Selbst für sehr optimistische Annahmen erscheint eine Detektion von massiven Dark Stars für Rotverschiebungen $z > 3$ unmöglich.

Aktuellste Ergebnisse verschiedener Experimente zum direkten Nachweis von WIMPs (Weakly Interacting Massive Particles, ein vielversprechender Dunkle Materie Kandidat), favorisieren eine niedrige WIMP Masse (< 100 GeV). Zusätzlich häufen sich die Hinweise darauf, dass Pop III Sterne möglicher Weise weniger massiv sind als zunächst angenommen wurde ($< 50\,M_\odot$). Daher wurde im zweiten Teil der Arbeit die Evolution von durch den Einfang von WIMPs dominierten Sternen mit dem Programmpaket 'DarkStars' für unterschiedliche WIMP-Szenarien, sowie eine Vielfalt an verschiedenen WIMP-Umgebungsdichten und Sternmassen berechnet. Es folgt, dass Dark Stars, deren Leuchtkraft durch die Annihlihation von WIMPs dominiert wird, wahrscheinlich in der zentralen Region von Dunkle Materie Halos entstanden sind, da die WIMP-Umgebunsdichte des Sterns in den weiter außen liegenden Regionen des Halos zu niedrig ist. Weil leichte Sterne gewöhnlich nicht in der zentralen Region des Halos entstehen, sind Dark Stars vorraussichtlich schwerer als $20\,M_\odot$.

Die hier vorgestellten Studien lassen sich durch Untersuchungen zum Einfluss verschiedener Sterngeschwindigkeiten und der mittleren Geschwindigkeit der WIMPs erweitern.

Contents

Chapter 1

Introduction

Within living memory mankind has been fascinated by the twinkling objects, called stars, emerging in the sky each night. This curiosity basic in human nature is the foundation for the spirit of research grasping the ancient Greeks as much as todays scientists. The ultimate goal is to finally answer the question raised by Goethes Faust:

"Dass ich erkenne, was die Welt im Innersten zusammenhält"

Mankind seeks fundamental knowledge about the principles of nature. Mathematical models are used to describe physical processes and phenomena. The modern astronomy, studying the most distant and oldest objects in the Universe, and particle physics, searching for the most fundamental components of matter, are just two of many branches of this far-reaching development. Astroparticle physics resides at the interface of both ambitious fields, trying to explain astrophysical phenomena by employing fundamental particle interactions.

Explaining the nature of the non-luminous matter component, called dark matter (DM), is most crucial to both scientific fields. This study combines considerations about the nature of the dark matter particle and fundamental questions concerning the nature of the first stars forming in the history of the Universe.

Since the first stars formed in high density DM regions the self-annihilation of dark matter particles may constitute an additional energy source for the first stars. This additional energy supply may be important during the formation of the first stars as well as during later stages of the evolution, altering their stellar properties. These altered stellar properties (low temperature, large radius, long lifetime) should condense in unique spectral features of DS helping to distinguish DS from normal first and contemporary stars. A direct detection of stars at high redshifts (light that has been emitted a long time ago) generally proves to be very difficult, thus the first part of this study is devoted on studying possible spectral features useful for identifying DS and probing the detectability of massive DS with the upcoming James Webb Space Telescope (JWST), which has been designed for studying early objects.

The second part of this study is dedicated to a detailed analysis confronting dark matter powered stars with recent results from experiments searching for dark matter particles and from studies of early star formation. The evolution of relatively low mass dark matter powered stars is calculated and interpreted in this light. Implications for the DM properties, star formation scenarios, and properties of the DM halo are discussed.

This study is arranged as follows: In the second chapter, a general introduction into the physical topics important to this study is given. Evidences for the existence of dark matter,

dark matter properties and possible candidates are discussed. A general introduction into the mechanisms important in the formation of the first stars (and DS) is given. The stellar evolution code 'DarkStars', which was used for calculating the evolution of relatively low mass DS, is introduced. Additionally, the basics of radiative transfer important for calculating stellar atmosphere spectra are given. The PHOENIX code, used in this study to calculate spectra of massive DS, is introduced.

In the third chapter, results of the analysis of DS atmospheres, calculated with PHOENIX, and the calculations concerning the detectability of DS are presented. The analysis of the stellar evolution of relatively low mass DS is carried out in Chapter 4. Detailed considerations concerning the implications of the results for DM properties, early star formation, and DM densities are also discussed in Chapter 4.

The results of this study are summarized, and a short outlook is given in Chapter 5.

Chapter 2

Theory

2.1 WIMPs as Dark Matter Candidates

In 1933 it was noted for the first time by Zwicky (1933), that there seemed to be more matter in the Coma cluster, than could be seen by visible observations. Additional astrophysical evidence for a non luminous mass component in the Universe, called Dark Matter (DM), has been provided over the following decades by measurements of the mass content of galaxy clusters via gravitational lensing, of orbital velocities of galaxies (as shown for the spiral galaxy NGC 6503 in Figure 2.1), of the expansion of the Universe using Supernovae 1a as standard candles, of the cosmic microwave background (CMB), as well as the measured abundances of the light elements in the early Universe (Big Bang Nucleosynthesis) (Bertone et al. 2005).
Today it is assumed that baryonic matter only makes up a small fraction of the total matter content in the Universe. It only accounts for $\approx 4.6\%$ of the energy density of the Universe, while DM accounts for $\approx 23\%$ and the majority of energy exists in the form of dark energy ($\approx 72\%$) as shown in Figure 2.2.

Such DM is non luminous (i.e. no electromagnetic interactions), it is stable or long lived, cold (or maybe warm), non baryonic, but gravitationally interacting. The Standard Model (SM) of particle physics does not provide a DM candidate. The only possibility would be the neutrinos, but they could not account for all the DM, because their mass is too small. Supersymmetry (SUSY) solves some of the major problems of the SM. It makes the unification of the gauge coupling constants possible and almost naturally solves the hierarchy problem (Bertone et al. 2005). Every SM fermion and boson has a SUSY partner (Figure 2.3) with the spin being different by one half to their SM partners. SUSY particles can not exclusively decay into SM particles, if conservation of R-parity is assumed[1].

Thus, the Lightest Supersymmetric Particle (LSP) would be stable or very long lived and might be a good DM candidate, meeting all of the above criteria. Nevertheless, SUSY must be broken, because otherwise the SM particles and their SUSY partners would not have the same mass, otherwise they would already have been detected. Depending on the specific theory the LSP might be the Neutralino (mixture of the Bino, Wino and Higssino, SUSY-partner of SM gauge and Higgs bosons) or the Gravitino. Both particles are examples for Weakly Interacting Massive Particles (WIMP), which are Majorana particles and thus able to self-annihilate into

---

[1]In the Minimal Supersymmetric Standard Model all SUSY particles have R-parity -1 and all SM particles 1 and the R-parity operator is given by $R_p = -1^{2s+3B+L}$ where s is the spin, B the baryon number and L the lepton number.
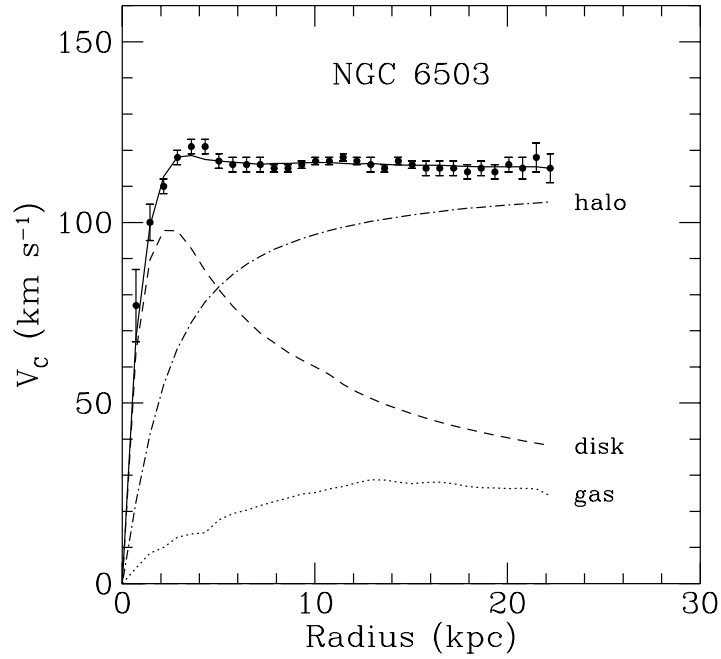
Figure 2.1: Rotational velocity of the spiral galaxy NGC 6503. The contribution of the different matter components contained within the radius r is given in terms of the radial velocity. The dotted line shows the contribution of the luminous matter in the disk, the dashed line shows the contribution of the gas in the interstellar medium and the dotted-dashed line the required DM contribution in the halo in order to reproduce the measured rotation curve (Begeman et al. 1991).
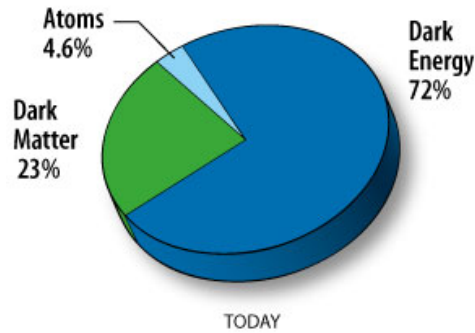
Figure 2.2: The energy density content of the Universe nowadays (Image credit: NASA/WMAP Science Team 2011).
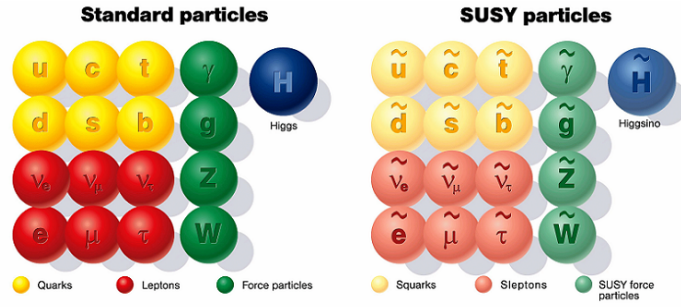
Figure 2.3: The particles of the SM and their SUSY partners (Image credit: The University of Glasgow)
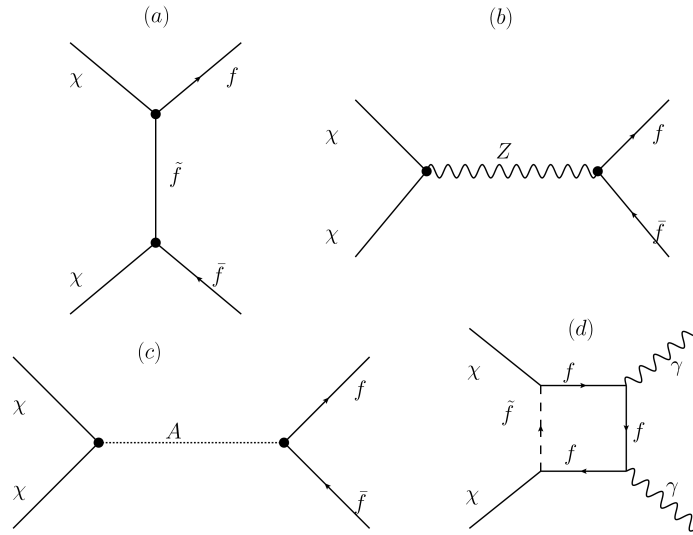
Figure 2.4: Feynman diagrams for Neutralinos annihilating into fermions (a, b, c), and one example diagram for Neutralino annihilation into Photons (d).

SM particles[2]. In Figure 2.4 the tree level Feynman diagrams for Neutralino annihilation into fermions (a,b,c) and one of several possible diagrams (d) for the annihilation into photons are shown exemplary. In principle the Neutralino can also annihilate into the SM gauge bosons and the Higgs. Thanks to crossing symmetries the Feynman diagrams b) and c) in Figure 2.4 can be rotated by 90 degrees into diagrams for Neutralino fermion scattering.

WIMPs are very prominent DM candidates because they would automatically produce the correct relic density. In the early Universe WIMPs are in chemical and thermal equilibrium, because they can self annihilate into SM particles and be produced out of SM particles as long as the WIMP density is high enough. As the Universe expands, the temperature and the number density of the DM particles decreases following a Maxwell-Boltzmann distribution

$$n_\chi \sim e^{-\frac{m_\chi}{k_{\mathrm{B}}T}}, \tag{2.1}$$

where n_χ is the number density of WIMPs, m_χ the WIMP mass, and T the temperature and

---

[2]Gravitino must not be a Majorana particle.

k_B the Boltzmann-constant.

Consequently, the annihilation rate decreases and at some point the WIMPs decouple from thermodynamic equilibrium and freeze out. A fixed number of WIMPs is left, but the WIMP density decreases further because the Universe continues to expand. Using some simplifying assumptions, an order of magnitude approximation of the relic density of WIMPs is given by (Bertone et al. 2005)

$$\Omega_\chi h^2 \approx \frac{3\text{x}10^{-27}\,\text{cm}^3\,\text{s}^{-1}}{\langle \sigma_a v \rangle}. \tag{2.2}$$

Here Ω_χ is the energy density of WIMPs, $h = H_0/100\,\text{km s}^{-1}\text{Mpc}^{-1}$, where $H_0 \approx 70\,\text{km s}^{-1}\text{Mpc}^{-1}$ is the Hubble parameter, and $\langle \sigma_a v \rangle$ is the thermally averaged and velocity weighted annihilation cross-section. The results of WMAP thus require an annihilation cross-section of $\langle \sigma_a v \rangle = 3 \times 10^{-26}\text{cm}^3\text{s}^{-1}$ (Komatsu et al. 2011). WMAP also measured that the Universe is flat, which means that the total energy density $\Omega = 1$. It is given by the energy density from matter ($\Omega_M = \Omega_\chi + \Omega_{\text{Baryons}}$, where Ω_{Baryons} is the energy density provided by baryons) and the dark energy density Ω_Λ.

2.1.1   Detection of WIMPs

Aside from finding the Higgs particle one of the major discoveries in the near future would be the detection of WIMPs. In principle, WIMPs can be produced and detected in collider experiments or via direct detection experiments, through their interaction with baryonic matter. Alternatively, they can be detected in indirect searches, where the radiation produced in dark matter annihilation and decay is studied. Examples are Ice Cube, which searches for neutrinos originating from DM annihilation, or H.E.S.S., which studies the gamma rays produced in WIMP annihilations (Bertone et al. 2005 and references therein).

In this study, we focus on direct detection experiment because their results will be used in Chapter 4. Thus, a short and general introduction is given. All direct detection experiments follow the same principle ideas: WIMPs are everywhere in the Universe, so they should be regularly passing through the earth, where they can interact with regular matter. They may be scattered from nuclei and transfer energy to the nuclei. The nucleon will recoil and its recoil energy may be detected. One of the major differences between different direct detection methods is the way this recoil energy is measured and the target material used. The recoil energy either manifests in a vibration (a phonon in a crystal lattice) or can be passed on to the electrons of the atoms, causing ionization or excitation of the electron. In the second case a photon is emitted, which can be measured as scintillation light. DAMA/LIBRA (Bernabei et al. 2008), for example, measures scintillation light and uses sodium iodide NaI as target material, CRESST measures photons and ionization using $CaWo_4$ (Angloher et al. 2011) and XENON uses ionization and scintillation with xenon as target material (Angle et al. 2008).

The rate at which such scatterings occur depends on the density and the velocity distribution of the WIMPs in the solar neighborhood, as well as the scattering cross-sections. The differential scattering rate per unit mass is given by

$$\frac{\text{d}R}{\text{d}E} = \frac{\rho_\chi \sigma_s}{2m_\chi \mu^2} \mid F(E) \mid^2 \int_{v_{\text{min}}}^{v_{\text{esc}}} \frac{f(\vec{v},t)}{v}\,\text{d}^3v. \tag{2.3}$$

Here ρ_χ is the ambient WIMP density given by approximately $0.3\,\text{GeV/cm}^3$ in the solar neighborhood, σ_s is the scattering cross-section, m_χ is the WIMP mass taking values between

$10 - 10^4$GeV, $\mu = m_\chi m_N/(m_\chi + m_N)$ and m_N is the nucleon mass. $\mid F(E) \mid$ is the energy dependent form factor of the nucleus. $v_{\min}$ is the minimum WIMP velocity and v_{esc} the escape velocity of the halo, consequently the maximum velocity a WIMP in the galactic halo can obtain. $f(\vec{v}, t)$ is the WIMP velocity distribution in the galactic halo, which can be approximated by an isothermal and spherical distribution

$$f(\vec{v}, t) \propto \exp\left(-\frac{(\vec{v} + \vec{v}_E)^2}{2\sigma_v}\right). \tag{2.4}$$

$\vec{v}_E$ is the speed of the earth, σ_v the velocity dispersion of the distribution given by the circular speed $v_0 \sim 230$km/s divided by $\sqrt{2}$.

WIMPs can scatter either via an axial-vector interaction, where it couples to the spin content of the nucleon, or a scalar interaction independent of the spin. In the first case the cross-section depends on the total angular momentum (to be exact it is proportional to $\sigma_{\mathrm{SD}} \propto J(J+1)$, where J is the total spin), the cross-section for spin-independent coupling depends on the mass of the target nuclei ($\sigma_{\mathrm{SI}} \propto A^2$, where A is the mass number of the material). Thus, a higher scattering rate can be achieved by using target nuclei with high masses.

Some of the experiments try to reject background signals by searching for an annual modulation (e.g. DAMA/LIBRA) of the WIMP arrival rate, which is caused by the movement of the earth around the sun relative to the overall movement of both through the galaxy. As the Solar System moves through the galaxy, the WIMPs seem to be moving towards the system (kind of a WIMP wind). Depending on the time of year the earth either moves towards the wind, increasing the rate at which the WIMPs arrive or away from it, decreasing the WIMP arrival rate

DAMA/LIBRA and CoGeNT have already claimed to see annually modulated signals (Bernabei et al. 2008 and Aalseth et al. 2011). CRESST has also seen a signal, but the statistic is too small to see any modulation. However, all of these signals are inconsistent with limits from the XENON experiment, which has not yet found any signal. At energies below ~ 10 GeV the XENON sensitivity decrease rapidly. Small changes in the energy or the systematic uncertainties would make some of the CRESST, DAMA/LIBRA and CoGeNT allowed regions feasible (Collar 2011). The current results of direct detection experiments are summarized in Figure 2.5.

2.2   Star Formation and Evolution

Stars form from interstellar gas clouds. The basic formation mechanisms are presented here following Ryan and Norton (2010). Such a cloud consists of hydrogen, helium and possibly metals, which are in atomic and partially molecular form depending on temperature and density of the gas. The atoms in the gas have a kinetic energy due to the temperature of the gas and a potential energy due to their gravitational interactions with the other atoms. The potential energy of a cloud is approximately given by

$$E_{\mathrm{grav}} \sim -\frac{\mathrm{G}M^2}{R}, \tag{2.5}$$
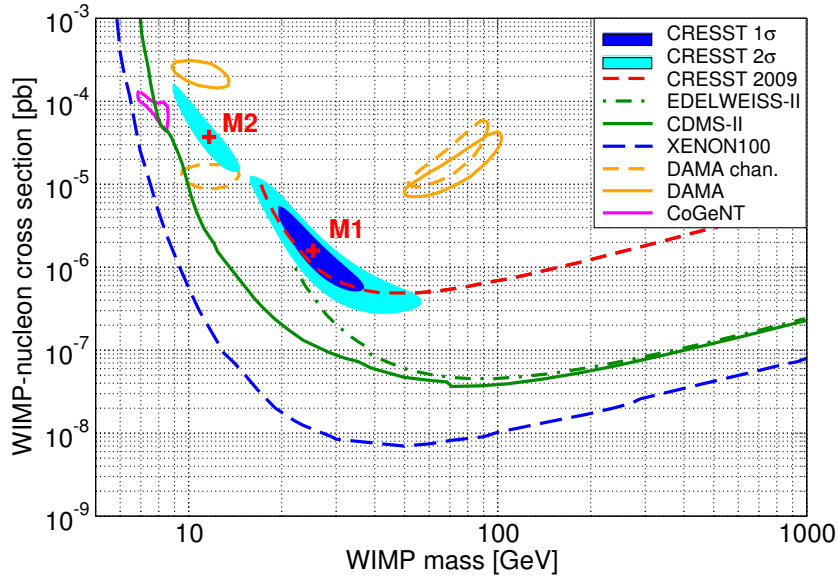
Figure 2.5: Current status of the of the search for WIMPs by direct detection experiments. The exclusion limits from XENON100, CDMS-II and EDELWEISS-II are shown and the CRESST limit from 2009. Additionally the signal regions of CoGeNT and DAMA/LIBRA (with and without ion channeling) are shown, as well as the CRESST detection regions which have been calculated with respect to the global likelihood maximum M1. In addiation there is another global likelihood M2 shown (Angloher et al. 2011).

where G is the gravitational constant, M is the total mass of the cloud, and R is the radius of the cloud. The kinetic energy of all particles in the cloud is given by

$$E_{\text{kin}} = \frac{3}{2} N k T. \tag{2.6}$$

Here, N is the total number of particles in the cloud, k is the Boltzmann constant, and T is the temperature of the gas cloud. If the kinetic energy exceeds the absolute value of the potential energy the cloud tends to expand, while it tends to collapse if the gravitational energy exceeds the kinetic energy. Thus, the condition for the collapse of such a gas cloud is given by

$$\mid E_{\text{grav}} \mid > E_{\text{kin}}. \tag{2.7}$$

This relation can be translated into a limit for the mass or density that a cloud must exceed in order to collapse due to self gravity, if it has a certain temperature T, radius R and composition $\overline{m}$ (average mass of the particles in the gas)

$$M > \frac{3\text{k}T}{2\text{G}\overline{m}} R \equiv M_J, \tag{2.8}$$

$$\rho > \left(\frac{3\text{k}T}{2\text{G}\overline{m}} \right)^3 \frac{3}{4\pi M^2} \equiv \rho_J. \tag{2.9}$$

This limiting mass (density) is called Jeans mass M_J (Jeans density ρ_J). If such a cloud collapses adiabatically, meaning without any exchange of heat, the relationship between temperature and density of the gas is given by

$$T \propto \rho^{\gamma - 1}, \tag{2.10}$$

where γ is the adiabatic index depending on the number of degrees of freedom of the particles making up the gas and takes values between 1 and 5/3.

Thus, if the cloud contracts, the temperature rises until the kinetic energy balances the potential energy so that a state of equilibrium is reached. The same holds for an expanding gas cloud. Therefore, no gas cloud contracts adiabatically, so that cooling and heating mechanisms must be considered.

A gas cloud can be heated by cosmic rays, while it is cooled via escaping photons, which are emitted when atoms or molecules are de-excited, or they are emitted as thermal infrared radiation from dust. Approximately cooling dominates for temperatures above 20 K (for solar metallicity stars), while heating dominates below. Thus, a stellar cloud, for example dominated by cooling, decreases its temperature, but does not expand or contract until the temperature at which heating and cooling balance each other is reached.

In case that the resulting combination of temperature and density leads to conditions in which gravitational energy dominates over kinetic energy, the cloud collapses at an almost constant temperature until it becomes opaque to its own radiation. However, the temperature does not immediately rise freely because first, the liberated potential energy dissociates molecules and ionizes atoms. Afterwards, the temperature and density rise almost adiabatically and the cloud approaches hydrostatic equilibrium. Even though, attaining hydrostatic equilibrium slows the collapse, it is not halted as energy is radiated away. Furthermore, usually the conservation of angular momentum leads to the formation of an accretion disk during the collapse of the protostellar cloud. The material in the disk rains onto the protostar, which leads to an increase in the final mass of the star. The accretion process is stopped by feedback mechanisms. In contemporary stars, the radiation pressure on the dust grains in the circumstellar disk gets so high that the gas in the disk is radiated away (for the first stars other feedback mechanisms are important; see Section 2.3).

This stage in the formation defines the transition from an protostellar cloud to a protostar, so that the star is considered a pre-main sequence (PMS) star. Gravitational energy powers the protostar in this stage of the evolution. The evolution of a star can be described by plotting the luminosity against the effective temperature of the star. Such a diagram is called a Herzsprung-Russel diagram (H-R diagram) and is often used to refer to or explain a certain step in the stellar evolution.

In order to maintain hydrostatic equilibrium the star must have a temperature greater than a minimum value called the Hayashi boundary. Protostars with temperatures cooler than this limit contract heating up until they have reached this minimum temperature. Afterwards the protostar contracts further, but the stellar temperature stays almost constant, so that the luminosity decreases. A star in this stage of the evolution thus takes an almost vertical track in the H-R diagram, called Hayashi track. Now the energy transport through the star is fully convective, because the protostar is cool and very opaque, so that radiative transport is inefficient. Stars with masses smaller than $0.5\,M_\odot$ start hydrogen burning at the bottom of the Hayashi track.

More massive stars join the Henyey track contracting and heating up further. Because of the increasing temperature the opacity decreases, so that the core becomes radiative and the star is not fully convective anymore. Finally the temperature gets so high that hydrogen burning starts and the collapse is halted. A star at this stage is called a Zero-Age-Main-Sequence (ZAMS) star.

From now on the energy is generated by hydrogen burning defining the main sequence, until hydrogen runs out and other nuclear fusion processes become important. Finally all of

the nuclear fuel is used up and the star ends its life in dependence on its mass for example in a Supernova explosion, as a white or black dwarf, a neutron star or a black hole.

In general, most contemporary stars form in large stellar clusters, because the large initial cloud fragments during the contraction process. This happens, because after the cloud has started to collapse, the Jeans mass is reached for smaller and smaller subregions of the cloud, so that eventually they start to collapse individually. Thus, several stars may form within a single gas cloud.

2.3 Formation of the First Stars

It is believed that the formation of the first stars started at z > 20 in mini-halos containing $10^5 - 10^6 \, M_\odot$ of matter. The matter in such halos, would consist of 15% baryons and 85% DM. The first stars form out of metal-free gas consisting of hydrogen and helium. These zero metallicity stars constitute the Population III. Here, the most important mechanisms of early star formation as well as the differences to contemporary star formation are discussed following Bromm and Larson (2004) and references therein.

In contemporary gas clouds cooling takes place mainly via thermal radiation from dust. In the first stars no metals and thus no dust exist, therefore, the cooling in the first stars proceeds via escaping photons emitted when hydrogen atoms or molecules de-excite. The virial temperatures of the small gas clouds in the early Universe are below the threshold $\sim 10^4$ K at which cooling by atomic hydrogen becomes efficient, so that the cooling must rely on molecular hydrogen H_2. It takes place via rotational-vibration transitions that occur, when for example hydrogen atoms collide with the H_2 molecules. H_2 cooling cannot proceed to temperatures lower than $100 \, \text{K}$, because the two lowest lying rotational energy levels have an energy spacing of $E/k_B = 512 \, \text{K}$. Collisions with particles (mostly H-atoms) from the high energy tail of the Maxwell-Boltzmann can lower the temperature somewhat more, but not below the mentioned 100 K. This leads to a characteristic temperature of 200 K. Above a critical density of 10^4 particles per cm^3, the de-excitation by collisions not cooling the gas compete with radiative de-excitation which cool the gas (Bromm and Larson 2004). Thus, at this characteristic values the gas is not efficiently cooled anymore and undergoes a phase of slow contraction in hydrostatic equilibrium.

If the mass of the cloud is above the Jeans mass (or more mass is accumulated until the Jeans mass is reached), a gravitational runaway collapse is triggered. Since turbulent velocity fields and magnetic fields influencing the stability of present-day molecular clouds are believed to be sub-dominant in primordial clouds, the Jeans criterion can be applied much better to primordial star formation than to present-day star formation. This gas cloud is the immediate progenitor of the final star or, in the case of sub-fragmentation, the total mass of the star cluster. Thus it sets an upper limit to the final stellar mass. Presently, it has not finally been determined whether the first stars form isolated, in binaries or even clusters. It has been suggested that sub-fragmentation may take place at densities above 10^8 cm^{-3}, because three body interaction may convert the gas into fully molecular form. This would lead to a sudden increase in cooling resulting in thermal instabilities. Nevertheless, several simulations have drawn very conflicting pictures (Abel et al. 2000, Abel et al. 2002, Bromm et al. 1999, Bromm et al. 2002) and the question whether the first stars form isolated or in clusters has not been finally answered.

The final mass of the star is set by the efficiency of the accretion process, which is very

different for present-day and primordial star forming regions. The matter accretion rate is proportional to the temperature in the region ($\propto T^{2/3}$). Thus, today it is much lower ($T \sim 10 \, \text{K}$) than when the first stars formed $T \sim 200 - 300 \, \text{K}$. Additionally, it is important how long the accretion continues. The usual termination process in present-day stars, where accretion is stopped because the disk evaporates due to the radiation pressure acting on the dust grains in the disk, is not important for primordial accretion disks. Alternatively, the formation of a HII region (Omukai and Inutsuka 2002) or the radiation pressure exerted by trapped $Ly - \alpha$ photons (Tan and McKee 2004) could turn off accretion.

Nevertheless, the typical mass scale of primordial stars is much higher than in present-day stars, where $1 \, M_\odot$ is a typical mass. For Pop III stars the typical mass scale is $\sim 100 \, M_\odot$. According to McKee and Tan (2008), normal Pop III stars grow to around $140 \, M_\odot$ and have temperatures $T >> 50000 \, \text{K}$.

In the halos where the first stars form a large amount of DM exists. Under the assumption of a WIMP scenario, DM particles can self-annihilate into SM particles, generating energy. The amount of energy produced in WIMP annihilation is high enough to eventually be an important heating source within a star or even during the collapse of the protostellar cloud. The energy produced by WIMP annihilation per unit volume is given by

$$Q_{\text{ann}} = \langle \sigma_a v \rangle \frac{\rho_\chi^2}{m_\chi}. \tag{2.11}$$

Here $\langle \sigma_a v \rangle$ is the thermally averaged and velocity-weighted annihilation cross-section, ρ_χ the local energy density of the WIMPs and m_χ the WIMP mass.

Spolyar et al. (2008) suggested that the energy production due to the presence of DM within a star forming region can significantly alter the properties of the first stars proposing the existence of an object called Dark Star (DS), whose main heating source is DM annihilation.

During the collapse of the protostellar cloud the DM is pulled alongside the baryonic matter and is thus accumulated also. Figure 2.6 shows the density profile of the DM before and after the collapse of the molecular cloud in the halo according to Freese et al. (2009) for the case that just a single protostar forms. The initial DM density profile according to Navarro et al. (1996) is shown, as well as the adiabatic contracted profile for hydrogen densities of 10^{13} and $10^{16} \, \text{cm}^3$, which is obtained in rough (factor two) agreement by two different methods. The gravitational torque of the baryonic matter leads to higher DM densities up to $10^{14} \, \text{GeV/cm}^3$ in the central region of the DM halo.

Increasing the DM density magnifies the number of annihilation processes taking place. The products of the DM annihilation (which are SM particles) thermalize with the core of the protostar and may contribute significantly to the energy produced by the star. Just about $\sim 1/3$ (for Neutralino DM) of the annihilation energy goes into neutrinos and leaves the star (recent simulations have suggested that the energy loss to neutrinos is more likely 10%, Scott et al. 2009). The luminosity of the DM L_{DM} is roughly given by

$$L_{\text{DM}} \sim \frac{2}{3} \int Q_{\text{ann}} \, \text{d}V, \tag{2.12}$$

where $\text{d}V$ is the volume element. This heating due to WIMP annihilation counteracts the cooling processes possibly halting the collapse of the protostellar cloud.

The temperature of the resulting object is very low, so it might be possible that accretion continues[3] much longer than in normal Pop III stars. Thus, according to Spolyar et al. (2009)

---

[3]Because of the small effective temperatures no ionizing radiation is emitted.
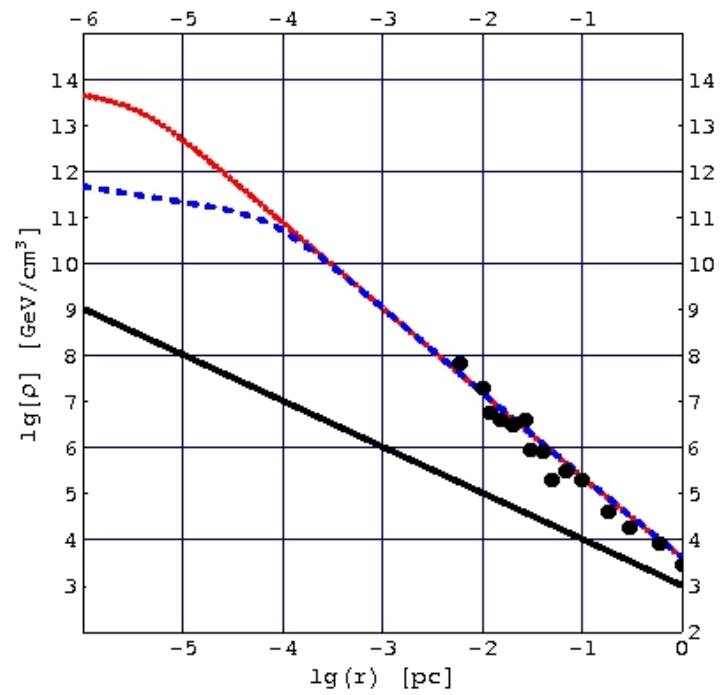
Figure 2.6: The initial DM density profile (solid black line) and the adiabatic contracted DM profile for a hydrogen density of 10^{13} (blue dashed line) and 10^{16}cm^3 (red dotted line) is shown. The black dots are calculated with an numerical method. For details see Freese et al. (2009)

.

the resulting DS are very heavy (500 - 1000 $M_\odot$), puffy (radius $\approx 1-10\,\mathrm{AU}$), cool ($T_\mathrm{eff} <$ 10 000 K) and bright ($10^6 - 10^7\,L_\odot$).

If the DM used up by DM heating is not replaced in some way from outside the star, the DS will run out of DM. The DM heating will be irrelevant and the star may contract and will continue its evolution along the ZAMS towards the main sequence. Thus such a DS exists only temporarily and its lifetime critically depends on the amount of DM available for burning.

It is not clear whether the DM heating is definitely able to halt the collapse (Ripamonti et al. 2008), otherwise the gas will collapse into a normal Pop III protostar. Dark matter particles can scatter of the nuclei in the protostar, loose energy and cam then be captured by the gravitational potential well of the star. The WIMPs thermalize with the star, which leads to a very high and very central DM density. Again, annihilation takes place and if the scattering cross-section is high enough, the energy produced by annihilation is high enough to effectively alter the evolution of the star and prolong its lifetime (Iocco 2008). Such a DS can in principle have an infinitive lifetime. It is only limited by the existence of a sufficient DM reservoir in the environment. Such DS have the same properties as normal Pop III stars when it comes to mass, but instead of being powered by hydrogen burning they are powered by WIMP annihilation. The WIMP annihilation leads to an expansion of the star, thus the density within the star is low and the radius is large (Freese et al. 2008b, also see Section 4).

Whether either kind of DS forms at all significantly depends on the DM parameters, the WIMP mass m_χ, the different scattering and annihilation cross-sections, and also very significantly on the ambient WIMP density ρ_χ. It has been investigated that DS may exist for a broad range of realistic parameters, especially for DM masses between 1 GeV and 10 TeV (Spolyar et al. 2009). One of the goals of this work is to find out how strong the DM influence is on stars whose DM source comes from scattering if parameters favored by the above mentioned direct detection experiments are considered.

The existence of such DS would have a significant impact on the Universe. They might change the way re-ionization took place (Furlanetto and Loeb 2003, Bromm et al. 2001), be important as precursors of black holes, or end their lives in a pair-instability supernova phase (Heger et al. 2003).

2.4 Stellar Evolution of Dark Stars: The 'DarkStar' Code

'DarkStars' (Scott et al. 2009, Scott et al. 2010) is a stellar evolution code that calculates the structure of Dark Stars during their lifetime depending on the different mechanisms of energy production within a star. It includes all the normal energy sources of a star and additionally includes WIMP annihilation and a full implementation of WIMP conductive energy transport. 'DarkStars' is based on the normal stellar evolution code EZ by Paxton (2004), which itself was derived from the STARS code developed by Eggleton (1971) (also see Eggleton 1972, Pols et al. 1995). In the following chapters, a general introduction into the calculation of the evolution of DS influenced by burning of captured DM will be given following Scott et al. (2009).

2.4.1 Stellar Structure

The conditions inside a star can be described by a set of four differential first order equations, which describe the stars mass distribution, pressure, luminosity and temperature in depen-

dence on the radial distance (or alternatively in terms of the mass inside a radius r) from the center of the star. They are based on simple assumptions such as hydrostatic equilibrium and spherical symmetry.

A stable star is in hydrodynamic equilibrium, which means that the gas pressure pointing outwards must balance the gravitational force on each volume element pointing inwards. Thus, the pressure is determined by the following equation given in terms of the integrated mass m inside a radius r

$$\frac{\mathrm{d}P(m)}{\mathrm{d}m} = -\frac{\mathrm{G}m}{4\pi r(m)^4}. \tag{2.13}$$

P represents the pressure, m the mass, G is the gravitational constant and r the radial distance from the center of the star (including a certain mass). The mass must be distributed homogeneously within the star, thus the second equation holds:

$$\frac{\mathrm{d}r}{\mathrm{d}m} = \frac{1}{4\pi r^2 \rho(r)}, \tag{2.14}$$

here $\rho(r)$ denotes the density at radius r in the star. The luminosity increases going outwards and can be described in terms of the different ways of energy production in the star

$$\frac{\mathrm{d}L}{\mathrm{d}m} = \epsilon_{\mathrm{nuc}} + \epsilon_{\mathrm{grav}} - \epsilon_{\nu} + \epsilon_{\mathrm{WIMP}}. \tag{2.15}$$

In this equation, L is the luminosity, ϵ_{nuc} the rate of energy produced in nuclear fusion processes and ϵ_{grav} the gravitational energy rate meaning the rate at which gravitational energy is converted into heat. The gravitational energy rate is high during the collapse of the protostellar cloud, or when the star contracts. ϵ_{ν} is the amount of energy produced in nuclear reactions, which leaves the star in the form of neutrinos. Finally, ϵ_{WIMP} is given by the energy production rate from WIMPs ϵ_{ann}, which itself consists of the energy rate produced by WIMP annihilation and the conductive energy transport rate $\epsilon_{\mathrm{trans}}$ ($\epsilon_{\mathrm{WIMP}} = \epsilon_{\mathrm{ann}} + \epsilon_{\mathrm{trans}}$). All of the energy rates are given per unit nuclear mass. The last equation links pressure and temperature, but is no more than a definition of the ∇ operator

$$\frac{\mathrm{d}\ln T}{\mathrm{d}m} = \nabla \frac{\mathrm{d}\ln P}{\mathrm{d}m}. \tag{2.16}$$

∇ represents the temperature gradient and will be replaced by specific expressions depending on the specific case considered for example by a radiative or a convective temperature gradient.

In 'DarkStars' the structure equations are solved using the method of relaxation. For the solution, another four grid equations are introduced, the grid is adaptive and has 199 mesh points.

2.4.2   WIMP Capture and Annihilation

The speed u at which the WIMPs in the halo move follows a velocity distribution $f(u)$. When the WIMPs cross the star they are eventually scattered by the nuclei in the star. The rate at which the WIMPs are scattered is determined by the velocity distribution of the WIMPs, the local escape velocity $v(r,t)$, the velocity a WIMP obtains by the time it reaches the radius r in the star $w(u,r,t) := \sqrt{u^2 + v(r,t)^2}$ (it is being influenced by the gravitational field) and the partial capture rate $\Omega_v^-(w)$. Following Gould (1987) the capture rate is given by

$$C(t) = 4\pi \int_0^{R_\star} r^2 \int_0^\infty \frac{f(u)}{u}\, w\, \Omega_v^-(w)\, \mathrm{d}u\, \mathrm{d}r. \tag{2.17}$$

The partial capture rate $\Omega_v^-(w)$ depends on the form factor of the different nuclei ('DarkStars' assumes a delta function for hydrogen and an exponential suppressed form factor for scattering on nuclei heavier than hydrogen), the local number density in the star, the total cross-section for the scattering of WIMPs on the different nuclei types (includes spin-dependent and spin-independent scattering), the masses of the nuclei and WIMP as well as some other quantities. It must also be taken into account that a WIMP of mass m_χ can only be scattered to velocities less than v, when the energy Δ lost in the collision obeys the following relationship:

$$\frac{u^2}{w^2} \leq \Delta \leq \frac{\mu}{\mu_+^2} \tag{2.18}$$

with $\mu \equiv \frac{m_\chi}{m_{\text{nuc}}}$ and $\mu_\pm \equiv \frac{\mu \pm 1}{2}$. The WIMP capture is based on generalized capture routines of DarkSUSY (Gondolo et al. 2003). Scattering is considered for the 22 most important nuclei, among these of course ^{1}H, ^{3}He and ^{4}He. The code also calculates and gives out the abundances of the seven most important elements.

Once the WIMPs are captured they can transport energy through the star. This theory of conductive energy transport makes it possible to evaluate whether WIMPs scattered to velocities higher than the local escape velocity and thus evaporate. In the best case all the energy taken from a hotter region of the star is returned to a cooler region, so that no energy leaves the star. This is naturally the case in local thermal equilibrium (LTE), where the density of the gas is so high that collisions dominate the energy transport, but not if the energy is transported globally. The Knudsen number is a good indicator for the type of the energy transport. It is defined as follows

$$K(t) = \frac{l(0,t)}{r_\chi(t)}. \tag{2.19}$$

$l(0,t)$ is the mean free path of the WIMP at the center of the star, while r_χ is the radius of a sphere of a uniform central density $\rho_c(t)$, which may be assumed to exist because WIMPs cluster so strongly in the star. Thus r_χ describes the sphere in which all the WIMPs reside. So if the mean free path is larger than r_χ the WIMPs typically travel out of this sphere before they deposit their energy (K>1).

In LTE the conductive energy transport can be calculated analytically (Gould and Raffelt 1990). For K > 1, this approximation breaks down, and there is no analytical way of determining the amount of conductive energy transport. Gould and Raffelt (1990) thus solved the Boltzmann equations by performing explicit Monte Carlo simulations. A detailed description how ϵ_{trans} can be calculated is given in Scott et al. (2009). In the cases considered here, evaporation can usually be neglected, because $E(t)$ is proportional to n_χ, while the annihilation rate is proportional to n_χ^2, thus for high capture rates and ambient densities, evaporation can be neglected, unless the WIMP mass is very close to the mass of the nuclei considered.

Furthermore, the WIMPs self annihilate at the following rate per unit volume

$$a(r,t) = \frac{1}{2} \langle \sigma_a v \rangle n_\chi(r,t)^2. \tag{2.20}$$

Thus, it is given by the product of the non-relativistic limit of the thermally averaged and velocity weighted annihilation cross-section $\langle \sigma_a v \rangle$ and the local number density of WIMPs $n_\chi(r,t)$ in the star squared. The total number of WIMPs annihilating in the star at a time t

can be calculated by integrating the annihilation rate per unit volume over the total volume of the star

$$A(t) = 4\pi \int_0^{R_\star} r^2 \, a(r,t) \, \mathrm{d}r. \tag{2.21}$$

The number density of WIMPs n_χ in the star can be calculated assuming that the WIMPs have thermalized with the stellar matter. This can happen either locally (LTE), so that the WIMP energies reflect the local temperature at every stellar radius, or the WIMPs can be isothermally distributed, which means that they reflect only a single overall temperature T_W. In the second case a Boltzmann distribution for particles in a potential well gives the local WIMP density. Calculating the number density in LTE, which means that the WIMPs travel less distances, is more complicated and has been done by Gould and Raffelt (1990a).

In order to calculate the WIMP number density distribution within the star, in both cases the total number of WIMPs must be known. In the case of scattered WIMPs the change of total number of WIMPs in time is given by the rate at which WIMPs are captured $C(t)$ and the rate at which they disappear again due to self-annihilation ($2A(t)$, because two WIMPs annihilate always) as well as the rate at which they evaporate $E(t)$

$$\frac{\mathrm{d}N(t)}{\mathrm{d}t} = C(t) - 2A(t) - E(t). \tag{2.22}$$

Finally, the energy per unit mass of nuclear matter produced by WIMP annihilation is given by

$$\epsilon_\mathrm{ann}(r,t) = \frac{2 \, a(r,t) \, m_\chi c^2}{\rho_\star(r,t)} - \nu_\mathrm{loss}(r,t). \tag{2.23}$$

Here, $a(r,t)$ is the local annihilation rate per unit volume, m_χ the WIMP mass, c the speed of light, $\rho_\star(r,t)$ the local density in the star, $\nu_\mathrm{loss}(r,t)$ is the fraction of energy produced in WIMP annihilation, which leaves the star in the form of neutrinos.

2.4.3   Equilibrium

The number of WIMPs in the star $N(t)$ is determined by a competition between annihilation and capture, if evaporation is neglected. If the capture rate is equivalent or smaller than the annihilation rate, capture and annihilation will balance each other

$$\frac{\mathrm{d}N}{\mathrm{d}t} = 0 \rightarrow C = 2A. \tag{2.24}$$

Thus, Equation 2.22 can be rewritten for equilibrium between capture and annihilation, where the capture rate C does not depend on the number of WIMPs within the star, and using the N-independent annihilation coefficient $A_c = 2A/N^2$

$$\frac{\mathrm{d}N}{\mathrm{d}t} = C - A_c N^2 \tag{2.25}$$

This differential equation is solved by

$$N(t) = \sqrt{C/A_c} \, \tanh\left(\frac{t}{\tau}\right), \tag{2.26}$$

where $\tau = 1/\sqrt{CA_c}$ is the equilibration timescale.This timescale is very short compared to the lifetime of the star (a few tenth or hundred years, Freese et al. 2008a). Therefore, the annihilation rate is given by

$$A(t) = \frac{1}{2}C \tanh^2\left(\frac{t}{\tau}\right) \tag{2.27}$$

Thus, the capture rate determines the annihilation rate in equilibrium. The capture rate in Equation 2.17 can be estimated by

$$C \approx 4.9 \times 10^{34} \left(\frac{M_\star}{M_\odot}\right)^{0.55} \left(\frac{\overline{v}}{10\text{km/s}}\right)^{-1} \left(\frac{\rho_\chi}{10^9\text{GeV/cm}^3}\right) \left(\frac{m_\chi}{100\text{GeV}}\right)^{-1} \left(\frac{\sigma_{\text{SD}}}{10^{-39}\text{cm}^2}\right) \tag{2.28}$$

only considering spin-dependent scattering and properties of Pop III stars (Freese et al. 2008a). $M_\star$ is the stellar mass, $\overline{v}$ the WIMP velocity dispersion, m_χ the WIMP mass and ρ_χ the ambient WIMP density. This formula will not be used in the following calculations of the stellar structure, but the important relationship

$$C \sim \frac{\rho_\chi}{m_\chi} \tag{2.29}$$

becomes very clear.

The dark matter luminosity is given by

$$L_{\text{DM}} = f \times A \times 2m_\chi, \tag{2.30}$$

where f is the fraction of energy produced by WIMP annihilation which goes into the stellar luminosity and does not leave the star (e.g. in the form of neutrinos). In equilibrium between capture and annihilation $C = 2A$, the DM luminosity is determined consequently by the capture rate. The important relationship

$$L_{\text{DM}} = f \times C \times m_\chi \sim \rho_\chi \tag{2.31}$$

follows. The energy loss rate from WIMPs annihilating into neutrinos has been set to 10 %, after evaluating explicit Monte Carlo simulations including various detection channels (Scott et al. 2009). Thus, the fraction f in Equation 2.31 is given by 0.9. This fraction is quite uncertain because the nature of WIMPs is still unknown. Often it is estimated that the fraction of energy going into neutrinos is 30% (Spolyar et al. 2008).

2.5 Radiative Transfer in Stellar Atmospheres

Stellar atmospheres emit a characteristic spectrum of light depending on their effective temperature, density and the element abundances. This spectrum can be calculated using the theory of radiative transport. Radiative transport is based on the idea that the energy is produced within the core of the star and then transported outwards through the atmosphere from where it is emitted. No energy is produced within the atmosphere, but its composition and the transportation mechanisms highly influence the resulting spectrum. In the following chapters, the basics of radiative transport are reviewed following the lectures of Hauschildt (2011) and Baron (2011).
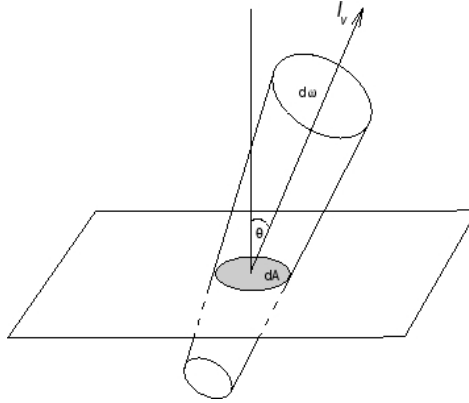
Figure 2.7: Illustration of the definition of the specific intensity I_ν (Hauschildt 2011).

2.5.1   Fundamental Quantities

The specific intensity I_ν is the characteristic quantity describing radiative transport. It is defined as the energy E passing through the surface element $\mathrm{d}A$ in the direction defined by $\cos(\theta)$ into the solid angle element $\mathrm{d}\omega$ per unit time $\mathrm{d}t$ and frequency interval $\mathrm{d}\nu$ (Figure 2.7). The specific intensity is a macroscopic quantity, which is essentially determined by efficiency of emission, absorption and scattering of photons while a ray of light passes through the stellar atmosphere.

$$\mathrm{d}E_\nu = I_\nu \, \cos(\theta) \, \mathrm{d}A \, \mathrm{d}\omega \, \mathrm{d}t \, \mathrm{d}\nu \tag{2.32}$$

Another important quantity is the mean intensity J_ν, which is the specific intensity averaged over all directions.

$$J_\nu = \frac{1}{4\pi} \oint_{4\pi} I_\nu \, \mathrm{d}\omega = \frac{1}{2} \int_{-1}^{+1} I_\nu \, \mathrm{d}\mu, \ \mu = \cos(\theta) \tag{2.33}$$

In thermodynamic equilibrium both quantities (I_ν and J_ν) are the same and determined by a single temperature. The radiation field is then given by a blackbody spectrum B_ν

$$J_\nu = I_\nu = B_\nu = \frac{2h\nu^3}{c^2} \frac{1}{\exp(h\nu/kT) - 1}. \tag{2.34}$$

The amount of scattering, absorption and emission of that the photons undergo in a specific ray is expressed in the theory of radiative transfer by introducing corresponding coefficients. The scattering, absorption and emission coefficients (σ_ν, κ_ν, ϵ_ν) depend on density, temperature and composition of the gas through which the photons pass and thus on the exact location in the star. For spherical symmetry it is assumed that the location in the star is determined by the radius r. Even though in the theory of radiative transport the optical depth is used instead of the radial coordinate r, because the optical depth describes the transparency of the atmosphere and thus is the more physical quantity. In general, the optical depth along a beam is defined as the geometrical thickness $\mathrm{d}s$ times the extinction coefficient χ_ν (includes absorption and scattering coefficients)

$$\mathrm{d}\tau_\nu(s) = \chi_\nu \, \mathrm{d}s. \tag{2.35}$$

Hydrostatic Equilibrium
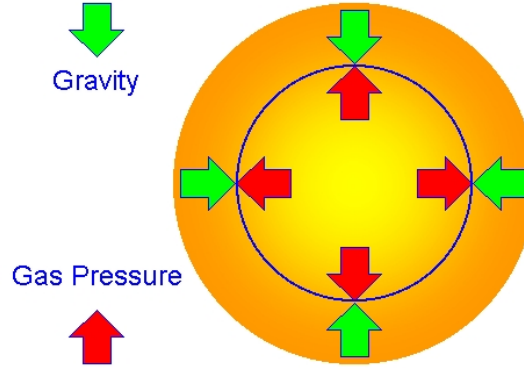
Figure 2.8: Illustration of the forces acting on a volume element of gas in a star (Image credit: Ohio State University 2006).

Since it is more reasonable that the optical thickness is zero outside the star and highest at the core, another definition of the coordinate system is used. The optical depth is defined along the z axis from the outside of the star to the inside of the star (for plane parallel geometry), so that the relationship between ds and dz is given by $\cos(\theta) = \frac{-dz}{ds}$, where θ is the angle between ds and dz. The following definition of the optical depth is used

$$d\tau_\nu = -\chi_\nu \, dz = \cos(\theta) \, d\tau_\nu(s). \tag{2.36}$$

2.5.2   Atmosphere Structure

The basic structure of the atmosphere is determined by the pressure and temperature gradient. Both can be derived from basic physical principals. A stable star can only exist in hydrostatic equilibrium, thus the pressure structure of the star is determined by the following differential equation, which describes the equilibrium state between gravitational force, gas pressure and radiation pressure.

$$\frac{dP_{\text{gas}}}{d\tau_\nu} = \frac{g(r)\rho}{\chi_\nu} - \frac{dP_{\text{rad}}}{d\tau_\nu} \tag{2.37}$$

$$\frac{dP_{\text{rad}}}{d\tau_\nu} = \frac{\pi}{c\chi_\nu} \int_0^\infty F_\nu \, d\nu \tag{2.38}$$

Here P_{gas} represents the gas pressure, P_{rad} the radiation pressure, τ_ν the optical depth as defined in Equation 2.36, χ_ν the extinction coefficient, $g(r)$ the gravitational acceleration at radius r, ρ the local density, c the speed of light and F_ν the specific net flux as defined in Equation 2.39. Figure 2.8 illustrates how the forces acting on a volume element of gas must cancel each other to reach a stable state. For consistency the gradient of the gas pressure is given in the dependence on optical depth, because the equation for radiation transport will also depend on the optical depth. The first term in Equation 2.37 reassembles the gravitational force downwards and the second term the radiation pressure outwards. Together they equal

the gas pressure. In principle Equation 2.37 can be solved, assuming that the gradient of the radiation pressure is known. However, it depends on the total radiation flux F_λ and χ_ν, which also depends on the temperature and pressure.

Furthermore, energy conservation must be guaranteed, while the energy is transported through the stellar atmosphere. Therefore, the specific net flux through the surface element dA (specific intensity integrated over all directions) integrated over all wavelengths must be equal for all optical depth (for plane parallel symmetry). The net flux F_ν is defined as follows

$$F_\nu = \oint_{4\pi} I_\nu \vec{n} \, d\omega = 2\pi \int_{-1}^{1} \mu I_\nu \, d\mu. \tag{2.39}$$

Here $\vec{n}$ defines the direction and $d\omega$ is again the solid angle element in which the light is emitted. The total and conserved radiation flux is consequently given by

$$F_{\mathrm{rad}} = \int_0^\infty F_\lambda d\lambda \equiv \sigma T_{\mathrm{eff}}^4 = \mathrm{const} \Longleftrightarrow \frac{dF_{\mathrm{rad}}}{d\tau} = 0. \tag{2.40}$$

Thus, it is determined by the temperature of a blackbody T_{eff}. An equivalent statement is that the gradient of the total radiation flux must be zero. In the case of a spherical symmetry, the flux F_ν is proportional to r^{-2}.

By solving this differential equation a temperature structure $T(\tau)$ can be derived. Nevertheless, again in order to calculate the temperature the specific flux is needed but not known. Section 2.6.4 shows how this problem can be solved by numerical iteration.

2.5.3   Radiative Transfer Equation (RTE)

The equation of radiative transfer describes how the specific intensity a ray of light changes when the ray passes through the atmosphere. Here, the specific intensity is equivalent to the number of photons in a ray of light of a certain frequency. The change in intensity is the same as a change of the number of photons in the ray by adding (emission) or removing (absorption, scattering) photons from a ray. This can be described macroscopically by a change in the intensity and mathematically by the following differential equation (radiative transfer equation RTE)

$$\frac{1}{c}\frac{\partial I_\nu}{\partial t} + \vec{n} \, \nabla I_\nu = \epsilon_\nu - \chi_\nu I_\nu = \chi_\nu(S_\nu - I_\nu). \tag{2.41}$$

This is a general equation for all geometries. The Nabla operator ∇ must be chosen for the geometry used. The equation states that the change of the intensity with time and direction is given by an emission coefficient ϵ_ν, which determines how many photons are added to the beam and an extinction factor consisting of the extinction coefficient χ_ν and the intensity itself. This is obvious because the number of photons that can be absorbed or scattered depends on the number of incoming photons. The extinction coefficient itself includes scattering and absorption coefficients. The inverse of the extinction coefficient is the mean free path. Here, only time-independent radiative transfer problems are considered, so that $\frac{\partial I_\nu}{\partial t} = 0$.

Equation 2.41 is usually rewritten in terms of the source function, which is defined as the ratio of the emission coefficient and the extinction coefficient ($S_\nu = \epsilon_\nu/\chi_\nu$) and shows the relative importance of emission to extinction. For simplicity plane parallel geometry is used
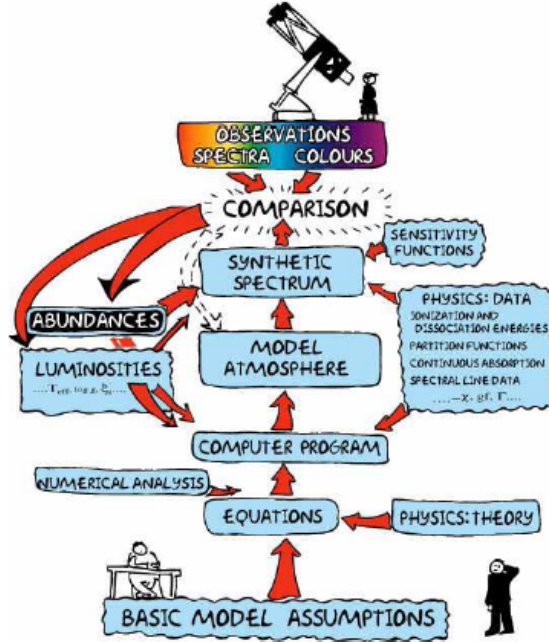
Figure 2.9: Interaction between theory and observation using a stellar atmospheric code (Hauschildt 2011).

here. The general ideas are the same as in every other geometry. The RTE in plane parallel geometry is given by

$$\mu \frac{\mathrm{d}I_\nu}{\mathrm{d}z} = \chi_\nu(S_\nu - I_\nu) \Longleftrightarrow \mu \frac{\mathrm{d}I_\nu}{\mathrm{d}\tau_\nu} = I_\nu - S_\nu. \tag{2.42}$$

2.6 The PHOENIX Code

PHOENIX is a general purpose model atmosphere code package, which is able to calculate the emission spectra of stars, planetary atmospheres, supernovae et cetera. It has been written by Hauschildt and Baron (1999) and is still under development. PHOENIX calculates the light originating from the photosphere. Figure 2.9 shows how theory and observation interact using a stellar atmospheric code. Using basic model assumptions like hydrostatic equilibrium, energy conservation and spherical symmetry, the main equations are implemented into the code and solved using numerical methods. This way the emission from a model atmosphere is calculated and the spectrum can be compared to observational spectra.

The comparison may give information about the abundances of certain elements or other quantities, which can be again used to improve the PHOENIX model atmosphere. PHOENIX consists of two main parts. The first set of differential equations determines the pressure structure of the star (and the atmosphere) starting from a given temperature and density structure. This is needed to calculate the opacities of lines, the continuum and molecules. The second part solves the radiative transfer equations and produces a model spectrum. PHOENIX uses a spheric symmetric and relativistic version of the RTE (Hauschildt 2011). Here, the plane parallel RTE is used to explain the way PHOENIX works. Even though, the RTE is more

complicated in the spheric and relativistic case the basic ideas are the same. The following sections explain how PHOENIX solves the RTE and are based on the lectures of Hauschildt (2011) and Baron (2011). Also, see Hauschildt and Baron (1999) for more information on the basic PHOENIX code and Hauschildt and Baron (2010) for information on the currently developed three dimensional radiative transfer framework PHOENIX/3D.

2.6.1   Solving the RTE

PHOENIX main goal is to self consistently solve the RTE. It is not very difficult to find a formal solution to the plane parallel RTE:

$$I_\nu(\tau, \mu) = I_\nu(\tau_1, \mu) \exp(-\frac{\tau_1 - \tau}{\mu}) + \frac{1}{\mu} \int_\tau^{\tau_1} S_\nu(t) \exp(-\frac{t - \tau}{\mu}) \mathrm{dt} \tag{2.43}$$

It gives the specific intensity depending on the optical depth and the direction in which the ray passes. The intensity is calculated by starting from a known value at a given optical depth τ_1 ($I_\nu = J_\nu = B_\nu$ can be used as the inner boundary condition, while $I_\nu = 0$ is the outer boundary condition.). From this starting value $I(\tau_1, \mu)$ the intensity of the next optical depth step can be calculated using Equation 2.43. This can be continued for every height (or equivalently optical depth) in the star. Nevertheless, this result is not well-defined, because the source function is unknown. So the goal of PHOENIX is to determine the source function and solve the RTE.

In local thermal equilibrium (LTE), the following relations hold $I_\nu = B_\nu$(2.34), so that $\frac{\mathrm{d}I_\nu}{\mathrm{d}z} = \frac{\mathrm{d}B_\nu}{\mathrm{d}z} = 0$ and $S_\nu = I_\nu = B_\nu$, so that $I_\nu = J_\nu = B_\nu = S_\nu$ holds in LTE, where no scattering occurs.

In the case of scattering, the source function can be written in terms of J_ν and B_ν

$$S_\nu = (1 - \beta_\nu)J_\nu + \beta_\nu B_\nu, \tag{2.44}$$

where $\beta_\nu = \frac{\kappa_\nu}{\kappa_\nu + \sigma_\nu}$ is called the photon destruction probability, κ_ν is the absorption coefficient and σ_ν the scattering coefficient. Now the real problem is to find J_ν (the intensity averaged over all directions), because once J_ν is known, the source function is known, and a formal solution can be performed to get the specific intensity. Thus, it is convenient to rewrite the RTE in terms of J_ν (in order to keep the equations as clear as possible, from now on the index ν will be omitted, but it should be remembered that the quantities here are still specific quantities and thus dependent on ν). This can be done by plugging Equation 2.44 into the formal solution and integrating over all directions. Thus, the RTE can be rewritten as some operator Λ_τ (Λ_τ represents a matrix) acting on the source function

$$J(\tau) = \Lambda_\tau[S]. \tag{2.45}$$

Again the source function is initially unknown. The solution is to perform a so called Λ iteration, where the inner boundary condition $J^{(0)} = B^{(0)}$ is used as a starting point because for high optical depth this is always true. Then the following iteration scheme is used until J converges.

$$J^{(n)} = \Lambda_\tau[\beta B] + \Lambda_\tau[(1 - \beta)J^{(n-1)}] \tag{2.46}$$

Unfortunately this method does not work when scattering dominates ($\beta \ll 1$). The iteration converges far from the true solution (Hauschildt 2011).

Therefore, PHOENIX uses the operator splitting method, where this problem does not occur. Another operator $\Lambda^\star$ is introduced, which corresponds to a small correction to the Λ (again the index τ is omitted, but of course all the quantities still depend on τ) operator. This way, the Λ operator can be rewritten as

$$\Lambda = \Lambda^\star + (\Lambda - \Lambda^\star). \tag{2.47}$$

Again, an iteration scheme is used, but this time it has the form

$$J_{\text{new}} = \Lambda^\star S_{\text{new}} + (\Lambda - \Lambda^\star) S_{\text{old}}. \tag{2.48}$$

By plugging Equation 2.44 in Equation 2.48, it is possible to write down an expression for J_{new}, which does not directly depend on Λ anymore.

$$J_{\text{new}} = [1 - \Lambda^\star (1 - \beta)]^{-1} (\Lambda S_{\text{old}} - \Lambda^\star (1 - \beta) J_{\text{old}}) \tag{2.49}$$

This way the major difficulty is inverting a matrix. Making an adequate choice of the $\Lambda^\star$ matrix improves the convergence behavior and thus can reduce the required computational power significantly.

However, there is still a problem left. In order to solve the RTE, the extinction, absorption, emission and scattering coefficients must be known. This means the opacities must be calculated (or guessed in the very first step of the iteration) before it is possible to solve the RTE.

2.6.2   Calculating Opacities

The opacities can be calculated, when the general structure of the star is known. This means for each mesh point (corresponding to a τ) the abundances of the elements, pressure, temperature and densities are known. Using them as input parameters, PHOENIX can calculate the opacities either in local thermal equilibrium (LTE) or non-local thermal equilibrium (NLTE). In LTE the energy distribution between the atoms, and therefore the distribution of atoms in the different atomic and ionization states, is determined by inelastic collisions. The medium is so opaque that photons transporting energy are quickly absorbed. This way the energy stays within the local environment. There is no coupling between different areas of the star. If the star is less dense the medium may become less opaque and the photons can travel further, thus connecting different areas of the star with different temperatures. The number densities n_i^j, where i stands for the atomic state and j for the ionization state, can be calculated using the Maxwell-Boltzmann distribution and the Saha equation in LTE. In NLTE, statistical equilibrium is assumed and the Rate-equations must be solved. In order to calculate the number densities, some results of atomic and molecular physics must also be used, e.g. Einstein coefficients.

In general, solving the Rate-equations instead of applying LTE is always a good choice, because they should give the same results for LTE as solving the Maxwell-Boltzmann and Saha equations. Nevertheless, it is more time consuming, so it may be more convenient to use LTE. Lines, line broadening via different effects, the existence of molecules and dust can also be included in these calculations. In this way absorption, scattering and emission coefficients are calculated.

2.6.3   Line Broadening

Every emitted spectral line is naturally broadened, because when a photon is emitted the Heisenberg uncertainty relation (Equation 2.50) holds and the photons energy is within a certain interval, but not sharply defined

$$\Delta E \Delta t \geq \frac{\hbar}{2}. \tag{2.50}$$

ΔE and Δt are the energy interval and the time uncertainty of the photon, $\hbar$ the Planck's constant. Thus, the line seen in a spectrum has a defined broadened shape with a defined width. The natural line broadening is well described through the spectral line width Γ

$$\Gamma = \hbar \Delta \omega, \tag{2.51}$$

where $\Delta \omega$ is the frequency interval into which the photon is emitted. The atoms in a gas move due to their thermal energy. The energy seen by the observer depends on the direction and speed of the movement of the emitting photon relative to the observer. The frequency of the photon is Doppler shifted, which leads to a further broadening of the line. In PHOENIX, there are additional effects included for the broadening of the spectral lines: The Stark Effect and the Van der Waals line broadening effects.

Stark broadening   The existence of the charged components in the atoms results in an electric field, which is a superposition of the electric fields of every atom in the star. Thus, when one of the atoms emits light, the atom is influenced by the electric field originating from all other atoms. This leads to the Stark line broadening. Due to the external electric field the energy levels within the atom are shifted or even dissociated in a way depending on the degree of degeneracy of the atomic level.

If the electron is in ground state, which means the level is not degenerated, an electric dipole moment is induced, because the probability of the electron position relative to the proton changes. This results into a changed Hamiltonian. Because the electric fields are small, this change can be written as a small perturbation

$$\hat{V} = e|\vec{E}|\hat{z}. \tag{2.52}$$

$\hat{V}$ represents the perturbation operator of the potential energy, e the elementary charge, $|\vec{E}|$ the absolute value of the electric field and $\hat{z}$ the direction operator, when the electric field is defined along the $\hat{z}$ axis. In first order, the energy shift disappears, but in second order it is proportional to the electric field squared. This means that higher energy levels are mixed into the ground state.

If the atomic state is degenerated, different degenerated atomic states overlap and are mixed. This leads to a dissociation of the states and a shift in energy of some of them. This shift is proportional to the electric field. Thus, this effect is called the linear Stark effect. In a star both effects are important. The electric field of all the other atoms is averaged over time at the place of the electron. Thus, the energy which is emitted varies depending on the strength of the electric field at the time of the emission and a broadened profile occurs (Stark effect line broadening). The linear and quadratic Stark effect profiles can be approximated by a Lorentz profile.
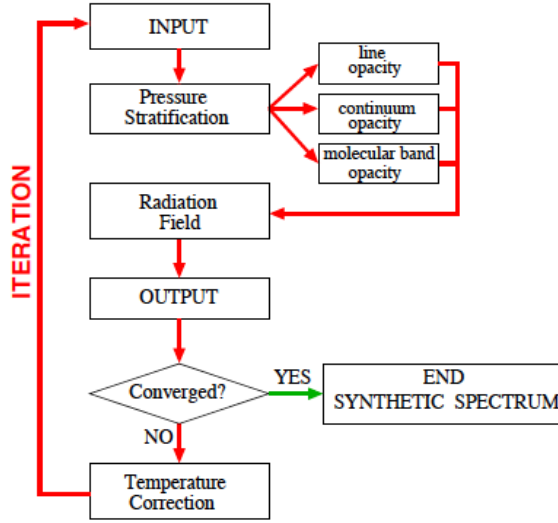
Figure 2.10: Iteration scheme used by PHOENIX (Hauschildt 2011).

Van der Waals broadening   The van der Waals line broadening is a result of the repulsive and attractive van der Waals forces between the molecules (or parts of the same molecule) in the gas. It is a force between two dipoles (either permanent or induced) and leads to a shift in the energies when a particle emitting a photon is perturbed by van der Waals forces. The energy shift is roughly given by the Lennard-Jones potential ($\Delta E \sim \frac{1}{r^6}$). Thus, this effect is usually more important in cool and very thick atmospheres. Again, a Lorentz profile may be used approximatively.

In general, the spectral lines are always influenced by all of these mechanisms and the resulting line profile is a superposition of these effects.

2.6.4   Input Parameters and Numerical Iteration

Combining everything discussed above it is possible to calculate detailed spectra of stellar atmospheres with PHOENIX. A star is well-defined by giving its abundances and three of the five parameters defining the star: the effective temperature T_{eff}, the stellar mass M, the stellar radius R, the gravitational acceleration at the surface $g(R)$ and the total luminosity of the star L. Nevertheless, only three of these quantities are needed, because they are connected by the following equation:

$$g = \frac{GM}{R^2} \tag{2.53}$$

$$L = 4\pi R^2 \sigma T_{\text{eff}}^4 \tag{2.54}$$

Here G denotes the gravitational constant and σ the Stefan-Boltzmann constant. Not every combination of these parameters is possible, because if mass, radius and the gravitational acceleration are chosen the luminosity and temperature can not be determined. Thus, arbitrary combinations of the five parameters are not possible. As mentioned before in order to solve the RTE, the opacities must be known. In order to calculate the opacities, the abundances,
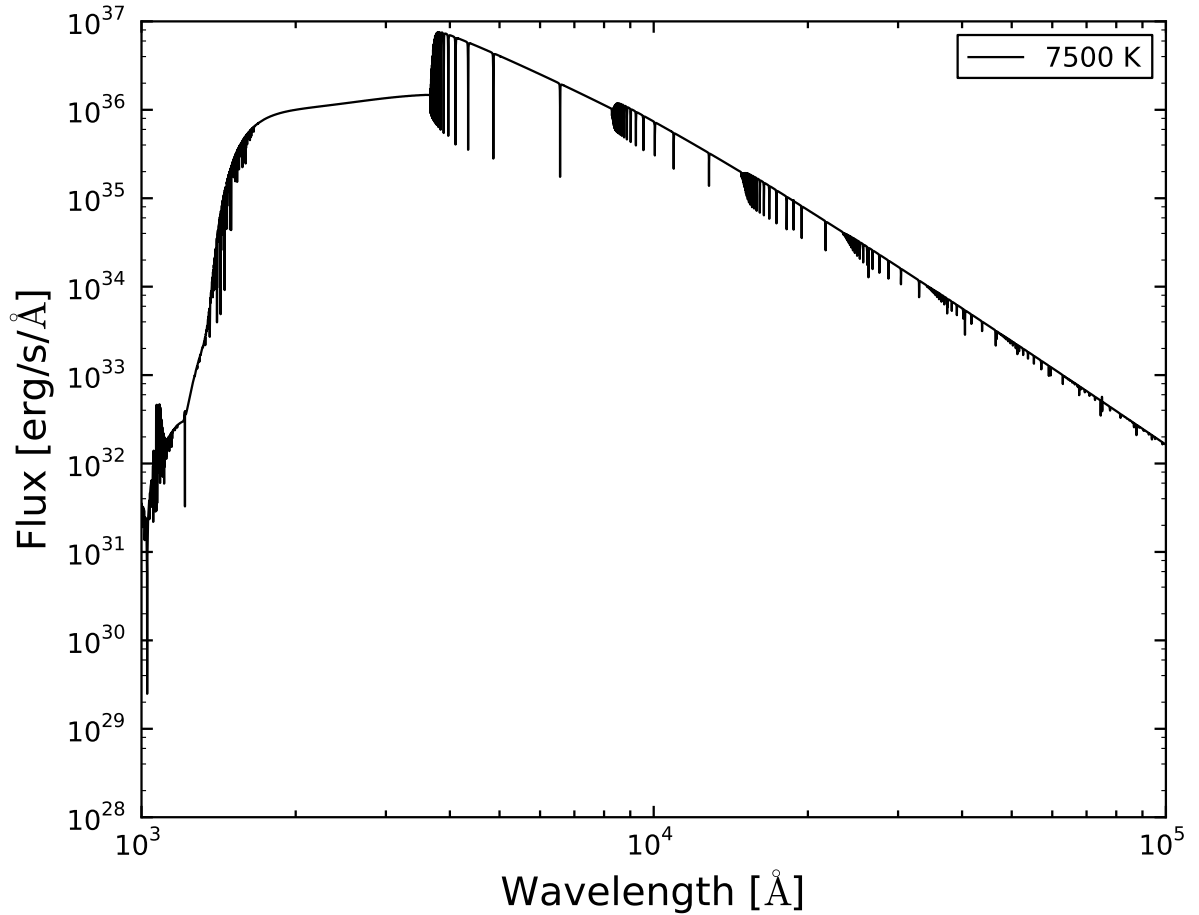
Figure 2.11: Example spectrum modeled by the PHOENIX atmospheric code.

the temperature, pressure and density structure must be given. Thus, PHOENIX uses an iteration scheme to find the right spectrum. This scheme is illustrated in Figure 2.10.

At first an initial density and temperature structure of the stellar atmosphere is guessed (often the structure of a similar star is used). Afterwards, the pressure structure is calculated, so that the opacities can be calculated in the next step. Now the RTE can be solved calculating a radiation field. The total radiation flux in each layer can be compared to the luminosity the star is supposed to have (energy conservation). In order to improve the atmosphere structure the temperature in each layer is corrected. Using the structure equations, the new pressure structure can be determined. These steps are repeated until the necessary temperature corrections become smaller than a preset limit of $1\,\mathrm{K}$ (only in LTE). Then, the atmosphere is converged. A example atmosphere is shown in Figure 2.11.

Chapter 3

Modelling of Dark Star Atmospheres

3.1 Motivation

3.1.1 Possible Detection Signatures

In order to detect and identify Dark Stars (DS), there must be ways to distinguish them from normal Pop III stars. The DS from Spolyar et al. (2009) have very low temperatures ($T_{\text{eff}} <$ 10 000 K) compared to normal Pop III stars, which easily have temperatures above 50000 K (McKee and Tan 2008). Here, stars with effective temperatures below 23000 K are considered, because above this temperature the existence of normal Pop III stars is more likely. Spectra of stars with lower effective temperatures peak at higher wavelength, thus their emission spectrum is redder. But there are some additional possibilities to identify DS: Molecular lines may be seen that are not seen in normal stars. A DS only consists of Hydrogen, Helium and Lithium. Lithium has its most important emission line at 6709 Å, which might be distinctive. Additionally, maybe other lines could help to identify a DS. This features will be explored in the next sections.

3.2 Parameter Studies

3.2.1 Dark Star Models: Input parameters

The spectrum emitted by a Dark Star mainly depends on the stellar properties mass, radius and effective temperature. In order to calculate the Dark Star atmospheres with PHOENIX these properties must be known. It was discussed in Section 2.3 that DS may form by adiabatic contraction of the baryonic gas and gravitational in-fall of the DM alongside the gas.

Spolyar et al. (2009) calculated the properties of DS formed by adiabatic contraction. Additionally, it is considered that the WIMPs may be scattered by the nucleons to lower energies and captured by the gravitational potential of the star. Their simulation starts with a $3M_{\odot}$ protostar ($M_{\odot}$ = solar mass), which accretes matter at a time-dependent rate adopted from Tan and McKee (2004). The protostar is approximately in hydrostatic and thermodynamic equilibrium. Thus, the DM heating balances the cooling mechanisms. The DS is build up in steps of $1M_{\odot}$. The structure is assumed to be polytropic and is calculated for every time step. The polytropes are between $n = 2/3$ for a fully convective star and $n = 3$ for a fully radiative star. Gravitation is included as an energy source, which becomes important when the star runs out of DM and contracts, as well as nuclear fusion, which also becomes

important when the star's DM supply runs out. Finally, repopulation of the star with DM due to capture is also considered.

The resulting stars are very heavy (500 - 1000 $M_\odot$), puffy (radius $= 1 - 10\,\mathrm{AU}$), cool ($T_\mathrm{eff} < 10\,000$ K) and bright ($10^6 - 10^7\,L_\odot$). Because the temperature of the star is so low, accretion continues longer than for normal Pop III stars (radiative feedback kicks in later) and the stars can grow to higher masses (according to McKee and Tan (2008) normal Pop III stars only grow up to around $140\,M_\odot$ and have temperatures $T >> 50000\,\mathrm{K}$). In the case of minimal capture (half of the luminosity is produced by fusion and half of DM burning) the final mass of these DS is about 1% larger.

The atmospheres for some of the DS calculated by Spolyar et al. (2009) are modeled in this work. The most interesting cases are given in table 3.1.

m_χ	$M\ [M_\odot]$	$\log(g)$	$T_\mathrm{eff}[K]$
1GeV	106	-0,6	5400
1GeV	690	1,0	7500
1GeV	756	1,9	10000
100GeV	716	2,9	23000

Table 3.1: Properties of the stars formed by adiabatic contraction from Spolyar et al. (2009). M is the mass of the star,the gravitational acceleration $\log(g)$ and T_eff the effective temperature.

It should be noted that the stars in the paper of Spolyar et al. (2009) have quite different properties for the different WIMP masses. Which means that the logarithm of the gravitational acceleration $\log(g)$ and the effective temperature T_eff are quite different for about the same stellar mass.

Because these stars formed from the gas clouds in the early Universe, where the gas has not been enriched by metals originating from the explosion of previous stars, an primordial composition of the gas within the star is assumed. Thus, the gas consists of hydrogen ($x_\mathrm{H} = 12.0$), helium ($x_\mathrm{He} = 10.93$), and a very small amount of lithium ($x_\mathrm{Li} = 1.05$). [1] For stars with low temperatures, molecules can play an important role in the spectrum, thus molecular hydrogen H_2, lithium hydride LiH and liquid lithium Li(L) are included.

3.2.2 Line Broadening Effects: Van der Waals vs. Stark

For the stars calculated in this work typically either van der Waals or Stark broadening should be dominating the profile. Correctly, both effects should be considered simultaneously, nevertheless, PHOENIX can only include one effect at a time. Thus, all of the profiles were calculated for both broadening mechanisms and compared so that the more important mechanism can be identified.

Figure 3.1 shows the 5400 K star spectrum for both effects. The Stark broadening lines are deeper (blue spectrum). For the 7500 K star in Figure 3.2 the effects of the different line profiles can best be seen just below 2000 Å. The spectral lines are much more pronounced for Stark broadening compared to the case when van der Waals broadening is included. So

---

[1]The abundances x_i of the different elements are given by $x_\mathrm{i} = \log(n_\mathrm{i}/n_\mathrm{H}) + 12$, where n_i is the number density of the element i and hydrogen H)
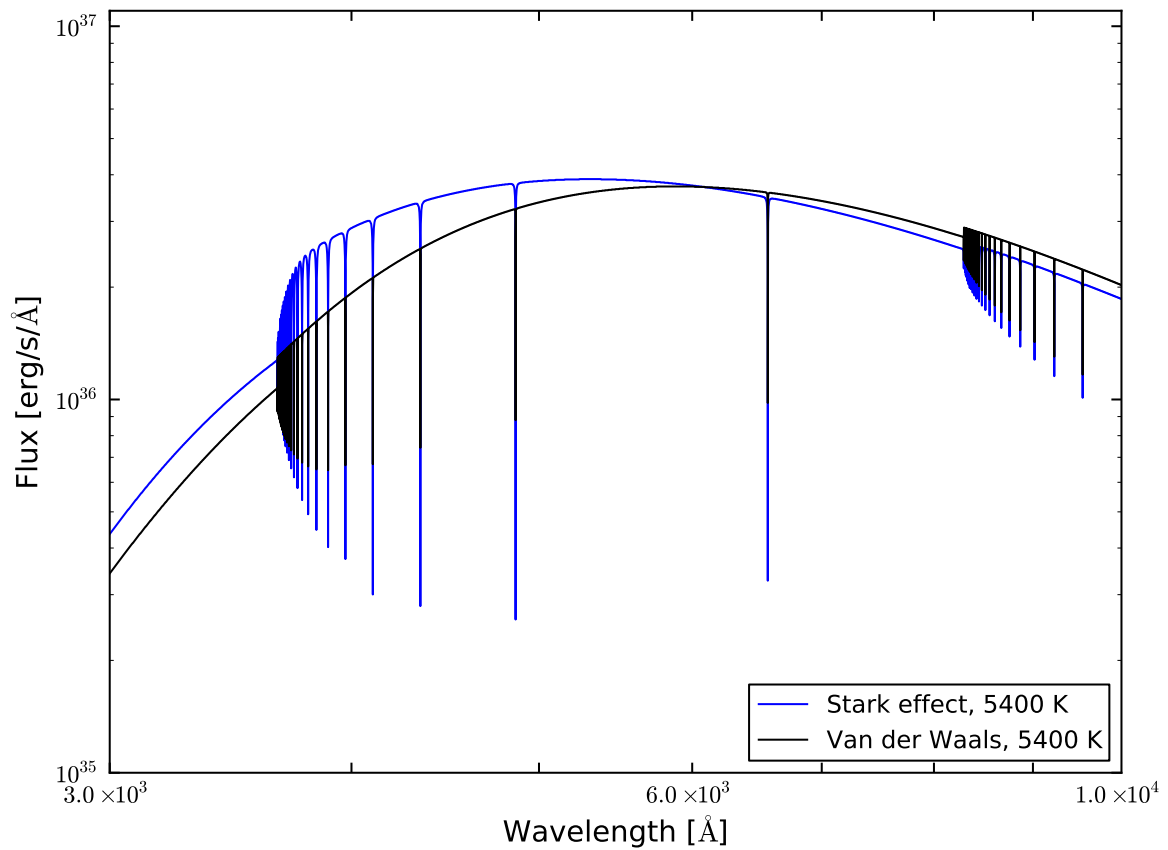
Figure 3.1: Spectrum of the 5400 K star with van der Waals (black line) and Stark broadening (blue line). The blue Stark broadened spectral lines are deeper than the black van der Waals broadend lines. Thus, the Stark effect is dominating.
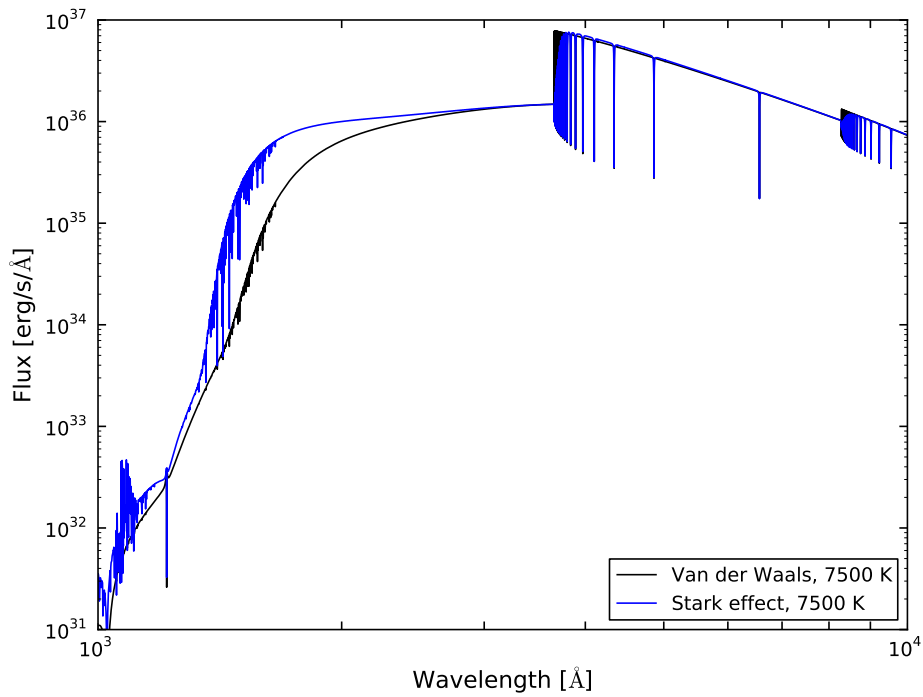
Figure 3.2: Spectrum of the 7500 K star with van der Waals and Stark broadening. The spectral lines below 2000 Å are deeper in the spectrum calculated with Stark broadening (blue line) than in the van der Waals broadened (black line) spectrum. Thus, the Stark effect is dominating.
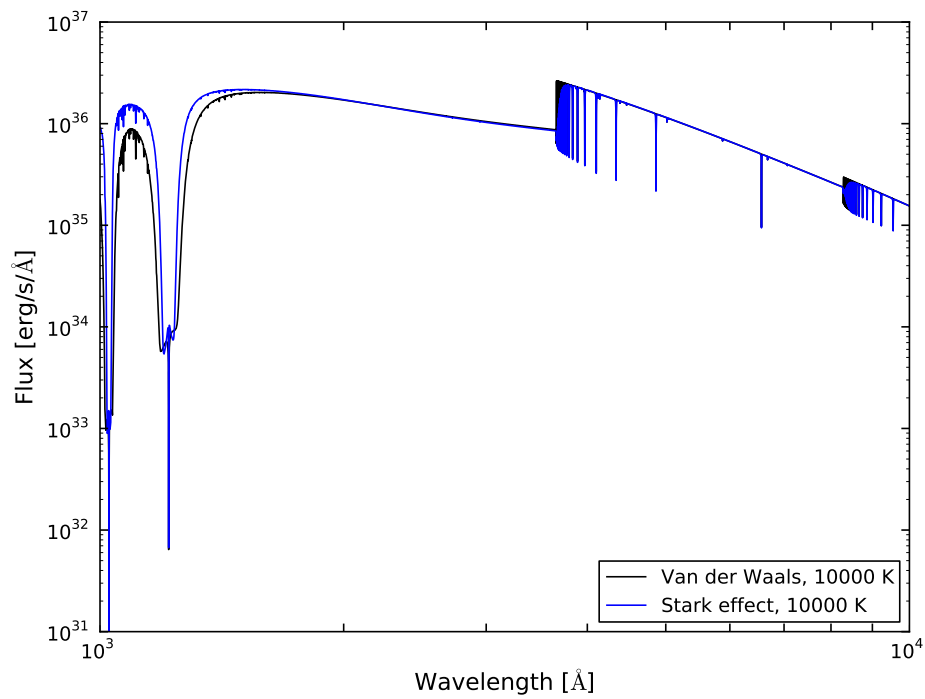
Figure 3.3: Spectrum of the 10000 K star with van der Waals and Stark broadening. The spectral lines in the black, van der Waals broadened spectrum and the blue, Stark broadened spectrum are approximately equally deep. Both effects are equally important.

for our temperatures the Stark effect seems to be dominant. Nevertheless, this cannot be generalized, because the importance of the two effects highly depends on the amount of the electron degeneracy, which depends on the local density and temperature. In Figure 3.3 a 10000 K star is shown for which both effects seem to be equally important (the spectral lines have approximately the same depth). Even though the H-α line (at about 6562 Å) is equally deep for both effects, it appears to be stronger broadened for the van der Waals effect than for the Stark effect. The lines just below H-α are a little more distinct as well (but not decisively). Consequently in order to determine the most important broadening mechanism the spectra for both effects should be calculated and compared. In the following chapters the spectra shown are usually calculated using Stark broadening (unless mentioned otherwise), because this is the dominating broadening effect for most of the stars considered here.

In Figure 3.1 also the continuum seems to change. The reason lies in the change of the flux in the lines causing a change of the flux in the continuum, because the overall flux must be conserved, and temperature, pressure and radius are adjusted. This effect can also be seen in Figure 3.2.

3.2.3   Local Thermal and Non-Local Thermal Equilibrium

PHOENIX can either calculate the population of the atomic states in local thermal equilibrium (LTE) or in non-local thermal equilibrium (NLTE). In local thermal equilibrium the occupation density of an atomic state is determined by collisions of the atoms, which is important when the material is thick and the radiation is reabsorbed locally and does not disperse the energy everywhere in the star.

Even though since DS might be very puffy, this might not be the case and the calculations must be done in NLTE. In LTE the population densities are calculated solving the Maxwell-Boltzmann equation and the Saha equations. In NLTE statistic equilibrium is assumed and the rate equations are solved. In PHOENIX the number of atomic levels which are included in the rate equations can be given. It is set to zero for LTE calculations and 999 for NLTE calculations. This number of atomic levels is sufficient because most of the atoms have significantly less than 999 levels.

Figure 3.4 shows the spectrum of the 10000 K star with van der Waals broadening calculated in LTE and NLTE. It is obvious that the NLTE line profiles are much deeper and the molecular lines below H_α are only seen in the NLTE spectrum (blue spectrum), probably because there is a threshold value for the width of a spectral line, which must be exceeded. This can also be seen for the other spectral lines between 3000 and 10000 Å. These spectral lines are deeper when the spectrum was calculated in NLTE (blue line) compared to the same spectrum in LTE (black line). This result holds also for all other spectra. In general, it is advisable to do the calculations in NLTE, because even if it is not necessary and the calculations could be done just as well in LTE, the NLTE spectrum should reproduce the LTE spectrum. Nevertheless, calculating an NLTE spectrum is more expensive on computing power. Calculating an LTE spectrum takes between 30 and 45 minutes, an NLTE spectrum more than four hours. All spectra that will be presented here are calculated in NLTE.

Nevertheless, before calculating every spectrum in NLTE with the different broadening mechanisms enabled, it was calculated in LTE (without the different broadening mechanisms, but including molecules). This was done in order to ensure that a spectrum really converged. In the LTE mode, PHOENIX considers the atmosphere as converged when the necessary change in temperature in each layer is smaller than a preset threshold value of 1 K. This is not
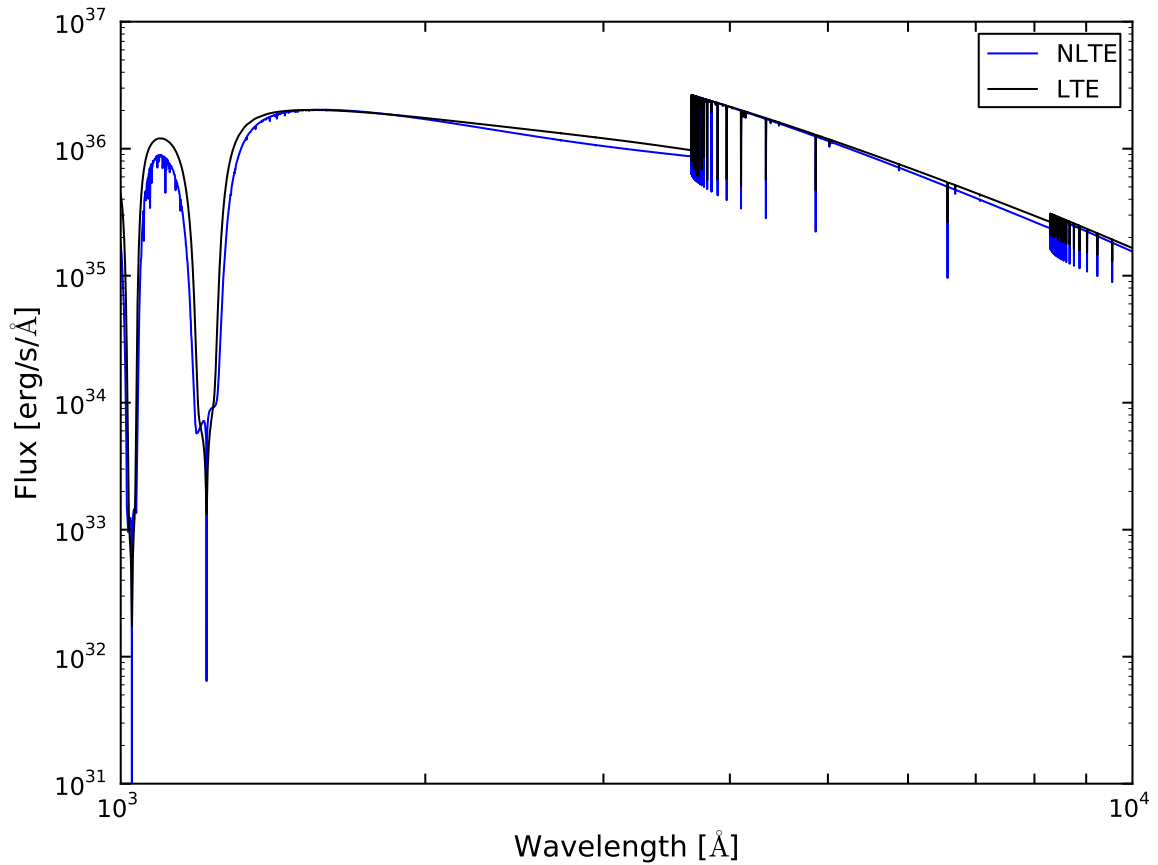
Figure 3.4: Spectrum of the 10000 K star calculated in LTE and NLTE. The spectral lines below 2000 Å can only be seen in the blue, NLTE spectrum and not in the black, LTE spectrum. The spectral lines between 3000 Å and 10000 Å are deeper in the spectrum calculated in NLTE than in the LTE spectrum.

done in NLTE, instead PHOENIX runs for a preset number of iterations. The only way to make sure that the model really converged is to check in the output file whether the temperature changes in the last few iterations are small and do not oscillate. Here, an atmosphere is considered to be converged when the LTE version converged and the temperature changes in NLTE were small for the last few iterations and did not oscillate.

3.3 Results

Molecular Lines

Figure 3.5 shows the spectra of all of the DS calculated via adiabatic contraction with temperatures between 5400 K and 23000 K. The Ly-α and Ly-β lines are labeled, as well as the Balmer and the Paschen series (see also 3.10) and several lines coming from molecular hydrogen right above and below Ly-α. These molecular lines can only be seen in stars with temperatures between roughly 7000 K and 10000 K. Below 7000 K (here in the 5400 K star) the temperature is not high enough in order to excite the molecular states. If the temperature gets too high, the molecules are dissociated the lines disappear (no molecular hydrogen exists in such stars).

In normal stars with just a small amount of metals, these molecular lines will not be seen because they would be dominated by lines from the metals which are located at the same wavelengths. Therefore, the existence of molecular hydrogen in a stellar spectrum is a good indicator for a low temperature Pop III star or DS. Since normal Pop III stars are usually expected to have higher temperatures, it is more likely to observe a low temperature DS.

Furthermore, it is obvious that some additional lines show up in the 23000 K spectrum. The origin of these lines will be explored in the next two sections.

Lithium Lines

In order to identify lines that might be emitted from the small amount of lithium (Li) atoms in a DS (Li exists in the first stars because they form from the primordial gas as described in Section 2.3), two different approaches were made. It was concentrated on the 23000 K star, because this star showed lines which are not obviously either atomic or molecular hydrogen (H) lines.

The first approach is to mark wavelengths at which Li lines are possible (Figure 3.6). Additionally, the DS atmosphere is recalculated with an extremely elevated Li abundance (the Li abundance is set to the H value) to make the possibly existing Li lines more prominent. In such a mega lithium star, all the Li lines that could possibly exist in a DS atmosphere should be intensified and easy to see. If there are additional Li lines in a DS, the wavelength where amplified lines occur in the mega lithium star are the wavelength at which to look for Li lines in a DS.

The most important Li line is located at 6709 Å, thus the 23000 K spectrum was recalculated with a higher resolution of 100 wavelength points per Å. The results are shown in Figure 3.6 and depicted in greater zoom in Figure 3.7. In both Figures, the spectrum of the normal 23000 K DS and the mega lithium DS are shown as well as the position where the line is expected (red) and the position of the Balmer-α line (blue). In Figure 3.6, an additional line appears at 6709 Å in the spectrum of the mega lithium star. In the corresponding DS spectrum the marker of the 6709 Å Li line is located right next to a line in the spectrum,
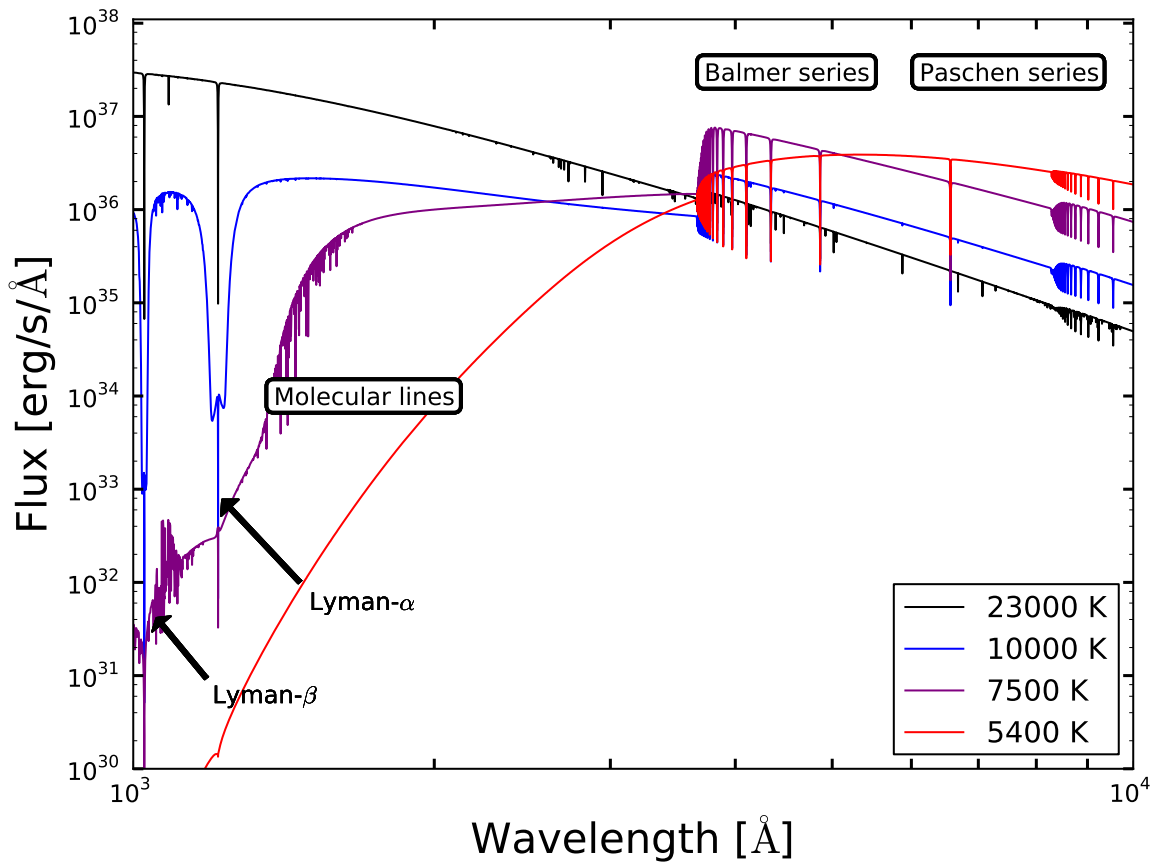
Figure 3.5: Spectrum of the 5400 K, 7600 K, 10000 K and 2300 K DS from adiabatic contraction. The different transition series (Balmer and Paschen), the molecular lines and the Ly-α and Ly-β lines are labeled.
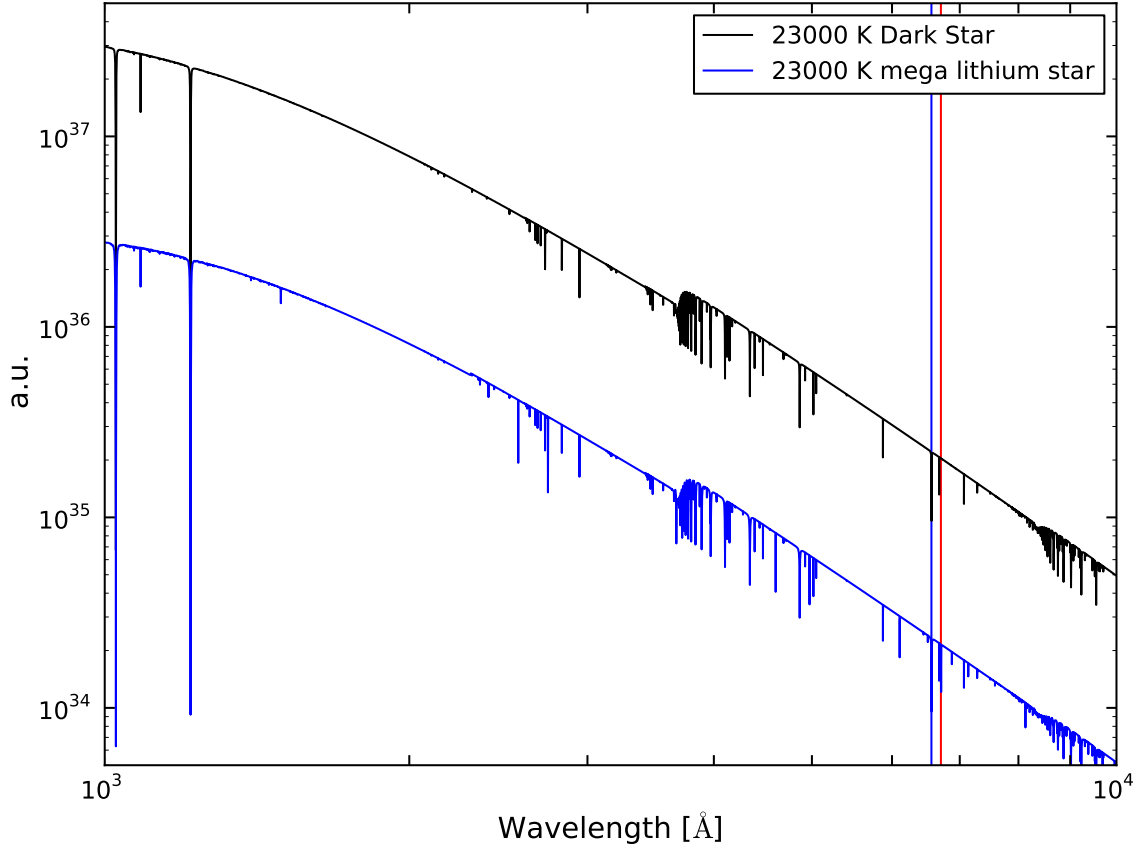
Figure 3.6: Spectra of the 23000 K DS and the 23000 K mega lithium star. The Balmer-α line and the most prominent Li line at 6709 Å are indicated by the blue and red vertical markers.

but their positions do not coincide exactly. This is confirmed by the close up view in Figure 3.7. Thus, the Li line is seen in the mega lithium star but not in the DS. Furthermore, in the mega lithium star, the 6709 Å Li line is small compared to Ly$-\alpha$ or Ly$-\beta$ and can probably not be resolved.

There are several other Li lines that could in principle show up in the spectrum. For the sake of completeness, Figure 3.8 shows the DS and the mega lithium spectrum together with markers at the positions of all possible lines of neutral (light blue) and one time ionized (light pink) Li. Some of the lines in the mega lithium star coincide with the positions of the pink and light blue markers, but none is equivalent to a line in the normal DS. Again, even the Li lines showing up in the mega lithium star are not strong enough for detection. Summing up, no Li lines useful for identifying DS are found.

3.3.1   Influences of Nebular Emission

Stars in the early Universe form from collapsing dense gas clouds, but not all of the material ends up in the star, so that the stars in the early Universe are often surrounded by dense clouds of gas (Rybicki and Lightman 1986). The gas in these clouds absorbs the light which
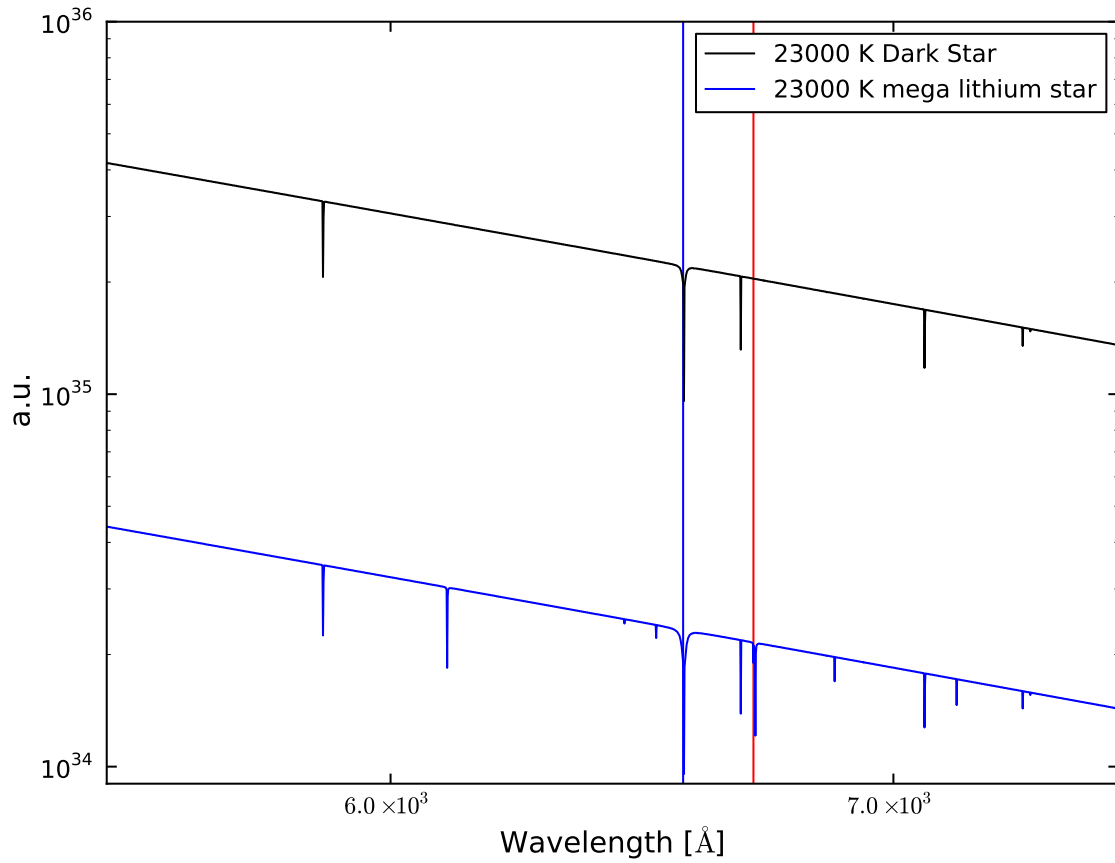
Figure 3.7: Zoom on the wavelength region around the possible Li lines in Figure 3.6. The spectra of the 23000 K star and the associated mega lithium star are shown. The Balmer-α line and the most prominent Li line at 6709 Å are indicated by the blue and red vertical lines. See text for a more detailed explanation.
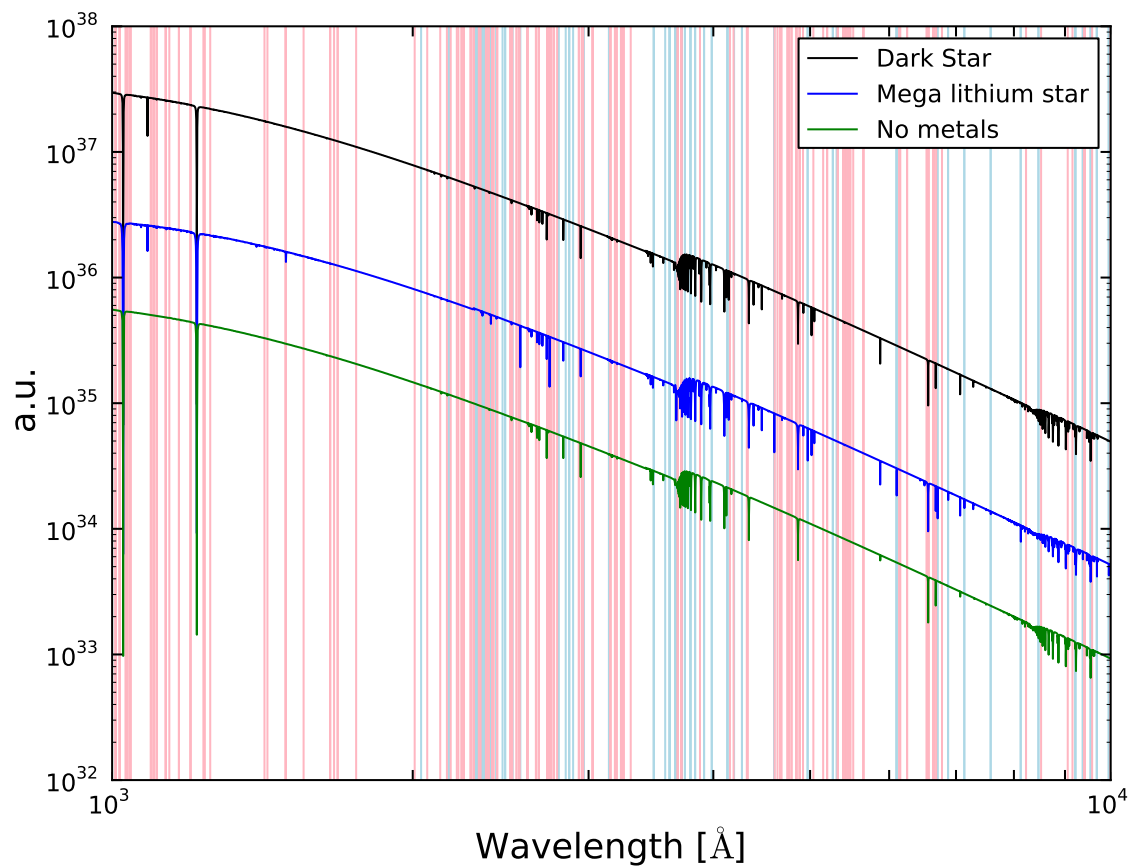
Figure 3.8: Spectra of the 23000 K DS and the associated mega lithium star, as well as a zero metallicity star. The light blue lines indicate the possible lines of neutral Li and the light pink lines of one time ionized Li.

Figure 3.9: Artist view of the molecular cloud surrounding a protostar in the early Universe (Image credit: NASA/WMAP Science Team 2007).

is emitted by the star and then re-emits it via different processes, shifting the energy of the photons to lower energies. This process can change the spectrum considerably. Thus, here the influence of the nebula emission is calculated following Fernandez and Komatsu (2006) and Dopita and Sutherland (2003) and references therein. The importance of the nebula emission is evaluated for DS.

The number of photons capable of ionizing the atoms in the cloud can be calculated directly from the PHOENIX spectrum. The specific total flux divided by the photon energy is integrated over all wavelength that are equivalent to photon energies above $13.6\,\mathrm{eV}$. The volume which characterizes this ionization is called the Stroemgren Sphere (Strömgren 1939). It is defined as the sphere with the radius at which the ionization rate equals the recombination rate. Thus, the volume of the sphere in which the gas is ionized can be calculated as follows. The ionization rate N_I per unit area at a radius R is given by

$$N_\mathrm{I} = \frac{Q_\mathrm{H}}{\frac{4}{3}\pi R^3}. \tag{3.1}$$

Q_H denotes the total number of ionizing photons. It is divided by the volume of the sphere of radius R.
The recombination rate is given by

$$N_\mathrm{R} = n_\mathrm{e}\, n_\mathrm{p}\, \alpha_\mathrm{B}. \tag{3.2}$$

Thus, it is determined by the number densities of electrons and protons $(n_\mathrm{e}, n_\mathrm{p})$ and the total recombination coefficient α_B, which includes recombinations to all levels. At the edge of the ionized region $N_\mathrm{I} = N_\mathrm{R}$ and the volume of the Stroemgren Sphere is given by

$$V_\mathrm{sphere} = \frac{Q_\mathrm{H}}{n_\mathrm{e}\, n_\mathrm{p}\, \alpha_\mathrm{B}}. \tag{3.3}$$

These electrons now interact in different ways with the atoms and produce photons again. But these photons are shifted to different energies compared to the original photons. Several processes play an important role and will be discussed in the following sections. The different radiative equations are calculated following Fernandez and Komatsu (2006) and Dopita and Sutherland (2003) and using references therein.

Stellar Contribution

The stellar spectrum is modeled by PHOENIX. The total specific luminosity emitted by the star is given by

$$L_\nu^\star = 4\pi R_\star^2 I_\nu. \tag{3.4}$$

Total absorption of photons with energies $h\nu > 13.6\,\mathrm{eV}$ is assumed. $R_\star$ is the radius of the star and I_ν represents the specific intensity defined in Equation 2.32.

Free-Free and Free-Bound emission

The electrons may be scattered due to the interactions with the protons or nuclei in the gas. During this process they are accelerated and therefore emit light. In a quantum mechanical description the electrons can be described as plane waves with an initial and a final energy. This process is called Free-Free emission.

Instead, the electron may be captured by atoms and emit light. The possible transition energies reach from the energy difference between the energy level and the ionization potential up to the highest energies the electron may have (Figure 3.10). The capture of a free electron will be preferred when its energy is only slightly above the ionization energy. The exact calculations can be done following Dopita and Sutherland (2003) by calculating overlap integrals of the wave functions of all possible initial and final energies (of course for the Free-Bound case the final energies are stepwise and the states are described by bound state wave functions). The correction to a classical calculation is given by the gaunt factor (Dopita and Sutherland 2003). The resulting total luminosity is given by

$$L_\nu^{\mathrm{cont}} = \frac{Q_{\mathrm{H}}}{n_{\mathrm{e}}\, n_{\mathrm{p}}\, \alpha_{\mathrm{B}}}\, \epsilon_\nu. \tag{3.5}$$

It is therefore given by the product of the Stroemgren Sphere and the emissivity per unit volume ϵ_ν. The volume emissivity is given by the following formula

$$\epsilon_\nu = 4\pi\, n_{\mathrm{e}}\, n_{\mathrm{p}}\, \gamma_{\mathrm{c}}\, \frac{\exp(-\mathrm{h}\nu/\mathrm{k}T_{\mathrm{g}})}{T_{\mathrm{g}}^{1/2}} \quad \mathrm{erg\, cm^{-3}\, s^{-1}\, Hz^{-1}}. \tag{3.6}$$

Again n_{e} and n_{p} are the number densities of electrons and protons, h is the Planck constant, ν the frequency, k the Boltzmann constant, γ_{c} is emission coefficient, T_{g} is the gas temperature in Kelvin, which can be assumed to be 20000 K (in approximation, see Fernandez and Komatsu 2006). α_B is the case B (the nebula is thick enough to prevent Lyman, except Lyman-α, series photons from escaping, while in case A the nebula is so thin that they can escape) recombination coefficient for hydrogen and is given by

$$\alpha_{\mathrm{B}} = \frac{2.06 \times 10^{-11}}{T_{\mathrm{g}}^{1/2}}\, \phi_2(T_{\mathrm{g}}) \quad \mathrm{cm^3\, s^{-1}} \tag{3.7}$$

The dimensionless function $\phi_2(T_{\mathrm{g}})$ is one for the gas temperature assumed here. It has been tabulated by (Spitzer 1978, Table 5.2). The emission coefficient γ_{c} comprises the difference between Free-Free and Free-Bound emission. It is given by

$$\gamma_{\mathrm{c}} := f_{\mathrm{k}}\, \overline{g}_{\mathrm{ff}} + f_{\mathrm{k}} \sum_{n=i}^{\infty} \frac{x_{\mathrm{n}}\, exp(x_{\mathrm{n}})}{n}\, g_{\mathrm{fb}}(n). \tag{3.8}$$
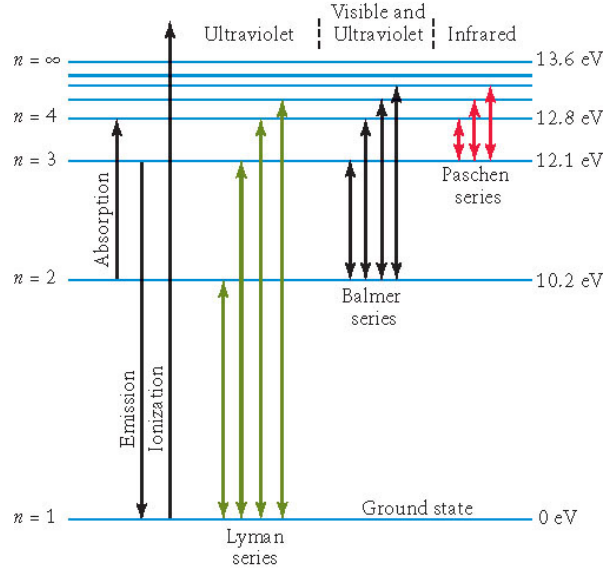
Figure 3.10: Schematic illustration of the hydrogen atomic levels and the possible transitions (University of Alberta 2012).

The first term is the contribution of the Free-Free emission. It consists of the constant $f_k = 5.44 \times 10^{-39}$ in CGS-units. It is no more than a collection of physical constants. $\overline{g}_{ff}$ is the Free-Free gaunt factor which resembles the difference between the quantum mechanical solution and the classical solution. It is thermally averaged and has approximately a value of 1.1 (Karzas and Latter 1961).

The second term describes the Free-Bound emission. Again, there is a gaunt factor for Free-Bound emission $g_{fb}(n)$, which now depends on n, which is the number of the atomic level to which the transition occurred. x_n is given by $x_n := E_{Ry}/(kT_g n^2)$ with $E_{Ry} = 13.6\,\text{eV}$. Most important is the understanding of the sum. This can be done with the help of Figure 3.10, assuming that a photon with a given energy is measured. The question is from which transition it originates. If it has an energy above 13.6 eV it can come from a transition to any of the atomic levels. The probabilities for all possible levels must be added up. This way you get a sum from the lowest possible level indicated by i and infinity (all higher levels). The sum starts from $i = 1$. For photons of lower energies, for example a photon with an energy below 13.6 eV but above 3.4 eV, it can come from any transition up to level two. The scheme repeats when gradually going to lower energies. Thus effectively, there is a step function with different values of the sum, depending on the energy of the photon. The lowest possible atomic level is $i = 2$ and not one, because all photons with energies above 13.6 eV are immediately reabsorbed and ionize another hydrogen atom. This way, effectively there is no probability, that a photon comes from an $i = 1$ transition and the first addend starts at $i = 2$. Approximatively, the gaunt factor g_{fb} can be assumed to be constant and is given by $g_{fb} \simeq 1.05$ for all n.

The continuum emission is the superposition of all previously discussed processes

$$
\begin{aligned}
L_\nu^{\text{cont}}(m) \simeq & 3.32 \times 10^{22} \, \text{erg s}^{-1} \, \text{Hz}^{-1} \left[\frac{Q_{\text{H}}}{10^{49}\text{s}^{-1}} \right] \\
& \times \left[\overline{g}_{\text{ff}} + \frac{E_{\text{Ry}}}{kT_{\text{g}}} \sum_{n=i}^{\infty} \frac{\exp(E_{\text{Ry}}/(kT_{\text{g}}n^2))}{n^3} g_{\text{fb}}(n) \right] \exp(-h\nu/kT_{\text{g}}),
\end{aligned}
\tag{3.9}
$$

where again i depends on the photon energy and starts at $i = 2$. The luminosity does not depend on the number density of electrons and protons, because when the density increases not only the ionization rate but also the recombination rate increases. Thus, these two effects cancel.

Line contribution

The electron which is captured by an atom, may cascade down to lower atomic levels emitting light with energies equal to the energetic difference between the two levels taking part. Thus, the emission has a defined energy, the light is emitted into a line. In principle, there are many of these lines, as can be seen in Figure 3.10. The Lyman series includes level transitions from any higher atomic level to level one, while the Balmer series includes transitions to level two. For simplicity, only the dominant Lyman-α photons are considered here. The luminosity is given as follows

$$
L_\nu^{\text{line}}(m) = f_{\text{ly}\alpha} \, h\nu_{\text{ly}\alpha} \, \phi(\nu - \nu_{\text{ly}\alpha}) \, Q_{\text{H}}.
\tag{3.10}
$$

$h\nu_{\text{ly}\alpha} = 10.2 \, \text{eV}$ and $\nu_{\text{ly}\alpha} = 2456$ THz. $f_{\text{ly}\alpha}$ is the fraction of ionizing photons that are converted to a Lyman-α photon in the end and then they emit light in the above explained fashion. Finally, all ionizing photons end up in a $n = 2 \rightarrow n = 1$ transition. Every electron that recombines to $n \geqslant 3$ emits a Lyman series photon when transferring to the ground state. This photon is absorbed again, exiting a neighboring atom which emits another photon when transferring to either the ground state or any other atomic state. Eventually, this is repeated until all electrons end up in the $n = 2$ state. Thus, they can go to the ground state either directly from $2p \rightarrow 1s$ emitting a line photon. Or they go indirectly via a two photon decay from $2s \rightarrow 1s$. The probability for the first process is about $2/3$ and $1/3$ for the second. Thus, $f_{\text{ly}\alpha}$ equals 0.64, because the exact value depends on the gas temperature (Spitzer 1978). The two photon decay is treated in the next section. ϕ is the line profile, which is for simplicity taken to be a delta function.

Two- photon emission

As mentioned in the previous section about $1/3$ of the time there is a transition from $2s \rightarrow 1s$ via a two-photon decay. Normally this process would be forbidden, because of the conservation of angular momentum (a photon carries spin one away). To conserve momentum two photons are needed for such a transition. First, one photon is emitted, when the electron transits to a virtual state, which is somewhere in between the 1s and the 2s state energetically. Simultaneously, another photon is emitted, so that the electron transits to the ground state. Since the virtual state has no fixed energy, the two photons are emitted into a continuum (they may have any energy from zero to 10.2 eV). The probability for such a two photon decay is the

product of the probabilities of the two transitions. Following the calculations of Dopita and Sutherland (2003) the luminosity is given by

$$L_\nu^{2\gamma}(m) \quad = \frac{2h\nu}{\nu_{\mathrm{ly}\alpha}} \left(1 - f_{\mathrm{ly}\alpha}\right) P\left(\frac{\nu}{\nu_{\mathrm{ly}\alpha}}\right) Q_{\mathrm{H}} \tag{3.11}$$

$$= 4.24 \times 10^{22} \ \mathrm{erg\,s^{-1}\,Hz^{-1}} \left[\frac{Q_{\mathrm{H}}}{10^{49}\mathrm{s^{-1}}}\right] \frac{\nu P(\nu - \nu_{ly\alpha})}{\nu_{\mathrm{ly}\alpha/2}}. \tag{3.12}$$

In this formula, $(1 - f_{\mathrm{ly}\alpha})$ gives the fraction of photons which are converted to two-photon emission photons. The function P gives the normalized probability to get a photon with a frequency in the range $\mathrm{d}\nu/\nu_{\mathrm{ly}\alpha}$. Fitting Table 4 of Brown and Mathews (1970), the following formula can be derived for this probability with $y = \nu/\nu_{\mathrm{ly}\alpha}$:

$$P(y) = 1.307 - 2.627\,(y - 0.5)^2 + 2.563\,(y - 0.5)^4 - 51.69\,(y - 0.5)^6 \tag{3.13}$$

The overall probability is normalized to one ($\int_0^1 P(y)\,\mathrm{d}y = 1$), but this fitting formula gives $\int_0^1 P(y)\,\mathrm{d}y = 1.0047$ (Fernandez and Komatsu 2006).

Resulting Spectrum

In Figure 3.11 all the important emission processes are shown for the 23000 K star. The spectrum seen by an observer is the sum of the nebula emission and the spectrum of the star for photons with energies below 13.6 eV (above 911 Å). The nebula emission is dominated by the stellar spectrum for higher energies, just for energies below 0.1 eV (above 124000 Å) the nebula emission becomes more important and dominates the spectrum. The Free-Free emission process is most important at this lower wavelength and the two-photon emission at higher wavelength. Nevertheless, for energies above 0.1 eV the spectrum is not significantly altered. Most important is that the peak is not shifted to lower energies. Thus, nebula emission does not play an important role for the detectable spectra of DS with temperatures below 23000 K. For hotter DS with temperatures of about 40000 K, the nebula emission becomes more important, but these stars are very similar to normal Pop III stars and thus not of interest here.

3.3.2   Detectability with the James Webb Space Telescope

In order to detect the light from DS at high redshifts, very powerful instruments are needed. The James Webb Space Telescope (JWST) was designed for the observation of the most distant objects, just as the first stars (Gardner 2006). It is supposed to shed light on the mechanisms important in the early star formation, the birth and evolution of galaxies and the epoch of re-ionization.

The near infrared camera (NIRCAM), which is planned to be part of the JWST is most suitable for searching for DS in the near infrared. Figure 3.12 shows the spectrum of the 5400 K DS (this star was chosen, because it has the highest flux of the considered stars at the wavelength where the field of operation of the NIRCAM is located) for different redshifts z.

The red-shifted spectra are calculated with the following formula from Peebles (1993)

$$S'_{\lambda'} = \frac{L_\lambda}{4\pi((a_0)r(z))^2(1+z)^3} \ \text{with } \lambda' = (1+z)\lambda. \tag{3.14}$$
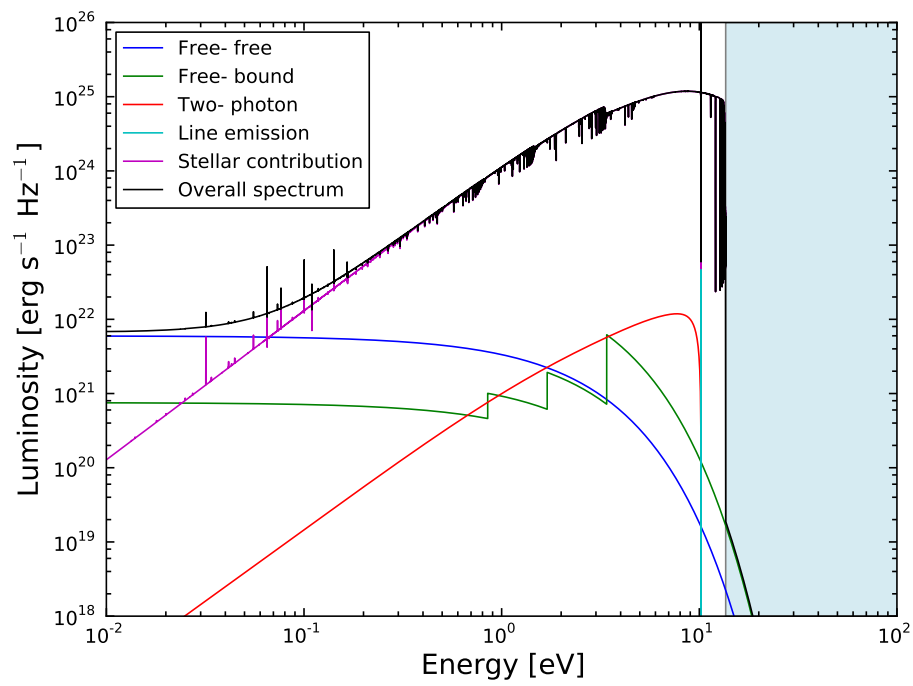
Figure 3.11: The nebula emission for the 23000 K star. The light blue area shows where the photons are energetic enough to ionize the gas. All important nebula emission processes are shown as well as the resulting overall emission.

Here, $L_\lambda = 4\pi R^2 I_\lambda$ represents the total specific flux emitted from the star with radius R and specific intensity I_λ at wavelength λ. As the light travels the Universe expands and the light is red shifted so that the wavelength arriving at the observer is λ'. The light from an object at distance $r(z)$ spreads over the area $4\pi a_0 r(z)$ (a_0 is the current scale factor) at the present epoch. $a_0 r(z)$ can be calculated using the formula for the angular size distance (Peebles 1993) for the case that the space curvature is negligible

$$H_0 a_0 r(z) = \int_0^z \frac{c}{E(z)} \mathrm{d}z. \tag{3.15}$$

E(z) denotes given by the cosmological equation for the expansion rate of the Universe (Peebles 1993)

$$\frac{\dot{a}}{a} = H_0 E(z) = (\Omega (1+z)^3 + \Omega_R (1+z)^2 + \Omega_\Lambda)^{\frac{1}{2}}. \tag{3.16}$$

Here, Ω is the matter energy density (baryons and dark matter), Ω_R is the spatial curvature density and Ω_Λ is the vacuum energy density as they are today. A flat geometry which means $\Omega_R = 0$, $\Omega = 0.3$ and $\Omega_\Lambda = 0.7$ is considered. The current Hubble constant is given by $H_0 = 70\,\mathrm{km\,s^{-1}Mpc^{-1}}$. Thus, $E(z)$ itself is a dimensionless function.

The sensitivities of the NIRCAM are also shown in Figure 3.12. On the website of the Space Telescope Science Institute (2012), they are given in nano Jansky (nJy) at the central frequency given in μm. Thus, they are given per unit frequency interval $= 10^{-32}\,\mathrm{erg\,s^{-1}\,cm^{-2}\,Hz^{-1}}$. In order to stay consistent with the previously used units the sensitivities were converted to $\mathrm{erg\,s^{-1}\,cm^{-2}\,cm^{-1}}$ and the central frequencies to wavelength in Å. The sensitivities are given for a $10\,\sigma$ detection and an observation time of 10000 seconds.

The plot also shows the sensitivities which have been rescaled for a longer observation time of 4 days (which was about the maximum observation time for the JWSTs predecessor Hubble) at a $10\,\sigma$ and a $5\,\sigma$ detection level. This can be done, considering that you need only 1/2 of the flux if your observation time is twice as long, or more generally

$$\Gamma_2 = \Gamma_1 \times \frac{1}{N} \ \text{ if } \ t_2 = Nt_1. \tag{3.17}$$

Here, Γ_1 is the flux (rate at which the particles are detected) measured when the observation time is t_1, and Γ_2 is the flux which would be measured if the observation time was t_2. The factor N scales between the observation times and thus also between the resulting fluxes. For a Poisson distribution (a Poisson distribution is assumed, because just very few photons are measured) the significance is defined as follows

$$S = \frac{N_S}{\sqrt{N_S}}. \tag{3.18}$$

Here $N_S = t\,\Gamma$ is the total number of detected particles, which is given by the rate of particles coming from the source Γ and the observation time t.

For a constant observation time the significance of the detection changes with the flux as follows

$$\frac{S_1}{S_2} = \sqrt{\frac{\Gamma_1}{\Gamma_2}}. \tag{3.19}$$

If just a 5σ detection is needed instead of an 10σ detection, only a quarter of the flux is needed. The 5400 K star on Figure 3.12 could principally be detected (the sensitivity markers
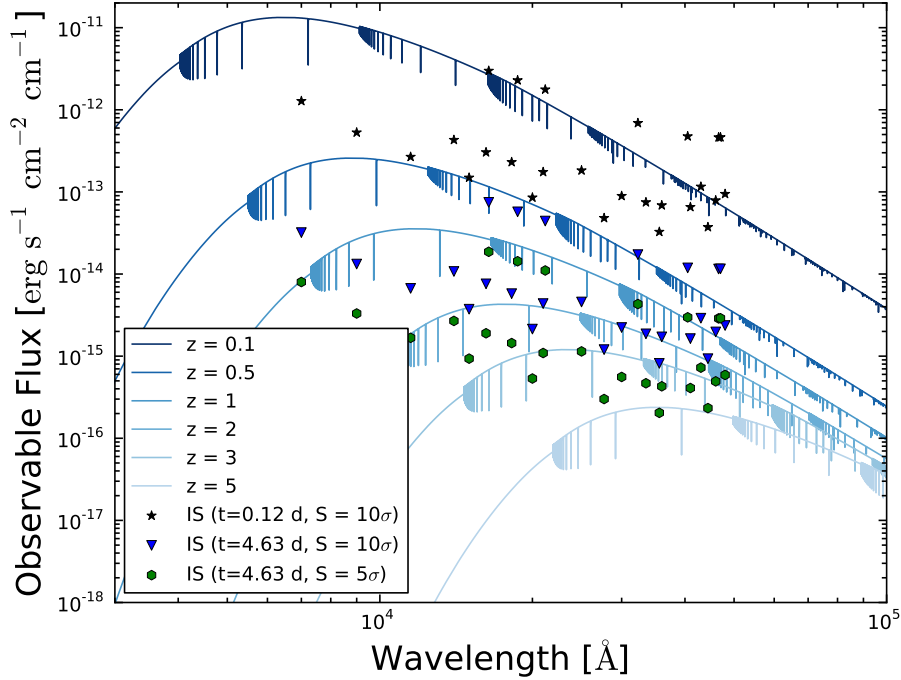
Figure 3.12: Rescaled NIRCAM sensitivities indicated by colored markers together with the spectrum of the 5400 K star at different redshifts.

are lower than the flux emitted by the DS) for redshifts up to $2 - 3$ with the NIRCAM at a significance level of 10σ (or 5σ) for an observation time of 4 days.

Thus, it is interesting to see how many stars are expected at the different redshifts in the field of view (FOV) of the NIRCAM. Since the FOV of the NIRCAM is not clear yet for this estimate the FOV of the Hubble Ultra Deep Field (11 square minute-of-arc region in the southern sky, Beckwith et al. 2006) and the Hubble Deep Field (covers area of the sky which is 2.5 arc minutes across, Ferguson et al. 2000) surveys are adopted. The number of objects is given as the product of the number density n and the proper volume element δV

$$\mathrm{d}N = n\,\delta V \ \text{ with } \ n = n_0 \left(\frac{a_0}{a}\right)^3 \tag{3.20}$$

This considers that the total number of objects is conserved and the initial number density is n_0. The proper volume element δV is given by the area at redshift z which is subtended by the field of the solid angle element $\delta\Omega$ within which the objects are counted $\delta A = (a_0 r(z))^2 \delta\Omega$ and the linear depth of the object sample between redshift z and $z + \mathrm{d}z$

$$\frac{\mathrm{d}l}{\mathrm{d}z} = \frac{H_0^{-1}}{(1+z)E(z)}, \tag{3.21}$$

because $\mathrm{d}l = \frac{\mathrm{d}a}{\dot{a}}$. This gives the volume element

$$\delta V = \frac{H_0^{-1}\delta z}{(1+z)E(z)}\frac{((a_0 r(z))^2 \delta\Omega)}{(1+z)^2} \tag{3.22}$$

48
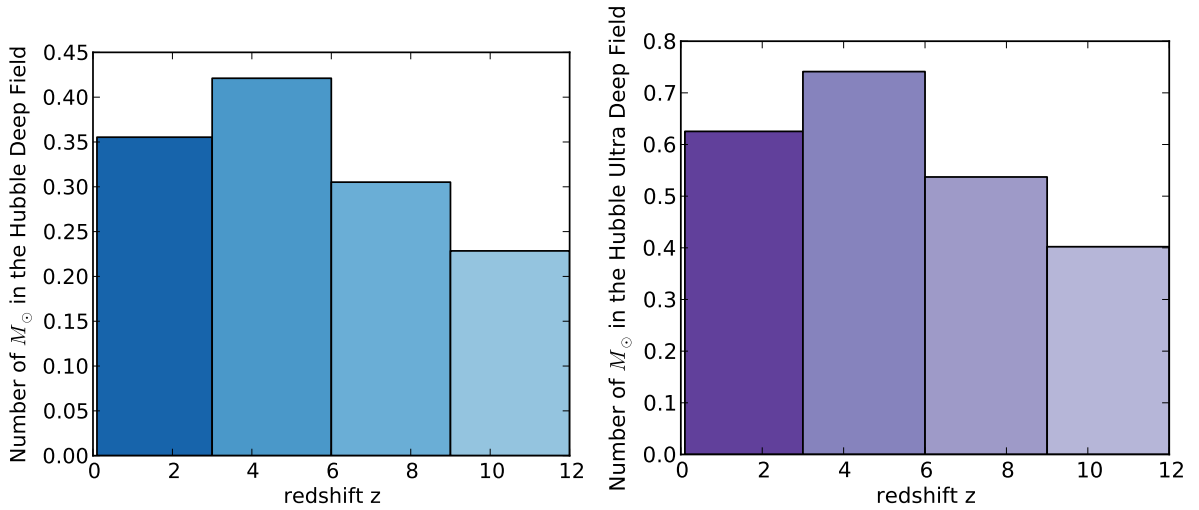
Figure 3.13: Number of stars expected in the Hubble Deep Field (covers area of the sky which is 2.5 arc minutes across, Ferguson et al. 2000) in the left-hand panel and the Hubble Ultra Deep Field (11 square minute-of-arc region in the southern sky, Beckwith et al. 2006) in the right-hand panel for different redshift intervals Δz.

and thus the predicted number of objects per steradian and unit redshift

$$\frac{\mathrm{d}N}{\mathrm{d}z} = n_0 \, H_0^{-3} \, F_n(z) \ \ \text{with} \ \ F_n(z) = \frac{[H_0 \, a_0 \, r(z)]^2}{E(z)}. \tag{3.23}$$

This number must be multiplied by the solid angle element covered by the FOV

$$\Omega = 2\pi(1 - \cos(\theta)). \tag{3.24}$$

Since Equation 3.23 is differential in time, the number of stars expected can only be calculated in redshift intervals. The results of these calculations are shown in Figure 3.13. Roughly 0.6 stars are expected in the Hubble Ultra Deep Field and 0.35 in the Hubble Deep Field if an initial number density of $n_0 = 10^{-5} M_\odot \, \mathrm{Mpc}^{-3}$ stars following Trenti and Stiavelli (2009) is considered. The expected number of stars scales with the initial number of stars and the number of stars decreases with the stellar mass, because the number of expected $M_\odot$ is shown in Figure 3.13. It is not considered that stars have a limited lifetime.

In conclusion, even for very optimistic values for the size of the FOV (Hubble Deep Field), the observation time (4 days) and the initial number density of stars ($n_0 = 10^{-5} M_\odot \, \mathrm{Mpc}^{-3}$) the number of stars with a mass of $1 \, M_\odot$ expected is ~ 0.6. For higher mass stars even considerably less stars are expected, for example 0.06 stars with $100 \, M_\odot$. Additionally, even when no background is assumed, the stars can probably only be detected with a significance of $10 \, \sigma$ ($5 \, \sigma$) up to redshifts of two (three).

A similar study by Zackrisson et al. (2010) focused on DS in the early Universe (z > 6). They come to the conclusion that the massive DS by Spolyar et al. (2009) are too faint to be detected by the JWST, but could possibly be detected if gravitational lensing by foreground galaxy clusters could be utilized. The spectra used by Zackrisson et al. (2010) were calculated by the stellar atmospheric codes MARCS (T < 8000 K) and TLUSTY (T > 10000 K). It was

not possible to calculate stellar spectra of stars between those two temperatures. A comparison of the spectra of Zackrisson et al. (2010) with spectra calculated by PHOENIX shows good agreement of the principal shape of the spectrum, nevertheless Zackrisson et al. (2010) did not use a real primordial abundances so that the spectral line features of DS could not be seen in their spectra. Nevertheless, PHOENIX is also capable of calculating spectra between 8000 and 10000 K.

Chapter 4

Evolution of Dark Stars in the Early Universe

4.1 Motivation

In the last section, it was shown that a detection of large DS, predicted by Spolyar et al. (2009), forming via adiabatic contraction, is very unlikely. The capture of WIMPs by the gravitational potential of a star after they have been scattered by the atomic nuclei is another process able to supply early stars with DM. It has been suggested that the burning of such WIMPs might prolong the lifetimes of DS even to the present-day (Iocco 2008). Nevertheless, Sivertsson and Gondolo (2011) found that the lifetimes of the previously discussed massive DS are not significantly prolonged because a rapid depletion of WIMPs from the dark matter halo traveling on orbits crossing the star takes place.

Furthermore, Stacy et al. (2011) employ numerical simulations in order to follow the density evolution of the DM corresponding to the collapse of a gas cloud. Stacy et al. (2011) found that the overall DM density does not increase compared to the initial density profile. In fact it even decreases by a small amount. Additionally, a few gravitational sinks, which are the predecessors of the first stars, form. These sinks are a lot less massive ($\approx 1\,M_\odot - 40\,M_\odot$) than the previously considered DS.

Recent results from direct detection experiments (DAMA/LIBRA, CRESST, XENON100) indicate a low mass ($10 - 50\,\mathrm{GeV}$) WIMP. The results of these experiments are combined with the results on DM halos and star formation in the early Universe discussed above to investigate the formation and evolution of DS under such conditions.

4.2 Parameter Studies

4.2.1 WIMP Scenarios

The properties of the DM itself highly influence the capture and annihilation rates within the DS. Thus, reasonable values for the mass of the DM particle, the spin-dependent and spin-independent, as well as the annihilation cross-section must be used. The resulting WIMP luminosity, path in the H-R diagram, and all other properties of a DS are influenced by them. Here, the recent results of the direct detection experiments DAMA/LIBRA (Bernabei et al. 2008), CRESST (Angloher et al. 2011), and XENON (Angle et al. 2008, Aprile et al. 2011)
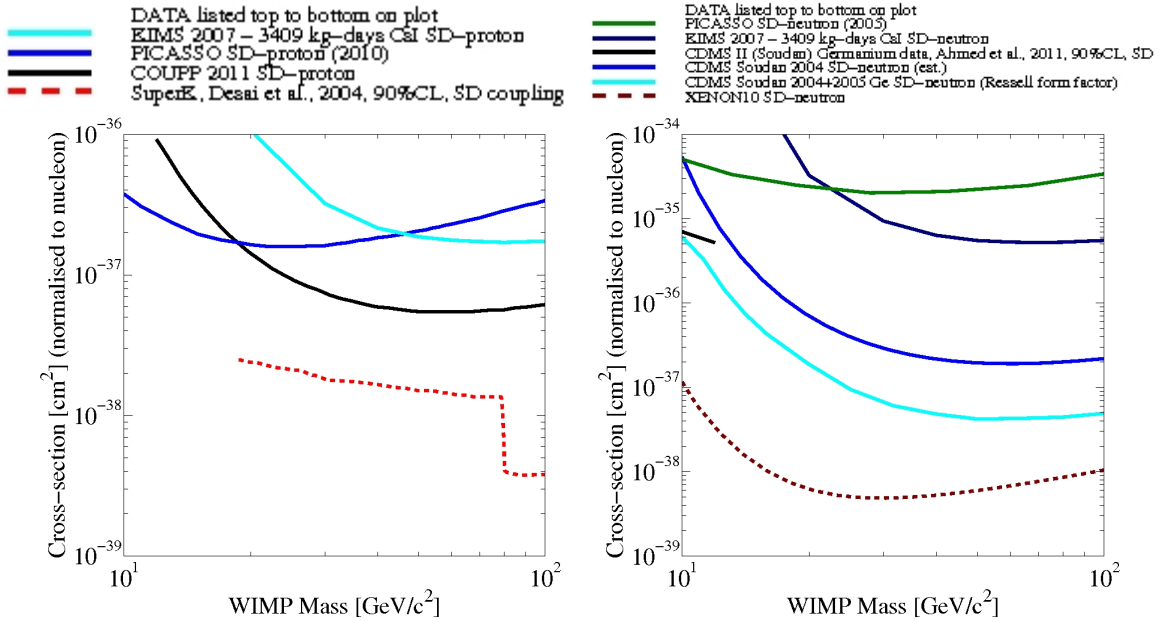
Figure 4.1: Current results of several direct detection experiments for the spin-dependent scattering cross-section on protons (left panel) neutrons (right panel) (Desai 2011).

are considered. Three different scenarios were chosen in agreement with the results of these experiments.

The DAMA/LIBRA experiment has measured a modulated signal at $8.9\,\sigma$ confidence level in a region around a small WIMP mass of $\approx 12\,\mathrm{GeV}$. The DAMA/LIBRA signal region is indicated by blue lines in Figure 4.2.

CRESST has also identified two possible signal regions with two global likelihood maxima M1 and M2. The mass of the second signal region around M2 is similar to that of DAMA/LIBRA. Thus, here the first region around M1 is considered in addition. The values of M1 are used for the CRESST scenario (see Table 4.1 and green lines in Figure 4.2).

The XENON collaboration has not detected a signal and thus gives limits (purple lines in Figure 4.2). The minimum spin-independent cross-section excluded by XENON is measured at a WIMP mass of $50\,\mathrm{GeV}$. The spin-independent cross-sections for the DAMA/LIBRA and CRESST scenarios are relatively high. Thus, for comparison this value is taken for the XENON scenario. The exact values used in this study are given in Table 4.1.

The results of DAMA/LIBRA and CRESST are not consistent with the XENON limits, because XENON excludes the results from both experiments. Nevertheless, XENON is not very sensitive for WIMP masses below $\sim 10\,\mathrm{GeV}$, thus the results might still be consistent (Collar 2011). This is another reason for considering all three scenarios.

In consistency with the current measurements shown in Figure 4.1, the spin-dependent scattering cross-section for scattering on protons and neutrons was set to $\sigma_{\mathrm{SD}} = 10^{-39}\mathrm{cm}^2$ (Desai 2011). The annihilation cross-section is set to $\langle \sigma_a v \rangle = 3 \times 10^{-26}\,\mathrm{cm}^3/\mathrm{s}$, because this value delivers the correct relic abundance of WIMPs as measured by WMAP (Komatsu et al. 2011). It is important to note that the annihilation cross-section does not essentially influence the properties of a DS. According to Section 2.4.3 capture and annihilation will be in equilibrium after the equilibrium timescale τ_{eq} (at the most a few hundred years, Freese
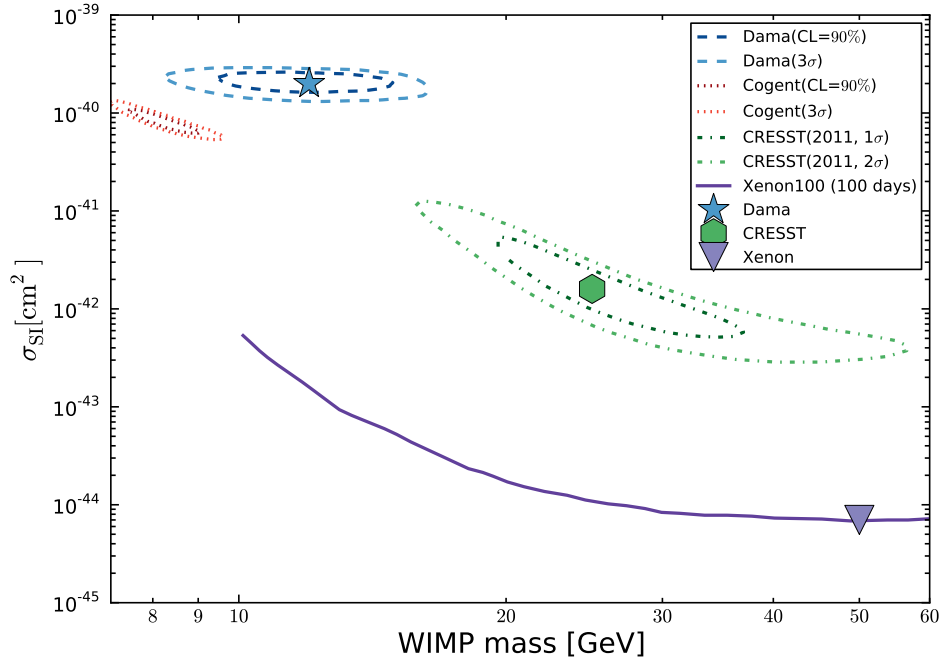
Figure 4.2: Overview of the current results obtained by several direct detection experiments (DAMA/LIBRA, CoGeNT (Aalseth et al. 2011), CRESST, XENON100). The stars indicate the values that were chosen for the different scenarios, which are used in this study (DAMA/LIBRA, CRESST, XENON100).

et al. 2008a). In equilibrium, the dark matter luminosity is determined by the capture rate and thus the annihilation cross-section only influences the required time to reach equilibrium.

Scenario	m_χ[GeV]	σ_{SI}[cm^2]
DAMA/LIBRA	12	2.0×10^{-40}
CRESST	25	1.6×10^{-42}
XENON	50	7.0×10^{-45}

Table 4.1: Parameters chosen for the different scenarios as shown in Figure 4.2. The column titled Scenario gives the name of the experiment the values are associated to. m_χ is the WIMP mass and σ_{SI} the spin-independent scattering cross-section.

4.2.2   Parameters of the Dark Matter Halo

Other important parameters, determining the capture and thus annihilation rates, are the WIMP density in the halo and their velocity distribution, as well as the velocity of the star. Stacy et al. (2011) follow the evolution of the gas and the DM within a collapsing molecular cloud by numerical simulations employing different initial DM density profiles (Case A: $\rho_{\mathrm{DM}} \propto$

53

r^{-2} and Case B: $\rho_{\mathrm{DM}} \propto r^{-1}$).[1] The sink particle method is used in order to represent accreting star forming regions.

First only the DM is evolved for 50000 years ('no-gas' case). The resulting DM density profile (black lines in Figure 4.3) is used to initialize a simulation which also includes gas ('with-gas' case). At the beginning of this simulation, the maximum gas density (gravitational sink) and the maximum DM density are both located at the center of the mini-halo.

In addition to the first sink, several more gravitational sinks and a disk form in the 'with-gas' simulation. The interaction of the newly formed protostars (sinks) with the disk leads to a separation of the positions of the protostars and the DM density peak. Thus, the protostars move within the DM halo from high to low DM densities. Figure 4.3 shows the initial DM density profile (red line), the final density profile of the 'no-gas' evolution (black dotted line) and the 'with-gas' evolution after 10000 years (blue dashed triple-dot line) and after 20000 years (blue long dashed line). The protostar disk system causes a gravitational scattering of the DM, which leads to a decrease of the DM density in course of the simulation (blue long dashed line is below blue dashed triple-dot line).

Additionally to the central gravitational sink of $28\,\mathrm{M_\odot}$, a second $17\,M_\odot$ sink forms. This second sink forms at a relatively small distance from the central sink but moves outwards in the course of the simulations, thus it moves from higher DM densities ($10^{10}\mathrm{GeV/cm^3}$) to lower DM densities ($10^7\,\mathrm{GeV/cm^3}$). Later on in the simulation, at least one additional small sink of about $\approx 1\mathrm{M_\odot}$ forms which also moves through the DM halo, however, it moves from a higher distance (lower DM density) to lower distance (higher DM density). In the other simulations, protostars form at smaller distances from the central DM density, thus possibly higher DM densities can occur (up to $10^{12}\,\mathrm{GeV/cm^3}$).

In the following sections, the effects of scattering on DS approximately as heavy as the sinks forming in the simulations of Stacy et al. (2011) are explored. It must be distinguished between the central star at a high DM density up to $10^{15}\,\mathrm{GeV/cm^3}$ and protostars forming and moving further outwards.

4.2.3   Stability of the Dark Matter Halo

The WIMPs in the DM halo surrounding the protostar can also self-annihilate. Since this DM hallo supplies the star with WIMPs, the ambient WIMP density must be stable in the long term. This might not be the case for very high ambient WIMP densities. Here, in the central regions of the minihalo ambient WIMP densities up to $10^{15}\,\mathrm{GeV}$ are possible. Thus, it must be evaluated whether these ambient WIMP densities are stable for reasonable long periods of time (which are at least a few Gyr in this context). The evolution of the ambient WIMP density is given by the solution of Equation 2.20 describing the rate WIMPs annihilate. The differential equation to be solved is given by

$$\frac{\mathrm{d}\rho_\chi}{\mathrm{d}t} = -\frac{1}{2}\langle\sigma_a v\rangle \frac{\rho_\chi^2}{m_\chi}. \tag{4.1}$$

This equation can be solved by

$$\rho_\chi(t) = \frac{\rho_0}{1 + \frac{\rho_0}{2}\frac{\langle\sigma_a v\rangle}{m_\chi}t}. \tag{4.2}$$

---

[1]Here, only Case A is considered due to the DM densities in Case B being too small for effective scattering of DM on stellar nuclei.
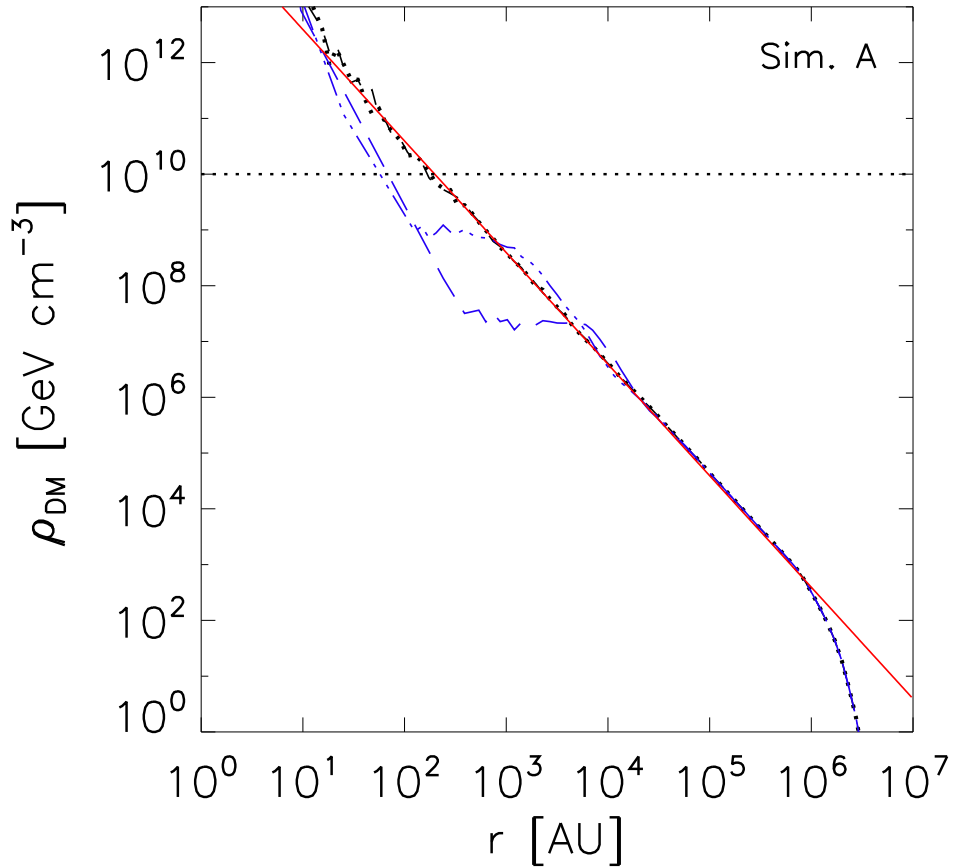
Figure 4.3: DM density profile from Stacy et al. (2011). The red lines resemble the initial profile, the black line the results of the evolution without and the blue line with gas. The dotted line indicates the DM density threshold, which is approximately needed to support a star via scattering.
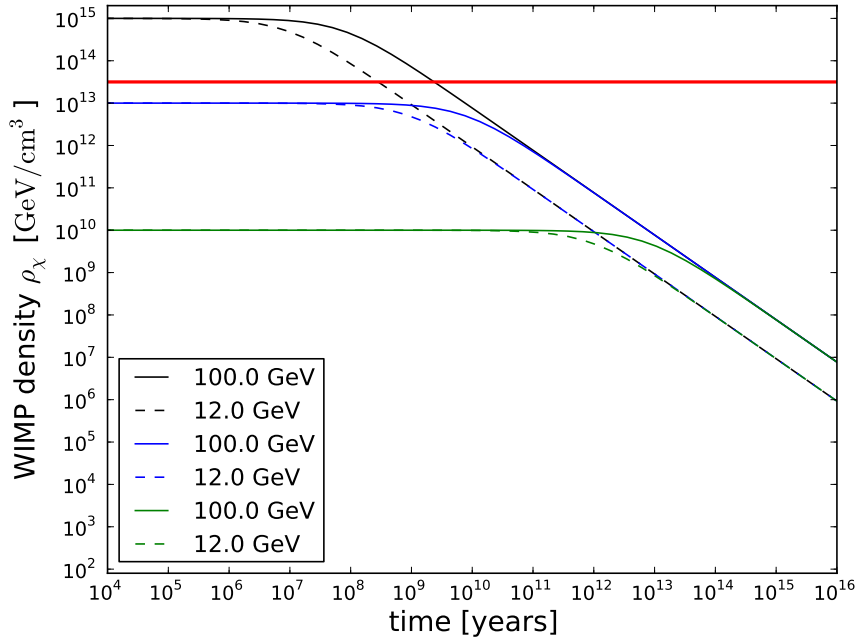
Figure 4.4: Ambient WIMP density evolution due to the self-annihilation of WIMPs. The ambient WIMP densities above the red line are not stable for a few Gyr (at least).

This Equation gives the evolution of the ambient WIMP density. From Figure 4.4 it can be concluded that the WIMP halo densities are stable at least for a few Gyr for the WIMP masses considered in this study if the initial ambient WIMP density does not exceed $10^{13.5}$ GeV (indicated by the red line). This is not the case for any of the scenarios considered here.

4.2.4 Stellar Evolution for Zero Metallicity Stars with the 'DarkStars' Code

The stellar evolution code 'DarkStars' by Scott et al. (2009) is used to calculate the evolution of stars that are embedded in DM halos with densities of $10^8 - 10^{13}$GeV/cm³. A constant local WIMP density is assumed, which means that when the star moves through the halo the density is the same everywhere.

Following the results from Stacy et al. (2011) and Sivertsson and Gondolo (2011) three stars of $1\,M_\odot$, $20\,M_\odot$ and $100\,M_\odot$ have been evolved with the 'DarkStars' code.

Solar values are taken as default for the WIMP velocity dispersion $\bar{v} = 270\,$km/s and the stellar velocity $v_\star = 220\,$km/s. Since the WIMP velocity dispersion (Equation 2.28) is probably a lot smaller in the early Universe (about 10km/s, Freese et al. 2008a), and the capture rate is elevated when the relative velocity of the WIMPs and the star is reduced, this choice can be considered conservative.

The evolution of the stars is initialized from normal zero age main sequence (ZAMS) models. These stars capture dark matter particles via scattering. The capture of WIMPs via scattering is included according to Equation 2.17, which is only valid if the WIMPs are not

gravitationally bound to the star (Scott et al. 2009, Sivertsson and Gondolo 2011).

'DarkStars' has been written for the purpose of exploring possible present-day Dark Stars in the center of our galaxy. Thus, it has not been designed for the evolution of DS in the early Universe, which almost exclusively consist of hydrogen (H) and helium (He). Nevertheless, the stellar evolution of the first stars must be calculated for zero metallicity stars.

'DarkStars' only includes a protostellar evolution, where the opacity tables are only available for hydrogen an helium. It is not taken into account that the composition of the star and thus the opacities change when hydrogen burning (and later helium burning) become important.

An analysis of the importance of the changing composition in the early stages of the evolution can evaluate whether the protostellar modus implemented in 'DarkStars' can be used for studying DS in the early Universe. Therefore, the evolution of the most important properties, i.e. temperature, density and luminosity, is compared for calculations in the protostellar modus and for the lowest metallicity (z = 0.0001) included in the 'DarkStars' package. The influences are evaluated for a normal star without WIMP capture and a star that is highly influenced by WIMP burning.

The Herzsprung-Russel diagram (H-R diagram), the central density and temperature as well as the different luminosities are shown in Figures 4.5 to 4.7 for a normal $100 \, \mathrm{M_\odot}$ star (left panel) and a $1 \, \mathrm{M_\odot}$ star with a ambient DM density of $10^{10} \, \mathrm{GeV/cm^3}$ (right panel) calculated in the Z = 0 protostellar mode (black line) and for Z = 0.0001 (red line).

For the $100 \, \mathrm{M_\odot}$ star in the left hand panels, the evolution is very similar for the first $2.9 \, \mathrm{Myr}$ before He burning sets in, which can be seen in Figure 4.7 showing the different contributing luminosities. Figure 4.5 and 4.6 confirm this.

For the $1 \, \mathrm{M_\odot}$ star in the right hand panels, the influence of the metallicity is even smaller, because the energy release is dominated by WIMP burning. The H-R diagram and the central density-temperature evolution are in principle identical, the main difference is that the low metallicity star moves a little bit quicker in the diagrams.

Thus, it can be concluded that the influence of the metallicity (or the wrong opacities) gets more important for stars that are less influenced by WIMPs. This is according to expectation, because if WIMP burning dominates, no hydrogen is burned and the composition does not change.

For this study, stars for which WIMPs are the dominating energy source are of major interest, so the simplified opacity assumptions in the protostellar mode will not influence the results. Some of the stars discussed in the next section will be less influenced by WIMPs, nevertheless, it can be concluded from this analysis that the resulting evolution is a good approximation until helium burning becomes important, because even for a normal star without WIMP burning the compositional changes are not very significant in the early stages of the evolution.

4.3 Analysis and Results

4.3.1 Properties of Dark Matter Influenced Stars

The evolution of the DS was calculated for the parameter sets discussed before (Table 4.1). It was possible to calculate a full evolution for several ambient densities ($10^8 - 10^{14} \, \mathrm{GeV/cm^3}$), all three scenarios (DAMA/LIBRA, CRESST, XENON) and all of the considered stellar masses (1, 25, $100 \, \mathrm{M_\odot}$). Roughly three different types of stars can be identified:
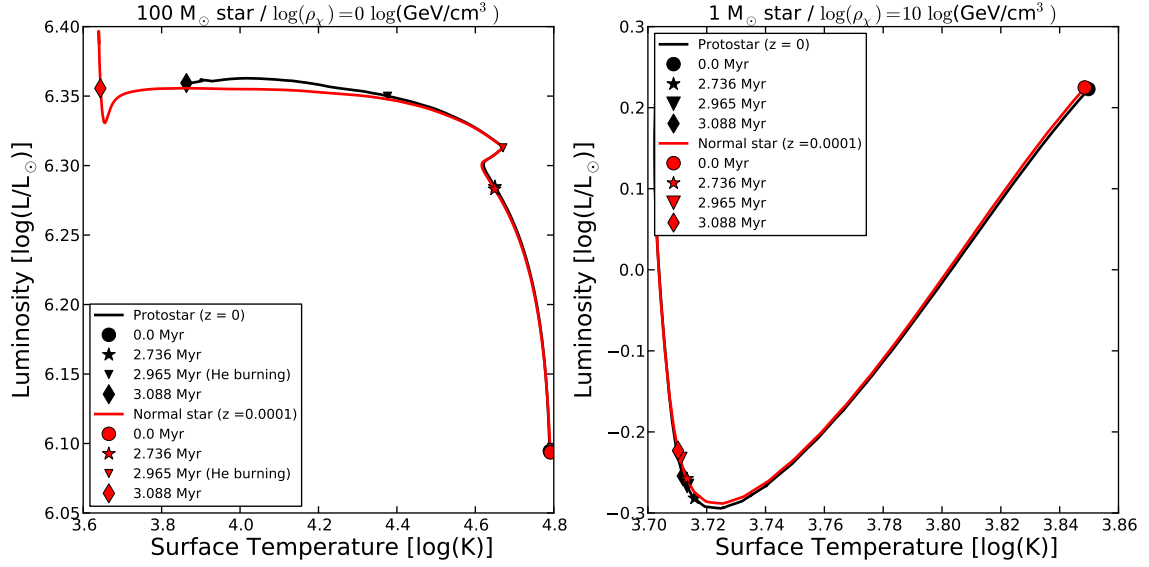
Figure 4.5: H-R diagramms for a $100\,\mathrm{M_\odot}$ star not influenced by WIMP annihilation (left panel) and a $1\,\mathrm{M_\odot}$ star in a $10^{10}\,\mathrm{GeV/cm^3}$ ambient WIMP density halo (right panel). The evolution is calculated in the $Z = 0$ protostellar mode (black line) and the $Z = 0.0001$ mode (red line). The black circles indicate defined timesteps in the evolution (see legend).
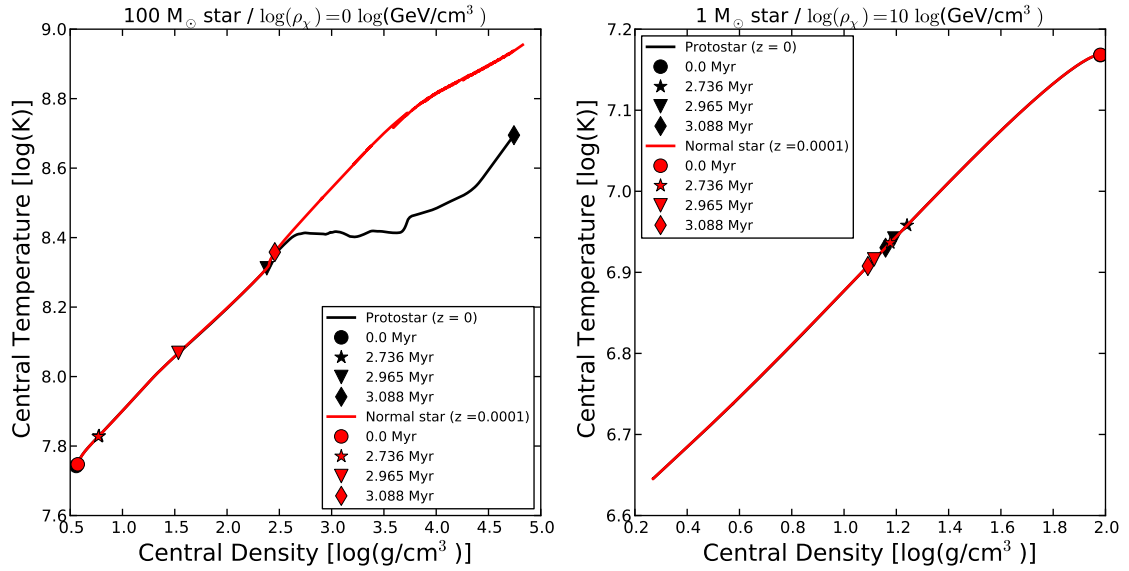
Figure 4.6: The central density vs. temperature evolution for a $100\,\mathrm{M_\odot}$ star not influenced by WIMP annihilation (left panel) and a $1\,\mathrm{M_\odot}$ star in a $10^{10}\,\mathrm{GeV/cm^3}$ ambient WIMP density halo (right panel). The evolution is calculated in the $Z = 0$ protostellar mode (black line) and the $Z = 0.0001$ (red line) mode. The black circles indicate defined timesteps in the evolution (see legend).
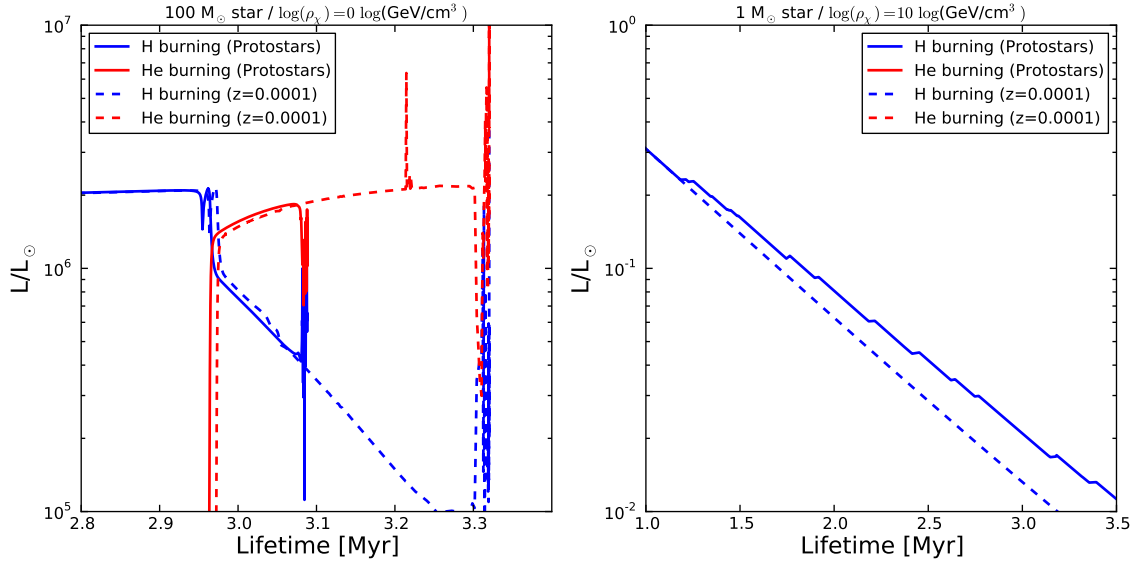
Figure 4.7: The evolution of the most important nuclear burning processes for a $100\,\mathrm{M_\odot}$ star not influenced by WIMP annihilation (left hand panel) and a $1\,\mathrm{M_\odot}$ star in a $10^{10}\,\mathrm{GeV/cm^3}$ ambient WIMP density halo. The evolution is calculated in the $\mathrm{Z}=0$ protostellar mode (solid lines) and the $\mathrm{Z}=0.0001$ (dashed lines) mode.

- If the combination of ambient densities and cross-section leads to a small amount of energy being produced by WIMP annihilation, the stellar evolution is almost not influenced by the WIMPs, and the stars evolution is not significantly altered (Not WIMP Influenced Star, NWIS).

- If the amount of energy produced by WIMPs is of the same order as the energy produced by fusion processes, the evolution of the star is altered by the WIMPs, thus the star is WIMP influenced (WIMP Influenced Star, WIS).

- In the case that WIMP burning dominates over the fusion processes by several orders of magnitude, the star is a real WIMP burner (WB) that would, in principle, live as long as the DM supply in its environment exists. Thus, the star has reached a stable equilibrium where all its energy is effectively provided by WIMP burning. In the calculations, this is indicated by the central hydrogen mass fraction changing by less than $10^{-14}\,M_\star/M_\odot$, as well as the logarithm of the central density and temperature (ρ_c and T_c), changing by less than 10^{-10} for four consecutive time steps. When this criterion is fulfilled, the simulation is stopped because the star will not develop any further.

The simulations for the other stars are stopped when the hydrogen in the core is exhausted (the central hydrogen mass X_c fraction drops below 10^{-6}). Additionally, the simulation is stopped when the stars lifetime exceeds the age of the Universe.

Nevertheless, sometimes the star started to change very quickly due to the inset of helium burning. Consequently, smaller and smaller time steps are required for the next evolutionary steps to be calculated, because 'DarkStars' requires that the number of WIMPs within the

star does not change by more than the current WIMP population. This way the required time step becomes smaller than the dynamic timescale and the simulation is stopped. Because the time after helium burning set in is not of interest for this study, these stars are still considered when the evolutionary phase, where DM burning is the dominating energy source, is explored. The same problem occurs when the ambient WIMP density at the beginning of the evolution is so high that the initial ZAMS model is adjusted so quickly that the time steps again get extremely small. This happens within the first few evolutionary steps. These stars are not considered here, but they should in principle be WB. This problem can be solved by evolving the star for a few time steps at a lower WIMP density and then using the resulting stellar model as an input for simulation with a higher ambient WIMP density.

Stars resulting from a certain parameter set can be identified by analyzing the most important properties of the star, e.g. temperature, density and luminosity.

Figure 4.8 shows the H-R diagrams for a $100\,M_\odot$ star in the CRESST scenario for three different ambient WIMP densities. Markers indicate defined lifetimes of the star, so that it is possible to evaluate the amount of time the star spends in a certain path on the diagram. These stars were chosen because the differences can be seen best.

The first star with an ambient WIMP density of $10^{10}\,GeV/cm^3$ is a NWIS following a normal path in the H-R diagram. At the beginning, the star moves along the main sequence powered by hydrogen burning. The luminosity increases, because central temperature and density increase (see left panel in Figure 4.9). Afterwards, the star contracts very quick, which marks the transition to shell hydrogen burning, and the temperature rises (left panel in Figure 4.9), so that helium burning sets in. Now, the star left the main sequence and moved to the red-giant branch, where the stellar envelope expands and the surface temperature drops, so that the total luminosity is maintained and the star moves horizontally across the H-R diagram.

The $10^{12}\,GeV/cm^3$ star (WIS) takes a similar path in the H-R diagram (middle panel in Figure 4.8) except at the very beginning of the evolution where temperature and luminosity shortly decrease (a behavior which is also seen in the WB in the right panel) before the normal main sequence evolutionary track of the NWIS is joined. Nevertheless, the WIS star moves significantly slower in the H-R diagram (middle panel of Figure 4.8) and the central temperature density diagram (middle panel of Figure 4.9) than the NWIS.

The right diagram in Figure 4.8 shows the H-R diagram for a typical WIMP burner. First, the luminosity and the surface temperature drop which is caused by the expansion and cooling of the star as a result result of the high radiation pressure from WIMP annihilation (density and temperature in the right panel of Figure 4.9 drops). Due to the low temperatures, hydrogen burning becomes ineffective and WIMP burning takes over (right panel of Figure 4.10). This leads to an increasing luminosity, while the surface temperature still drops, because of the continuing expansion of the star. Finally, the gravitational force and the radiation pressure get into hydrostatic equilibrium, and the star stabilizes in the H-R diagram, staying at this position in the H-R diagram forever (as long as the DM is supplied).

This behavior is very different from normal stars, shown in the first panel of Figure 4.8. Here, the luminosity increases with the lifetime while the surface temperature still drops. The H-R diagram for normal stars depends critically on the stellar mass, consequently the H-R diagram looks different for different masses. For WB this is not the case. The H-R diagrams all look essentially the same, independent of the mass.

The evolution of the luminosity of the three stars is shown in Figure 4.10. The Figure includes the most important fusion processes, creating energy as well as the WIMP burning
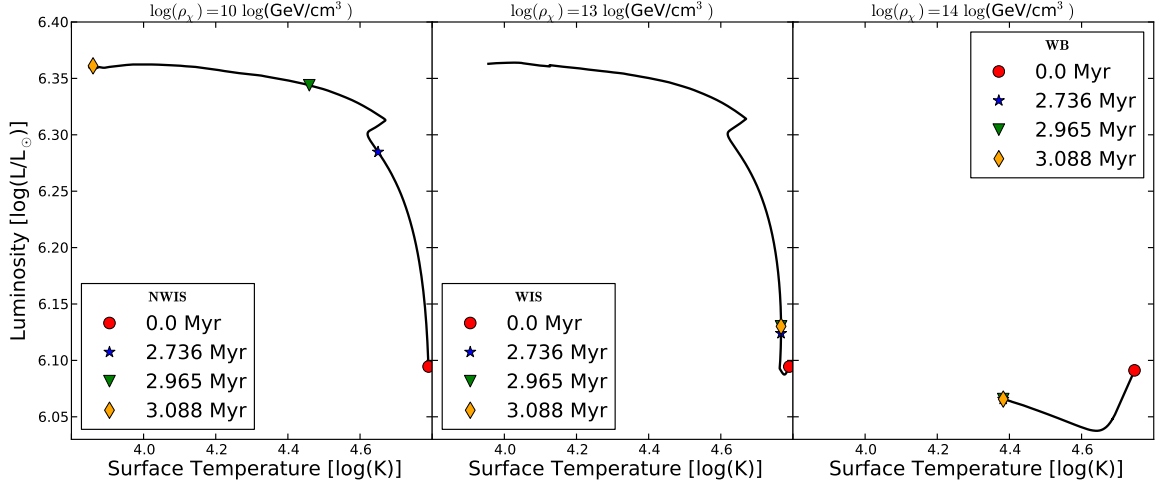
Figure 4.8: H-R diagram for the $100\,M_\odot$ star in the CRESST scenario for three different WIMP densities ($10^{10}\,\mathrm{GeV/cm^3}$, $10^{13}\,\mathrm{GeV/cm^3}$, $10^{14}\,\mathrm{GeV/cm^3}$).
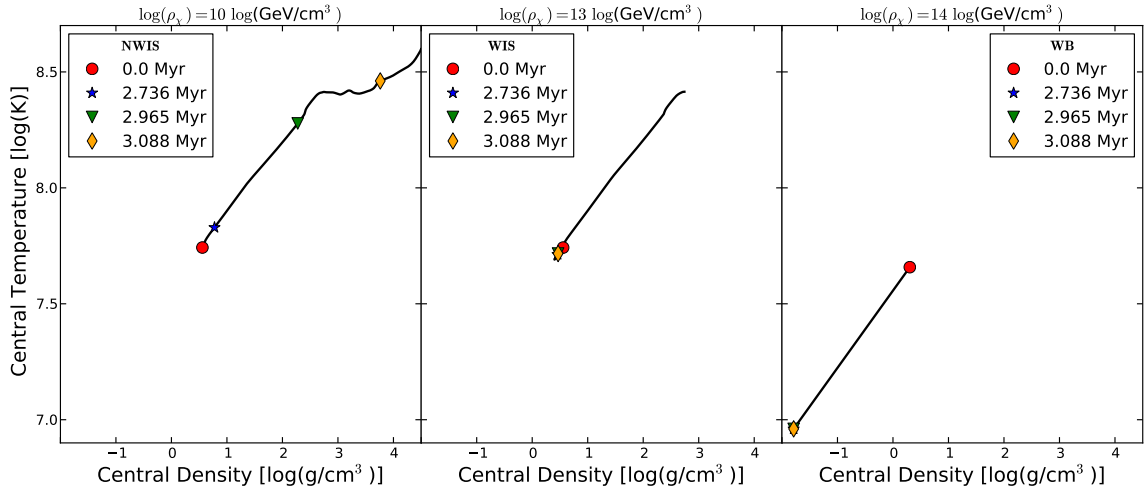
Figure 4.9: Evolution of the central density and temperature of the $100M_\odot$ star in the CRESST scenario for three different WIMP densities ($10^{10}\,\mathrm{GeV/cm^3}$, $10^{13}\,\mathrm{GeV/cm^3}$, $10^{14}\,\mathrm{GeV/cm^3}$). The symbols indicate the same time steps in the evolution as in Figure 4.8.
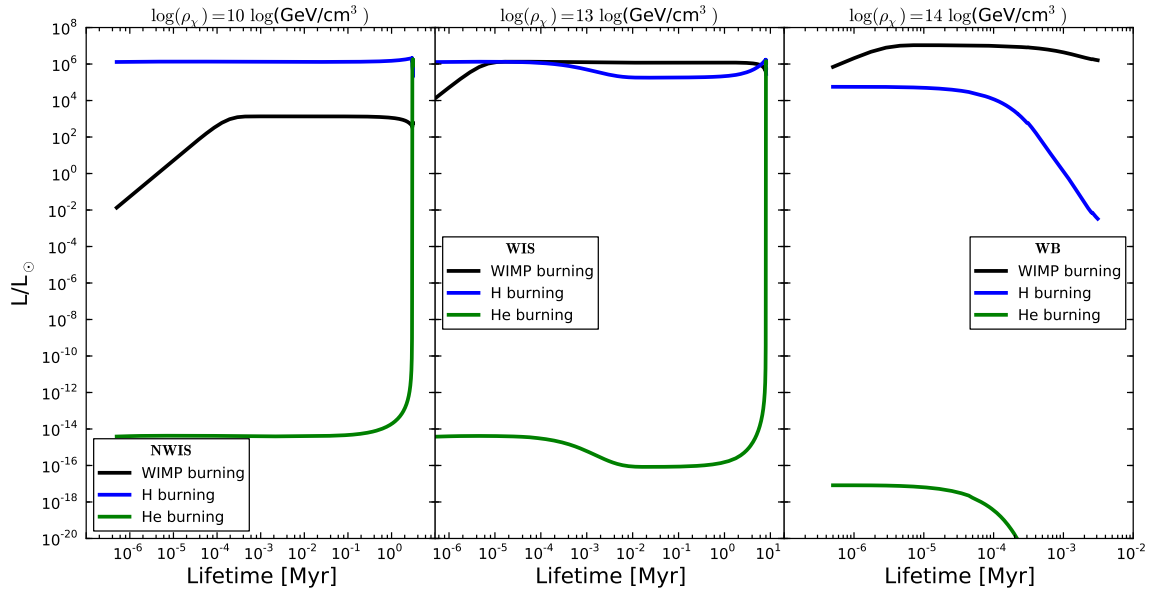
Figure 4.10: Evolution of the luminosities produced by the different burning process (H, He, WIMP burning) for the $100 M_\odot$ star in the CRESST scenario for three different WIMP densities (10^{10} GeV/cm^3, 10^{13} GeV/cm^3, 10^{14} GeV/cm^3).

luminosity, which will be discussed in detail in the next sections. In the left panel, the luminosities of the different fusion processes are shown for the NWIS. Hydrogen burning dominates for almost 2.7 Myr before helium burning takes over. The evolution of the luminosities is similar for the WIS in the middle panel, except that the hydrogen and helium luminosities drop a slightly after a few thousand years (10^{-3} Myr) and the take over of the helium burning occurs later at 7.8 Myr. The hydrogen luminosities for both cases are of the order $10^6\,L_\odot$, while they start at the order $10^4\,L_\odot$ in the WB in the right hand panel, but then drop within a few thousand years by several orders of magnitude, so that neither helium nor hydrogen burning is relevant. The simulation of the WB is stopped, but since it is a WB, it will be in this state forever (as long as enough DM is supplied).

Yoon et al. (2008) discussed the evolution of DS influenced by burning of captured DM similar to the approach presented here. Yoon et al. (2008) also find that the lifetimes of DS may be significantly prolonged and that stars might not undergo nuclear burning process for sufficiently high ambient WIMP densities. The total luminosities and effective temperatures are comparable to the ones found in our simulations. The agreement is very good for the total luminosity. The effective temperatures vary with the assumed WIMP properties and can thus not be directly compared. Nevertheless, the values are very similar (see Yoon et al. (2008) Figure 1).

4.3.2   Dark Stars vs WIMP Scenarios/Ambient Densities

It has been shown in the previous Section that the evolution and properties of the stars discussed dramatically change when the total energy supply of the star is dominated by WIMP burning. The relative importance of WIMP burning for the total energy budget of the star does not exclusively depend on the WIMP and halo properties, but also on the mass of the star, because the capture rate depends on the stellar mass (see Equation 2.28). Even though more massive stars capture more WIMPs, they also need more WIMP luminosity to be completely supported by WIMP burning. Thus, the luminosity produced by WIMP burning relative to the total luminosity of the star (nuclear reaction plus WIMP burning) is a good indicator to decide which type of energy production is dominant.

Figure 4.11 shows the WIMP (black), hydrogen (red) and helium (blue) luminosities normalized to the total luminosity for DAMA/LIBRA scenario stars of three stellar masses and a choice of ambient DM densities. For every parameter configuration, there is a swing in phase at the very beginning lasting approximately a few hundred years during which the WIMP luminosity grows, while the hydrogen luminosity is reduced before both stabilize on a constant level. This is a consequence of the fact that the stars are initialized as normal ZAMS (no WIMP influence) and then capture DM.

Afterwards, for NWIS, hydrogen burning (panel a, d) is the dominant energy source, for WIS hydrogen and WIMP burning are both important (panel b, e), while the luminosity produced by WIMP burning dominates in real WB (panel c, f, g). Once a WB has reached an equilibrium state, it will not change anymore and continue to burn WIMPs as long as the WIMP supply exists. In this case the simulation is stopped.

NWIS and WIS stars undergo a major transition when hydrogen runs out and He burning becomes the dominant energy source (also see the discussion about the red-giant branch in the previous Section). This transition occurs much earlier in NWIS and more massive stars (after roughly 2.5 Myr in the $100\,M_\odot$ star in panel a and 7 Myr in the $25\,M_\odot$ star in panel d of Figure 4.11) than in WIS (after roughly 5.3 Myr in the $100\,M_\odot$ star in panel b and 30 Myr in the $25\,M_\odot$ star in panel e of Figure 4.11), where WIMP burning again delays the evolution. [2]

Integrated luminosities   The overall importance of WIMP burning during lifetime of a star can be evaluated by looking at the integrated luminosity. In Figure 4.12, the integrated relative luminosities are given for each time step:

$$\frac{L_{\mathrm{int}}}{L_{\mathrm{burning}}} = \frac{\int_{t_0}^{t} L_i(t')\mathrm{d}t'}{\int_{t_0}^{t}\left(L_{\mathrm{DM}}(t') + L_{\mathrm{nuc}}(t')\right)\mathrm{d}t'}. \tag{4.3}$$

Here, L_{int} represents the integrated luminosity of type i (either DM oder hydrogen burning) between the starting time, where the star is initialized on the ZAMS, t_0 and the time t during the evolution of the star. L_{burning} is the same value for the luminosity produced by DM burning L_{DM} and the luminosity L_{nuc} produced by nuclear reactions. Thus, $L_{\mathrm{int}}/L_{\mathrm{burning}}$ gives the importance of the different burning processes (WIMP or hydrogen) relative to the

---

[2]The blue line of helium burning is only shown in panel a and e. The reason is the termination of the simulation (probably because the star changed too quickly) before helium burning becomes important enough to be seen in this choice of boundary coordinates. Nevertheless, the stars in panel b and d are normal NWIS and WIS and most likely start helium burning analogous to the stars in panel a and e.
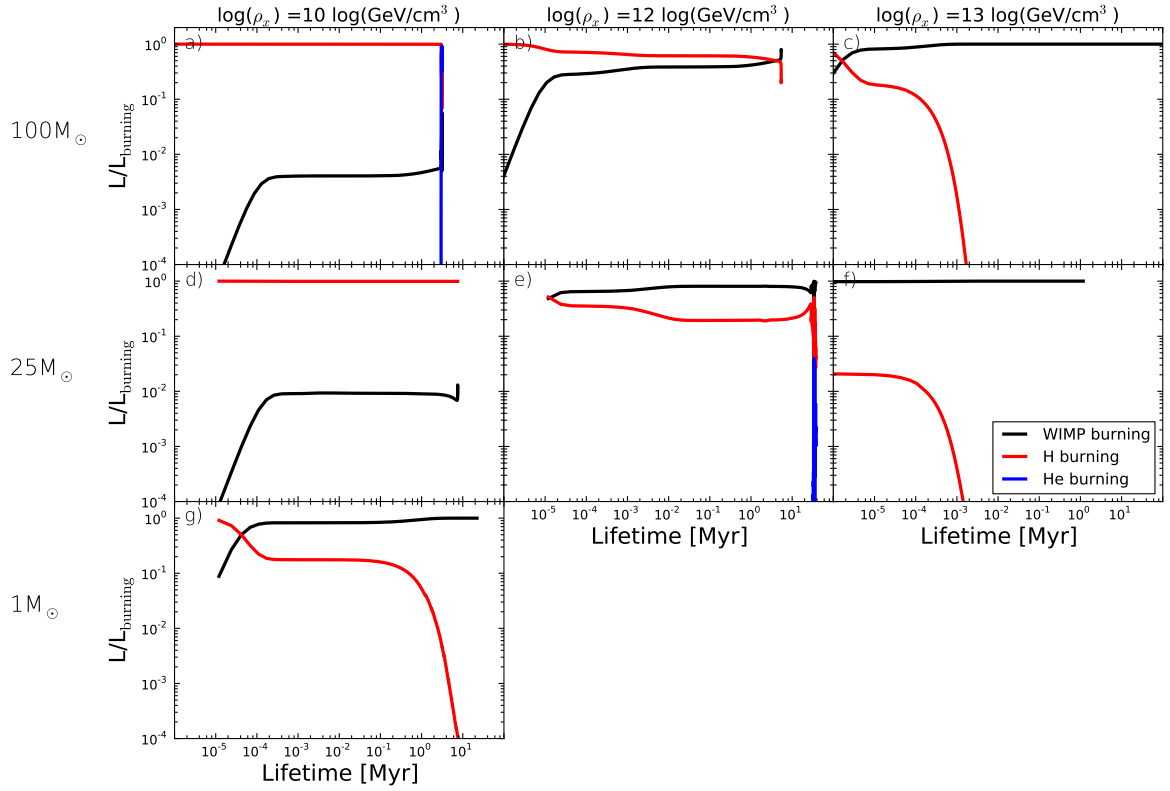
Figure 4.11: Diagram, showing the evolution of the relative luminosities produced by different process (H, He, WIMP), normalized to the total luminosity for three stellar masses and three ambient WIMP densities using the DAMA/LIBRA scenario.
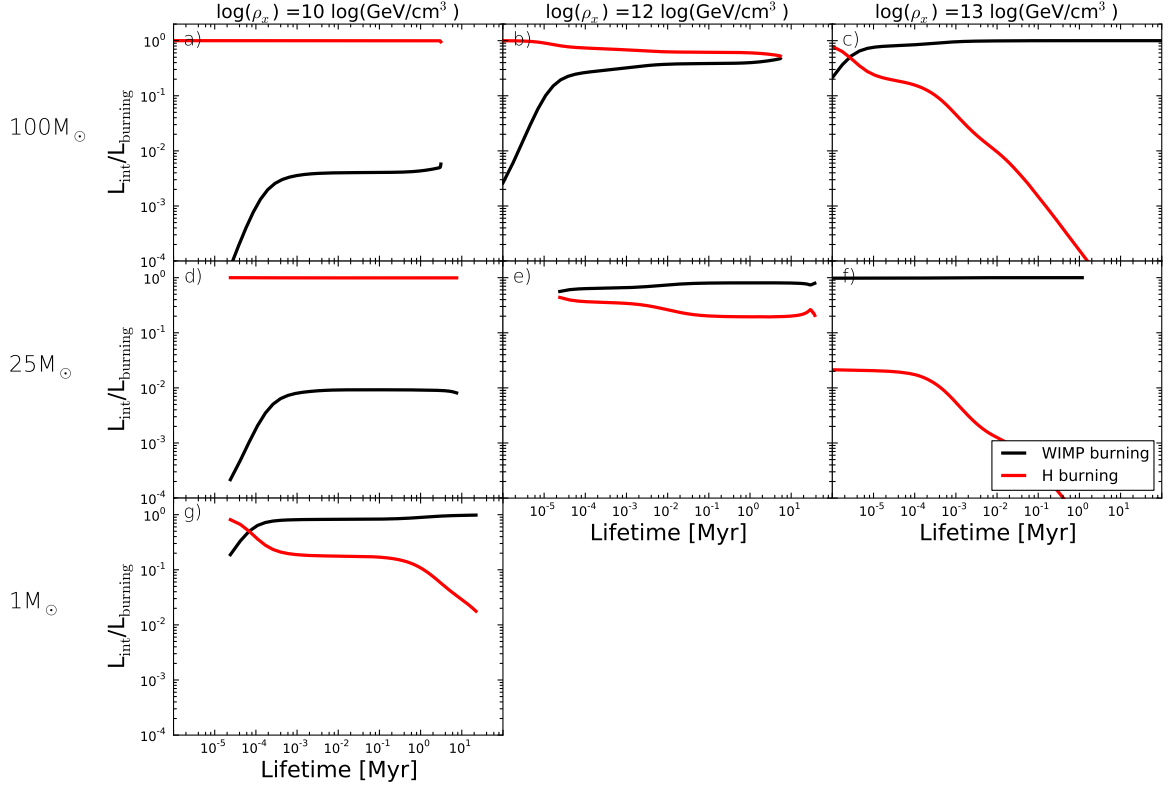
Figure 4.12: Diagram, showing the evolution of the integrated relative luminosities, produced by the different burning process (H, He, WIMP) for the same parameters as in Figure 4.10.

total luminosity produced by burning processes between t_0 and t.

Helium burning is not important for the total luminosity produced in the star over its lifetime and is therefore omitted from the Figure. Additionally, the evolution of the integrated luminosities is smooth for large timescales, which is natural because the quick changes in the luminosities at the end of the evolution are not important for the overall luminosity. Thus, the integrated WIMP luminosity in the stable phase is a good indicator for categorizing the stars as WB, WIS or NWIS. In order to use the stable phase and exclude the swing in phase, the first 1000 years are discarded. The values at the beginning of the stable phase, the end of the simulation and a mean value are taken into account for evaluating the importance of WIMP burning during the stable phase.

In the left panels of Figure 4.13, results for different ambient densities and WIMP scenarios are shown for every considered stellar mass. In every plot the values at the beginning of stable phase, the end of the simulation and a mean value of the integrated relative WIMP luminosity $L_{\mathrm{int}}/L_{\mathrm{burning}}$ are shown for all considered ambient densities and scenarios. Additionally, a gray shaded area is introduced indicating the area where the stars are WIMP burner (WB must have all of the three relative luminosity values above 0.8). The light blue shaded area indicates the area where the evolution and lifetime of the stars are significantly influenced by the WIMPs (WIS), again all three relative luminosity values must be between 0.1 and 0.8.

Additionally, some vertical lines are introduced, indicating realistic ambient density values for the different stellar masses following Stacy et al. (2011).

In the right hand panel, the lifetimes of the NWIS (white area in corresponding left panel) and the WIS (light blue shaded area in corresponding left panel) are shown. The lifetimes of the WB are not shown, since they live as long as WIMPs are supplied. Here, the lifetime is defined as the maximum age of the star in the simulation. This values can only be taken as an indicator, because some of the simulations have probably ceased too early due to the star changing too quickly (as explained before). Thus, the time until the hydrogen in the core is exhausted is probably longer and the lifetimes considered here are conservative lower limits.

In general, the relative WIMP luminosities for the DAMA/LIBRA scenario are greater than for the CRESST and XENON scenarios, because the capture rate (Equation 2.17) is higher for a higher scattering cross-sections. Thus, also the WIMP burning luminosity is increased. The relative integrated luminosities grow proportional to the ambient WIMP density, because the total WIMP luminosity is proportional to the ambient WIMP density according to Equation 2.31.

Low mass stars   Exemplary for low mass stars, the results for the $1\,M_\odot$ are displayed in the first row. In the DAMA/LIBRA scenario, the star is a WIMP burner at a relatively small ambient WIMP density of $10^{10}\,\mathrm{GeV/cm^3}$, while it becomes a WB at $10^{11}\,\mathrm{GeV/cm^3}$ in the other scenarios. The star is notably influenced by the dark matter at $10^9\,\mathrm{GeV/cm^3}$ in the DAMA/LIBRA scenario. Looking at the lifetimes of the star in the right panel in the first row of Figure 4.13, this interpretation is confirmed. In the DAMA/LIBRA scenario, the lifetime is significantly prolonged at an ambient WIMP density of $10^9\,\mathrm{GeV/cm^3}$, in the CRESST and XENON scenarios not for ambient WIMP densities smaller than $10^{10}\,\mathrm{GeV/cm^3}$. The NWIS have lifetimes of roughly 7000 Myr only. They are prolonged by 3000 to 6000 Myr in WIS, thus by a factor of 1.5 to 2.

The vertical dashed line in the left panel in Figure 4.13 indicates realistic ambient densities between $10^7\,\mathrm{GeV/cm^3}$ and $10^9\,\mathrm{GeV/cm^3}$ following simulation A from Stacy et al. (2011). Due to its small mass, the star is located relatively far outwards in the entire simulation of Stacy et al. (2011), where the DM densities are not very high. Even at the location of the star, where the DM density was highest, the DS would just be a WIS. Thus, it is very unlikely that the ambient WIMP density remains high enough for a long lasting support of low mass DS.

Nevertheless, it should be noted that in simulation B of Stacy et al. (2011) a low mass stars formed much closer to the central DM density peak, so that higher DM densities may also be possible. Nevertheless, movements of the star through the DM halo will always be more important for low mass stars, because of the gravitational interactions with other (possibly higher mass) objects and the ambient conditions will unlikely be stable in the long term. The plot can also be interpreted as the evolution of the relative luminosity when the star moves through the DM halo. The star may start as a WB and then undergo transitions to a WIS and to a NWIS or the other way around. Whether and how these transitions occur, depends critically on the speed at which the star moves.

Intermediate mass stars   Intermediate mass stars are very interesting, because stars of masses around $25\,M_\odot$ have formed in the gravitational center of the halo and further outwards in the disk in the simulations of Stacy et al. (2011). Exemplary, here the results for a $25\,M_\odot$ star are shown in the second row of Figure 4.13. For this intermediate mass star the transition

from a WIS to a WB takes place at $10^{13}\,\mathrm{GeV/cm^3}$ for all of the scenarios. [3] Here, the dashed vertical lines indicate again the maximum realistic ambient WIMP density and the minimum realistic ambient WIMP density for intermediate mass stars. The maximum value is given by the central halo density. The minimum value is given by the smallest ambient WIMP density at which an intermediate mass star is located in the simulations of Stacy et al. (2011). Thus an intermediate mass star, forming at the center of a DM halo, will be a WB. Intermediate mass stars, spending their lifetimes in areas of smaller DM densities, are unlikely to be significantly influenced by WIMP burning, because a ambient WIMP density as high as $10^{12}\,\mathrm{GeV/cm^3}$ is required for a WIS.

The analysis of the stellar lifetimes in the corresponding right panel shows again that the lifetime is prolonged for the WIS in the light blue shaded area ($10^{12}\,\mathrm{GeV/cm^3}$ and $10^{13}\,\mathrm{GeV/cm^3}$) by up to $40\,\mathrm{Myr}$, which is equivalent to six times the lifetime of NWIS (have just a lifetime of roughly 8 Myr).

High mass stars   In the simulations of Stacy et al. (2011), no stars with masses above $32\,\mathrm{M_\odot}$ formed. Nevertheless, it has been found previously that Pop III stars could be more massive than present-day stars, with a typical mass scale of $100\,M_\odot$ (Bromm and Larson 2004 and references therein). Such stars would form individually in the center of the DM halo (Abel et al. 2000 and Abel et al. 2002) or in small multiple systems (Bromm et al. 1999 and Bromm et al. 2002). Thus, the formation of for example a $100\,M_\odot$ star (third row in Figure 4.13) probably takes place in the center of the gravitational well. The maximum ambient densities in the simulations from Stacy et al. (2011), relevant for high mass stars, are indicated here as a dashed line. All of the stars calculated here are on the left side of this line thus it is absolutely possible that such stars are WB or WIS. The lifetimes of the WIS in the light blue shaded area are prolonged by roughly a factor of two.

It should be noted that recent results from (Hosokawa et al. 2011) predict a maximum Pop III mass of $50\,M_\odot$ due to feedback effects from ultraviolet radiation. Thus, this might be the maximum mass of high mass DS.

The DM luminosity of the stars is proportional to the ambient WIMP density and follows a power law. In double logarithmic scale, a power law is equivalent to a linear law, so that a linear regression can be performed and used to determine the ambient WIMP density for which the star becomes a WIMP burner. The linear regression is performed for all three relative luminosity values in order to find an estimate of a minimum and maximum ambient density at which the star will become a WB. Figure 4.14 illustrates the resulting best fit power laws. The slope is always close to one in consistence with the expectation that the luminosity is proportional to the ambient WIMP density. The shaded areas in the associated colors illustrate the range of ambient densities (the values are taken in order to be conservative for a relative WIMP luminosity of 0.9 indicated by the green horizontal line). The values in these areas are taken as an estimate for the ambient WIMP density at which the star becomes a WB.

In Figure 4.15, the results for different stellar masses are summarized. The mass of the star and the maximum and minimum values from the linear regression for the ambient density at which the star becomes a WB are given for all three scenarios. The area between maximum and minimum values are shaded in the colors of the scenarios (DAMA/LIBRA in purple, CRESST

---

[3]Nevertheless, a star for the DAMA/LIBRA scenario was calculated which already became a WIMP burner at $10^{12.5}\,\mathrm{GeV/cm^3}$.
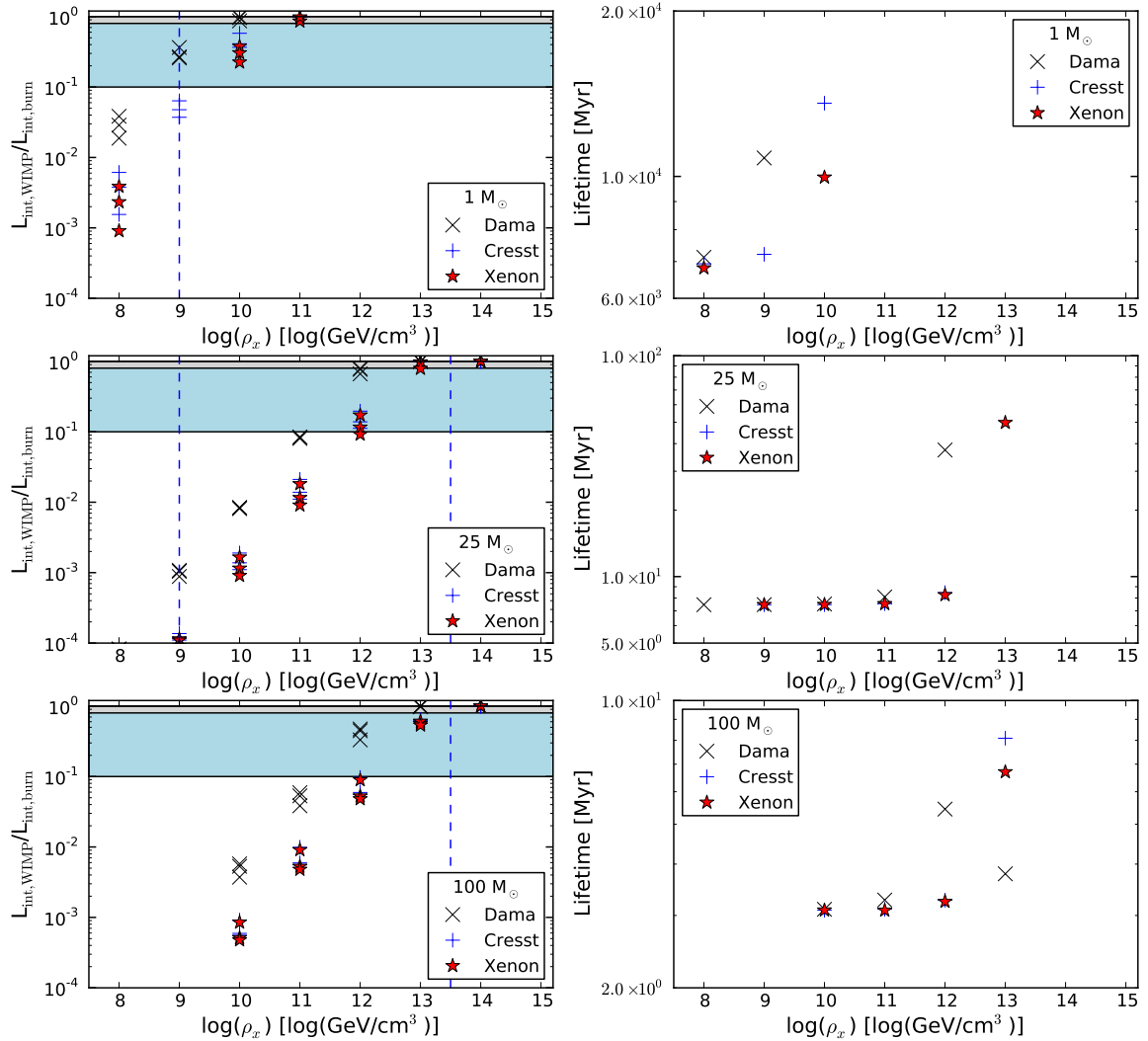
Figure 4.13: *Left:* The ambient densities vs. the relative luminosity $L_{\mathrm{int}}/L_{\mathrm{burning}}$ for a $1\,\mathrm{M_\odot}$, $25\,\mathrm{M_\odot}$, and $100\,\mathrm{M_\odot}$ star. Always the starting, final and mean values of the relative integrated luminosity in the stable phase are given. The gray shaded area indicates where the stars are considered WB (i.e. all three relative integrated luminosity values must be located in this area above 0.8). The light blue shaded area indicates the area where the evolution and lifetime of the stars are significantly influenced by the WIMPs (WIS) (all three relative luminosity values must be in this area between 0.1 and 0.8). The dashed line indicate realistic DM densities following Stacy et al. (2011). If two such lines are shown in a panel, the values between both are realistic. If only one is shown, the values *below* are realistic. *Right:* Lifetimes of the NWIS and the WIS.

in green and XENON in blue). The shaded areas indicate the ambient densities required for a star of a certain stellar mass to be a WB. Additionally, to the previously discussed example stellar masses the calculations have been carried out for two stars of $10\,M_\odot$ and $50\,M_\odot$. The black dashed line indicates the maximum long term stable WIMP density as discussed in Section 4.2.2.

For small stellar masses (i.e $1\,M_\odot$), ambient WIMP densities of $10^{9.4}\,\mathrm{GeV/cm^3}$ and $10^{10.8}\,\mathrm{GeV/cm^3}$ are required for the formation of a WB. Following Stacy et al. (2011), it is unlikely that small mass stars will stay in areas of the DM halo with high enough WIMP densities. Consequently, the long term existence of very low mass DS is unlikely even in the DAMA/LIBRA scenario.

Intermediate mass stars require even higher DM densities between $10^{11.5}\,\mathrm{GeV/cm^3}$ and $10^{13}\,\mathrm{GeV/cm^3}$ for stars of masses between $10\,M_\odot$ and $25\,M_\odot$. These ambient WIMP densities are also rather unlikely on long time scales. Nevertheless, in the central regions stable densities up to $10^{13.3}\,\mathrm{GeV/cm^3}$ are possible. Thus, an intermediate star must form in the central region of a DM halo in order become a WB.

The slope of the required WIMP density flattens when going to masses much above $25\,M_\odot$ and thus the ambient WIMP densities, required for the formation of high mass WB, is not much higher than for the intermediate WB (between $10^{12.5}\,\mathrm{GeV/cm^3}$ and $10^{13.2}\,\mathrm{GeV/cm^3}$). Additionally, it is more likely that higher mass stars form in the center of the DM halo, where such high DM densities are realistic following Stacy et al. (2011).

In conclusion, WB probably exclusively form in the central regions of the DM halos in the early Universe and usually have a mass larger than $20\,M_\odot$.

Considering that no indications for WB have been detected so far, several interpretations of our results are possible. Possibly, the ambient WIMP densities of roughly $10^{11.5}\,\mathrm{GeV/cm^3}$ to $10^{13.2}\,\mathrm{GeV/cm^3}$ required for the formation of WB did not exist (long enough) in the central regions of early DM halos to support the formation and allow the existence of WB on long timescales. A depletion of WIMPs crossing the star might be a possible reason for this. The capture by scattering may not proceed via the standard Gouldian prescription (Equation 2.17) for free WIMPs for Pop III Dark Stars. If the WIMPs are bound to the star, the velocities are different to free WIMPs, which reduces the capture rate, as suggested by Sivertsson and Gondolo (2011). On the other hand, in the case that such DM densities do exist, a significant number of DS can be expected to form and possibly even to still exist.

Also, the underlying assumptions about Pop III star formation are under ongoing debate. The initial prediction of very massive stars at a typical mass scale of $100\,M_\odot$ (Bromm et al. 1999, Bromm et al. 2002, Nakamura and Umemura 2001, Abel et al. 2000 and Abel et al. 2002) are possibly revised by recent results from Hosokawa et al. (2011), because no stars with masses above $50\,M_\odot$ formed in their radiation-hydrodynamic simulations due to radiative feedback from ultraviolet radiation emitted by the star. Thus, the mass scales (stars with mass < $100\,M_\odot$) likely for WB in our framework are supported by Hosokawa et al. (2011).

It must be taken into consideration that the detection of a WIMP signal by CRESST is only weak and the results from DAMA/LIBRA and XENON are contradictory. The upcoming XENON 1 tone experiment might even exclude the results from DAMA/LIBRA and CRESST more significantly. Thus it is possible that the WIMP properties considered here are not realistic. Maybe WIMPs have properties resulting in lower WIMP luminosities preventing the formation of long lived WB.

The results presented here are in general agreement with previous studies by Iocco et al.
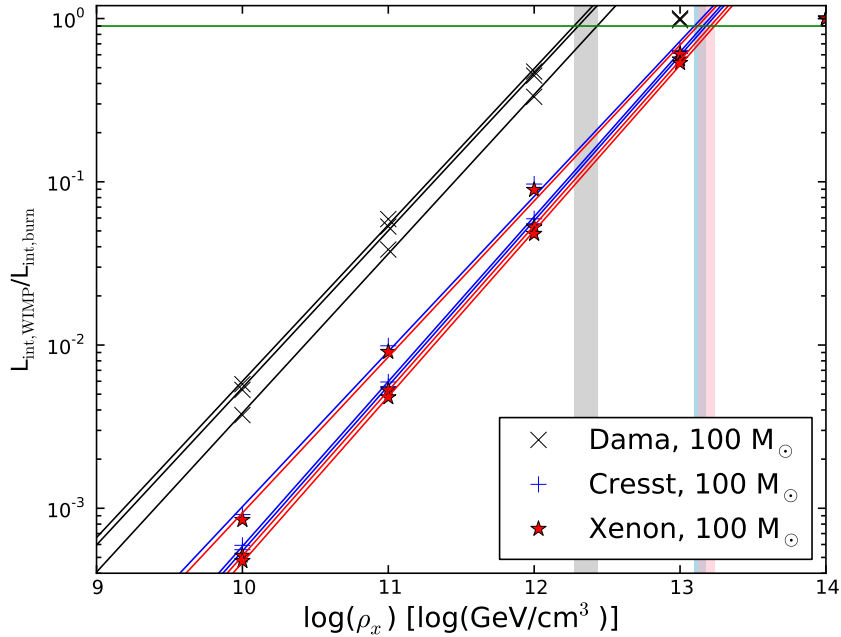
Figure 4.14: Illustration of the linear regression, for all three considered relative luminosity values (start, end, mean) and all scenarios for the $100_{\odot}$ star.

(2008). They also find that DS can be supported by burning of captured WIMPs as long as the environmental conditions remain unaltered. Since the details of the results depend on the environmental conditions, the WIMP properties and WIMP velocity dispersion, the agreement is only of qualitative, but not of quantitative nature. The parameters considered in this study are much more conservative and thus the ambient WIMP densities shown in Figure 4.15 required for the support of a WB are roughly two orders of magnitude higher than in a similar approach of Iocco et al. (2008). Nevertheless, the principle correlation of the stellar mass and the ambient WIMP density required for a WB are very similar (see Iocco et al. 2008 Figure 6).
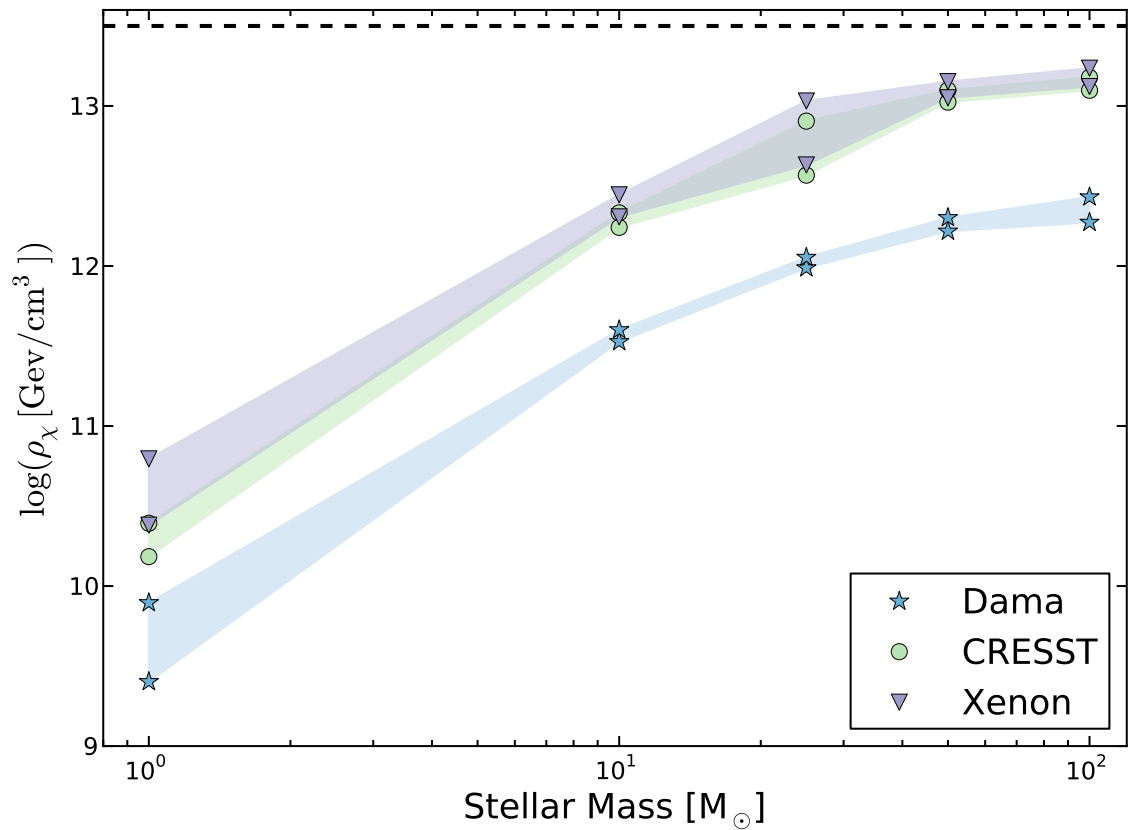
Figure 4.15: Summary of the results of the stellar evolution. The ambient density (maximum and minimum values of the linear regression) at which the star becomes a WB or a WIS for a certain stellar mass. The area between maximum and minimum values are shaded in the colors of the scenarios (DAMA/LIBRA in purple, CRESST in green and XENON in blue).

Chapter 5

Summary and Outlook

The general purpose model atmosphere code PHOENIX was employed for the calculations of stellar spectra of massive Dark Stars (DS). The DS properties were taken from Spolyar et al. (2009), who considered DS powered by Dark Matter (DM) pulled into the star due to the gravitational interaction of the DM with the gas during the formation of the star. The DS from Spolyar et al. (2009) are very massive, cool, but have high luminosities. It was possible to model stable atmospheres for a range of DS with effective temperatures between ~ 5000 K and ~ 24000 K. The importance of different line broadening processes as well as of calculations in local thermal equilibrium and non-local thermal equilibrium were explored. Possibilities of detecting DS with the James Webb Space Telescope (JWST) and identifying DS by unique spectral features have been investigated. Molecular hydrogen lines are a good indicator for low temperature Pop III or DS in the early Universe. Early stars consist exclusively of hydrogen, helium and a very small amount of lithium. No lithium lines useful for the identification of DS have been found. A detection of DS with the JWST proved rather unlikely. Even for optimistic values for the field of view (Hubble Deep Field), observation time (4 days), and the initial number density of stars ($n_0 = 10^{-5} M_\odot \, \mathrm{Mpc}^{-3}$), the expected number of stars is less than one. Additionally, even when no background is assumed the stars can probably only be detected with a significance of $10\,\sigma$ ($5\,\sigma$) up to redshifts of two (three). The influence of the absorption and re-emission by a nebula surrounding the star was evaluated. It was found that the nebula emission does not significantly alter the spectrum for low temperature DS.

Furthermore, the stellar evolution of DS, powered by the annihilation of WIMPs captured within the star after they have scattered from atomic nuclei, was calculated. For this purpose the DS evolution code 'DarkStars' by Scott et al. (2009) was used. Three different scenarios for mass and spin-independent scattering-cross-section were developed according to the results from the WIMP direct detection experiments DAMA/LIBRA, CRESST and XENON100. A scheme for characterizing first stars into Not WIMP Influenced Stars (NWIS), WIMP Influenced Stars where the properties and lifetimes of the star are altered by WIMP burning (WIS), and WIMP burner (WB), whose main power source is WIMP burning, is developed. The integrated luminosity due to WIMP burning normalized to the total luminosity of the star is taken as the crucial quantity for the characterization. Different ambient WIMP densities and stellar masses are explored following the results of Stacy et al. (2011). It is possible to define a boundary for the ambient WIMP density required to support WB in dependence on the stellar mass. This result is in qualitative agreement with a similar study by Iocco et al. (2008). A detailed analysis allows the statement that WB probably exclusively form

in the central region of the DM halo, because otherwise it would unlikely that the ambient WIMP density will be high enough for the support of a WB on long timescales. Because low mass stars do not usually form in the central region of the DM halo, it is likely that WB usually have masses above $20\,M_\odot$. The results can be interpreted in the light of the fact, that so far there has been no sign of a DM detection. Possibly the ambient WIMP densities of roughly $10^{11.5}\,\mathrm{GeV/cm^3}$ to $10^{13.2}\,\mathrm{GeV/cm^3}$ required for the formation of WB did not exist (long enough) in the central regions of early DM halos to support the formation and allow for the existence of WB on long timescales. A depletion of WIMPs on orbits crossing the star may take place, which is connected to the possibility that WIMP capture from a bound population of WIMPs (Sivertsson and Gondolo 2011) may proceed differently than for free WIMPs (the case considered in this study). On the other hand, if such ambient DM densities are possible we can expect the formation of DS.

Furthermore, the formation scenario of the first stars is under discussion, since Hosokawa et al. (2011) found an upper boundary $50\,M_\odot$ for the first stars due to feedback effects from ultraviolet radiation emitted by the star.

More uncertainties are given by the unknown nature of the WIMPs. Results of different direct detection experiments have not answered this question clearly, so that more realistic values for the WIMP scattering cross-section and mass may lead to lower DM luminosities preventing DS to form.

In this study, solar values for the dispersion of the WIMP velocities v and stellar velocity $v_\star$ were assumed. These values are probably not realistic for Pop III stars forming in the central regions of DM halos. The WIMP dispersion is expected to be of the order of $10\,\mathrm{km/s}$ and the star in the gravitational center of the halo is almost stationary. Figure 5.1 shows a first attempt of evaluating the influence of these parameters. Three cases were considered: A combination of the solar stellar velocity and the early dispersion of the WIMP velocity, as well as a combination of the early WIMP dispersion velocity value and the solar velocity both lead to a small increase of the DM luminosity. But the combination of an almost stationary star with a WIMP velocity dispersion, likely in the early Universe, leads to a DM luminosity increase of more than one order of magnitude. Thus, the results, given in this study, are conservative estimates and the next step would be to intensively explore the effects of different combinations of stellar and WIMP dispersion velocities.
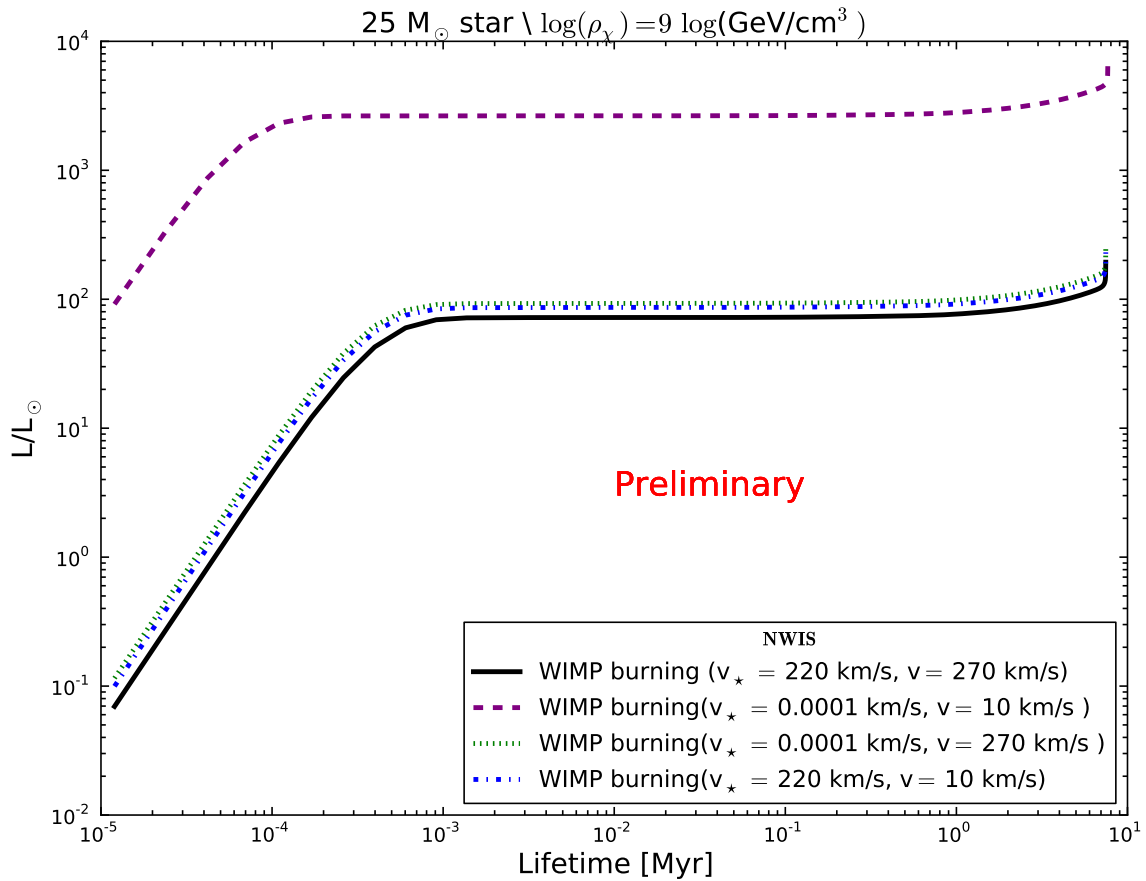
Figure 5.1: WIMP and hydrogen burning luminosities for the standard solar values of stellar velocity and WIMP dispersion velocity, as well three different combinations of the standard values and values for the WIMP dispersion velocity in the early Universe (v= 10 km/s) and the velocity of an almost stationary star ($v_\star = 0.0001$ km/s).

Bibliography

C. E. Aalseth, P. S. Barbeau, N. S. Bowden, B. Cabrera-Palmer, J. Colaresi, J. I. Collar, S. Dazeley, P. de Lurgio, J. E. Fast, N. Fields, C. H. Greenberg, T. W. Hossbach, M. E. Keillor, J. D. Kephart, M. G. Marino, H. S. Miley, M. L. Miller, J. L. Orrell, D. C. Radford, D. Reyna, O. Tench, T. D. van Wechel, J. F. Wilkerson, and K. M. Yocum. Results from a Search for Light-Mass Dark Matter with a p-Type Point Contact Germanium Detector. *Physical Review Letters*, 106(13):131301, April 2011. doi: 10.1103/PhysRevLett.106.131301.

T. Abel, G. L. Bryan, and M. L. Norman. The Formation and Fragmentation of Primordial Molecular Clouds. *Astrophys. J.*, 540:39–44, September 2000. doi: 10.1086/309295.

T. Abel, G. L. Bryan, and M. L. Norman. The Formation of the First Star in the Universe. *Science*, 295:93–98, January 2002. doi: 10.1126/science.295.5552.93.

J. Angle, E. Aprile, F. Arneodo, L. Baudis, A. Bernstein, A. Bolozdynya, P. Brusov, L. C. C. Coelho, C. E. Dahl, L. Deviveiros, A. D. Ferella, L. M. P. Fernandes, S. Fiorucci, R. J. Gaitskell, K. L. Giboni, R. Gomez, R. Hasty, L. Kastens, J. Kwong, J. A. M. Lopes, N. Madden, A. Manalaysay, A. Manzur, D. N. McKinsey, M. E. Monzani, K. Ni, U. Oberlack, J. Orboeck, G. Plante, R. Santorelli, J. M. F. Dos Santos, P. Shagin, T. Shutt, P. Sorensen, S. Schulte, C. Winant, and M. Yamashita. First Results from the XENON10 Dark Matter Experiment at the Gran Sasso National Laboratory. *Physical Review Letters*, 100(2):021303, January 2008. doi: 10.1103/PhysRevLett.100.021303.

G. Angloher, M. Bauer, I. Bavykina, A. Bento, C. Bucci, C. Ciemniak, G. Deuter, F. von Feilitzsch, D. Hauff, P. Huff, C. Isaila, J. Jochum, M. Kiefer, M. Kimmerle, J. . Lanfranchi, F. Petricca, S. Pfister, W. Potzel, F. Pröbst, F. Reindl, S. Roth, K. Rottler, C. Sailer, K. Schäffner, J. Schmaler, S. Scholl, W. Seidel, M. von Sivers, L. Stodolsky, C. Strandhagen, R. Strauß, A. Tanzke, I. Usherov, S. Wawoczny, M. Willers, and A. Zöller. Results from 730 kg days of the CRESST-II Dark Matter Search. *ArXiv e-prints*, September 2011.

E. Aprile, K. Arisaka, F. Arneodo, A. Askin, L. Baudis, A. Behrens, K. Bokeloh, E. Brown, T. Bruch, G. Bruno, J. M. R. Cardoso, W.-T. Chen, B. Choi, D. Cline, E. Duchovni, S. Fattori, A. D. Ferella, F. Gao, K.-L. Giboni, E. Gross, A. Kish, C. W. Lam, J. Lamblin, R. F. Lang, C. Levy, K. E. Lim, Q. Lin, S. Lindemann, M. Lindner, J. A. M. Lopes, K. Lung, T. Marrodán Undagoitia, Y. Mei, A. J. Melgarejo Fernandez, K. Ni, U. Oberlack, S. E. A. Orrigo, E. Pantic, R. Persiani, G. Plante, A. C. C. Ribeiro, R. Santorelli, J. M. F. Dos Santos, G. Sartorelli, M. Schumann, M. Selvi, P. Shagin, H. Simgen, A. Teymourian, D. Thers, O. Vitells, H. Wang, M. Weber, and C. Weinheimer. Dark Matter Results from 100 Live Days of XENON100 Data. *Physical Review Letters*, 107(13):131302, September 2011. doi: 10.1103/PhysRevLett.107.131302.

E. Baron. Radiative transfer in 7 lectures, June 2011.

S. V. W. Beckwith, M. Stiavelli, A. M. Koekemoer, J. A. R. Caldwell, H. C. Ferguson, R. Hook, R. A. Lucas, L. E. Bergeron, M. Corbin, S. Jogee, N. Panagia, M. Robberto, P. Royle, R. S. Somerville, and M. Sosey. The Hubble Ultra Deep Field. , 132:1729–1755, November 2006. doi: 10.1086/507302.

K. G. Begeman, A. H. Broeils, and R. H. Sanders. Extended rotation curves of spiral galaxies - Dark haloes and modified dynamics. , 249:523–537, April 1991.

R. Bernabei, P. Belli, F. Cappella, R. Cerulli, C. J. Dai, A. D'Angelo, H. L. He, A. Incicchitti, H. H. Kuang, J. M. Ma, F. Montecchia, F. Nozzoli, D. Prosperi, X. D. Sheng, and Z. P. Ye. First results from DAMA/LIBRA and the combined results with DAMA/NaI. *European Physical Journal C*, 56:333, August 2008. doi: 10.1140/epjc/s10052-008-0662-y.

G. Bertone, D. Hooper, and J. Silk. Particle dark matter: evidence, candidates and constraints. , 405:279–390, January 2005. doi: 10.1016/j.physrep.2004.08.031.

V. Bromm and R. B. Larson. The First Stars. , 42:79–118, September 2004. doi: 10.1146/ annurev.astro.42.053102.134034.

V. Bromm, P. S. Coppi, and R. B. Larson. Forming the First Stars in the Universe: The Fragmentation of Primordial Gas. , 527:L5–L8, December 1999. doi: 10.1086/312385.

V. Bromm, A. Ferrara, P. S. Coppi, and R. B. Larson. The fragmentation of pre-enriched primordial objects. , 328:969–976, December 2001. doi: 10.1046/j.1365-8711.2001.04915.x.

V. Bromm, P. S. Coppi, and R. B. Larson. The Formation of the First Stars. I. The Primordial Star-forming Cloud. *Astrophys. J.*, 564:23–51, January 2002. doi: 10.1086/323947.

R. L. Brown and W. G. Mathews. Theoretical Continuous Spectra of Gaseous Nebulae. *Astrophys. J.*, 160:939–+, June 1970. doi: 10.1086/150483.

J. I. Collar. A Realistic Assessment of the Sensitivity of XENON10 and XENON100 to Light-Mass WIMPs. *ArXiv e-prints*, June 2011.

Anand Desai. Dmtools, 2011. URL `http://dmtools.brown.edu:8080/`.

M. A. Dopita and R. S. Sutherland. *Astrophysics of the diffuse universe.* 2003.

P. P. Eggleton. The evolution of low mass stars. , 151:351, 1971.

P. P. Eggleton. Composition changes during stellar evolution. , 156:361, 1972.

H. C. Ferguson, M. Dickinson, and R. Williams. The Hubble Deep Fields. , 38:667–715, 2000. doi: 10.1146/annurev.astro.38.1.667.

E. R. Fernandez and E. Komatsu. The Cosmic Near-Infrared Background: Remnant Light from Early Stars. *Astrophys. J.*, 646:703–718, August 2006. doi: 10.1086/505126.

K. Freese, P. Bodenheimer, D. Spolyar, and P. Gondolo. Stellar Structure of Dark Stars: A First Phase of Stellar Evolution Resulting from Dark Matter Annihilation. , 685:L101–L104, October 2008a. doi: 10.1086/592685.

K. Freese, D. Spolyar, and A. Aguirre. Dark matter capture in the first stars: a power source and limit on stellar mass. , 11:14, November 2008b. doi: 10.1088/1475-7516/2008/11/014.

K. Freese, P. Gondolo, J. A. Sellwood, and D. Spolyar. Dark Matter Densities During the Formation of the First Stars and in Dark Stars. *Astrophys. J.*, 693:1563–1569, March 2009. doi: 10.1088/0004-637X/693/2/1563.

S. R. Furlanetto and A. Loeb. Metal Absorption Lines as Probes of the Intergalactic Medium Prior to the Reionization Epoch. *Astrophys. J.*, 588:18–34, May 2003. doi: 10.1086/374045.

J. P. Gardner. Science with the James Webb Space Telescope. *IAU Special Session*, 1, August 2006.

P. Gondolo, J. Edsjö, P. Ullio, L. Bergström, M. Schelke, and E. A. Baltz. Darksusy - a Numerical Package for Supersymmetric Dark Matter Calculations. In N. J. C. Spooner & V. Kudryavtsev, editor, *Identification of Dark Matter*, pages 256–261, March 2003. doi: 10.1142/9789812791313_0035.

A. Gould. Resonant enhancements in weakly interacting massive particle capture by the earth. *Astrophys. J.*, 321:571–585, October 1987. doi: 10.1086/165653.

A. Gould and G. Raffelt. Thermal conduction by massive particles. *Astrophys. J.*, 1990.

P. H Hauschildt. Stellar/planetary atmospheres, June 2011. URL `http://www.nhn.ou.edu/~baron/grk_lectures/index.html`.

P. H. Hauschildt and E. Baron. Numerical solution of the expanding stellar atmosphere problem. *Journal of Computational and Applied Mathematics*, 109:41–63, September 1999.

P. H. Hauschildt and E. Baron. A 3D radiative transfer framework. VI. PHOENIX/3D example applications. , 509:A36+, January 2010. doi: 10.1051/0004-6361/200913064.

A. Heger, C. L. Fryer, S. E. Woosley, N. Langer, and D. H. Hartmann. How Massive Single Stars End Their Life. *Astrophys. J.*, 591:288–300, July 2003. doi: 10.1086/375341.

T. Hosokawa, K. Omukai, N. Yoshida, and H. W. Yorke. Protostellar Feedback Halts the Growth of the First Stars in the Universe. *Science*, 334:1250–, December 2011. doi: 10.1126/science.1207433.

F. Iocco. Dark Matter Capture and Annihilation on the First Stars: Preliminary Estimates. , 677:L1–L4, April 2008. doi: 10.1086/587959.

F. Iocco, A. Bressan, E. Ripamonti, R. Schneider, A. Ferrara, and P. Marigo. Dark matter annihilation effects on the first stars. , 390:1655–1669, November 2008. doi: 10.1111/j.1365-2966.2008.13853.x.

W. J. Karzas and R. Latter. Electron Radiative Transitions in a Coulomb Field. *Astrophys. J., Suppl. Ser.*, 6:167–+, May 1961. doi: 10.1086/190063.

E. Komatsu, K. M. Smith, J. Dunkley, C. L. Bennett, B. Gold, G. Hinshaw, N. Jarosik, D. Larson, M. R. Nolta, L. Page, D. N. Spergel, M. Halpern, R. S. Hill, A. Kogut, M. Limon, S. S. Meyer, N. Odegard, G. S. Tucker, J. L. Weiland, E. Wollack, and E. L. Wright.

Seven-year Wilkinson Microwave Anisotropy Probe (WMAP) Observations: Cosmological Interpretation. *Astrophys. J., Suppl. Ser.*, 192:18, February 2011. doi: 10.1088/0067-0049/192/2/18.

C. F. McKee and J. C. Tan. The Formation of the First Stars. II. Radiative Feedback Processes and Implications for the Initial Mass Function. *Astrophys. J.*, 681:771–797, July 2008. doi: 10.1086/587434.

F. Nakamura and M. Umemura. On the Initial Mass Function of Population III Stars. *Astrophys. J.*, 548:19–32, February 2001. doi: 10.1086/318663.

NASA/WMAP Science Team. "fossil" galaxies may have helped end dark ages, November 2007. URL `http://www.nasa.gov/vision/universe/starsgalaxies/fuse_fossil_galaxies.html#backtoTop`.

NASA/WMAP Science Team. What is the universe made of?, June 2011. URL `http://map.gsfc.nasa.gov/universe/uni_matter.html`.

J. F. Navarro, C. S. Frenk, and S. D. M. White. The Structure of Cold Dark Matter Halos. *Astrophys. J.*, 462:563, May 1996. doi: 10.1086/177173.

Ohio State University. Astronomy 162: Introduction to stars, galaxies, the universe, 2006. URL `http://www.astronomy.ohio-state.edu/~pogge/Ast162/Unit2/Images/HSEq.gif`.

K. Omukai and S.-i. Inutsuka. An upper limit on the mass of a primordial star due to the formation of an Hii region: the effect of ionizing radiation force. , 332:59–64, May 2002. doi: 10.1046/j.1365-8711.2002.05276.x.

B. Paxton. EZ to Evolve ZAMS Stars: A Program Derived from Eggleton's Stellar Evolution Code. , 116:699–701, July 2004. doi: 10.1086/422345.

P. J. E. Peebles. *Principles of Physical Cosmology*. 1993.

O. R. Pols, C. A. Tout, P. P. Eggleton, and Z. Han. Approximate input physics for stellar modelling. , 274:964–974, June 1995.

D. Ripamonti, Ripamonti. E., F. Iocco, A. Bressan, R. Schneider, A. Ferrara, and P. Marigo. WIMP annihilation effects on primordial star formation. In *Identification of Dark Matter 2008*, 2008.

S. G. Ryan and A. J. Norton. *Stellar Evolution and Nucleosynthesis*. 2010.

G. B. Rybicki and A. P. Lightman. *Radiative Processes in Astrophysics*. June 1986.

P. Scott, M. Fairbairn, and J. Edsjö. Dark stars at the Galactic Centre - the main sequence. , 394:82–104, March 2009. doi: 10.1111/j.1365-2966.2008.14282.x.

P. Scott, J. Edjsö, and M. Fairbairn. The Darkstars Code:. a Publicly Available Dark Stellar Evolution Package. In H. V. Klapdor-Kleingrothaus & I. V. Krivosheina, editor, *Dark Matter in Astrophysics and Particle Physics, Dark 2009*, pages 320–327, December 2010. doi: 10.1142/9789814293792_0024.

S. Sivertsson and P. Gondolo. The WIMP Capture Process for Dark Stars in the Early Universe. *Astrophys. J.*, 729:51, March 2011. doi: 10.1088/0004-637X/729/1/51.

Space Telescope Science Institute. James webb space telescope: Nircam sensetivities, January 2012. URL `http://www.stsci.edu/jwst/instruments/nircam/sensitivity/`.

L. Spitzer. *Physical processes in the interstellar medium*. 1978.

D. Spolyar, K. Freese, and P. Gondolo. Dark Matter and the First Stars: A New Phase of Stellar Evolution. *Physical Review Letters*, 100(5):051101, February 2008. doi: 10.1103/PhysRevLett.100.051101.

D. Spolyar, P. Bodenheimer, K. Freese, and P. Gondolo. Dark Stars: A New Look at the First Stars in the Universe. *Astrophys. J.*, 705:1031–1042, November 2009. doi: 10.1088/0004-637X/705/1/1031.

A. Stacy, A. H. Pawlik, V. Bromm, and A. Loeb. Effect of Population III Multiplicity on Dark Star Formation. *ArXiv e-prints*, November 2011.

B. Strömgren. The Physical State of Interstellar Hydrogen. *Astrophys. J.*, 89:526–+, May 1939. doi: 10.1086/144074.

J. C. Tan and C. F. McKee. The Formation of the First Stars. I. Mass Infall Rates, Accretion Disk Structure, and Protostellar Evolution. *Astrophys. J.*, 603:383–400, March 2004. doi: 10.1086/381490.

The University of Glasgow. Physics beyond the standard model? URL `http://www.physics.gla.ac.uk/ppt/bsm.htm`.

M. Trenti and M. Stiavelli. Formation Rates of Population III Stars and Chemical Enrichment of Halos during the Reionization Era. *Astrophys. J.*, 694:879–892, April 2009. doi: 10.1088/0004-637X/694/2/879.

University of Alberta. Astronomy 122: Astronomy of stars and galaxies, January 2012. URL `http://www.ualberta.ca/~pogosyan/teaching/ASTRO_122/lect6/6268\_fig05\_25.jpg`.

S.-C. Yoon, F. Iocco, and S. Akiyama. Evolution of the First Stars with Dark Matter Burning. , 688:L1–L4, November 2008. doi: 10.1086/593976.

E. Zackrisson, P. Scott, C.-E. Rydberg, F. Iocco, B. Edvardsson, G. Östlin, S. Sivertsson, A. Zitrin, T. Broadhurst, and P. Gondolo. Finding High-redshift Dark Stars with the James Webb Space Telescope. *Astrophys. J.*, 717:257–267, July 2010. doi: 10.1088/0004-637X/717/1/257.

F. Zwicky. Die Rotverschiebung von extragalaktischen Nebeln. *Helvetica Physica Acta*, 6:110–127, 1933.

Danksagung

An dieser Stelle möchte ich mich herzlich bei allen bedanken, die zum Gelingen dieser Arbeit beigetragen haben. Zu allererst möchte ich mich bei Prof. Dr. Horns für die freundliche Aufnahme in seine Arbeitsgruppe bedanken und für die Gelegenheit, diese Diplomarbeit anfertigen zu können. Außerdem bedanke ich mich für die Möglichkeit und der deutschen Astroteilchen Schule in Obertrubach teilnehmen zu können. Ebenfalls gilt mein besonderer Dank Dr. Martin Raue für die interessante Aufgabenstellung und sorgfältige Betreuung dieser vorliegenden Arbeit. In gleichem Maße möchte ich mich bei Prof. Dr. Hauschildt, Andreas Maurer und Dr. Dennis Jack für ihre aufopfernde Hilfe bei der Fertigstellung dieser Diplomarbeit bedanken. Ohne sie wäre diese nicht zustande gekommen. Natülich bedanke ich mich bei der ganzen Arbeitsgruppe für die stets nette, kol- legiale und manchmal auch sehr heitere Arbeitsatmosphäre. Nicht zuletzt möchte ich mich bei meinem Verlobten Andi, meinen Freunden und meiner Familie für die Unterstützung während meiner Studienzeit bedanken.

Erklärung

Hiermit versichere ich, Franziska Laatz, dass ich die vorliegende Arbeit selbstständig verfasst und keine weiteren Quellen und Hilfsmittel als die angegebenen verwendet habe. Mit einer universitätsinternen Veröffentlichung bin ich einverstanden.

Hamburg, den 24.Februar 2012
Franziska Laatz